Doctoral Thesis, Periodical Part, Published Version

Emmert, Simon

Developing and Calibrating a Numerical Model for Microbially Enhanced Coal-Bed Methane Production

Mitteilungen. Institut für Wasser- und Umweltsystemmodellierung, Universität Stuttgart

Universität Stuttgart

Institut für Wasser- und Umweltsystemmodellierung

Mitteilungen

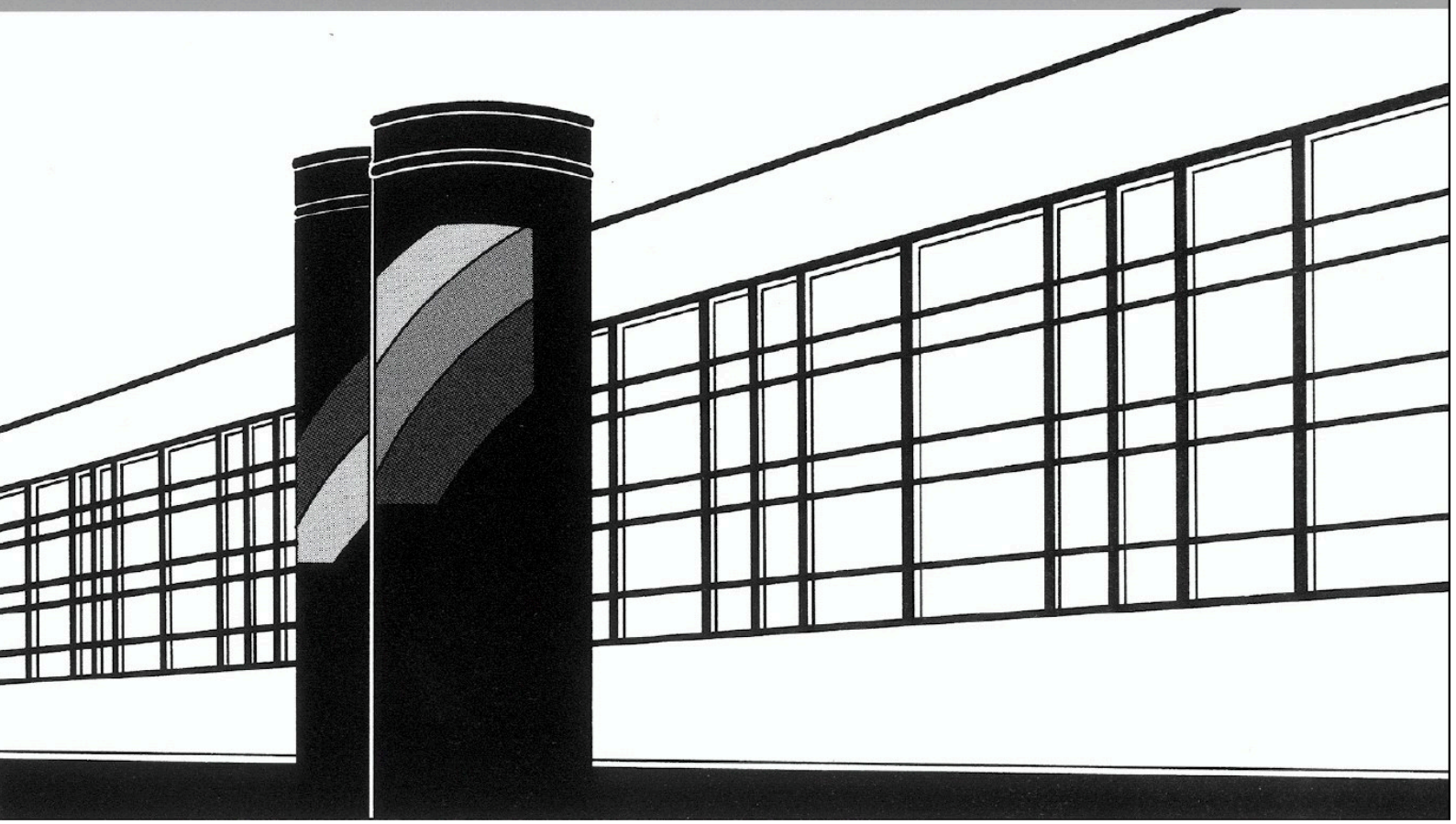

Heft 279 Simon Emmert

Developing and Calibrating a Numerical Model for Microbially Enhanced Coal-Bed Methane Production

Developing and Calibrating a Numerical Model for Microbially Enhanced Coal-Bed Methane Production

von der Fakultät Bau- und Umweltingenieurwissenschaften
der Universität Stuttgart und dem Stuttgart Center for Simulation Science
zur Erlangung der Würde eines
Doktor-Ingenieurs (Dr.-Ing.) genehmigte Abhandlung

vorgelegt von

Simon Emmert (geb. Scholz)
aus Schwäbisch Hall, Deutschland

Hauptberichter:	apl. Prof. Dr.-Ing. Holger Class
Mitberichter:	Prof. Robin Gerlach, Ph.D.
	Prof. Oliver Röhrle, Ph.D.

Tag der mündlichen Prüfung: 17.12.2020

Institut für Wasser- und Umweltsystemmodellierung
der Universität Stuttgart
2021

Heft 279

Developing and Calibrating a Numerical Model for Microbially Enhanced Coal-Bed Methane Production

von
Dr.-Ing.
Simon Emmert

Eigenverlag des Instituts für Wasser- und Umweltsystemmodellierung
der Universität Stuttgart

D93 Developing and Calibrating a Numerical Model for Microbially Enhanced Coal-Bed Methane Production

Bibliografische Information der Deutschen Nationalbibliothek
Die Deutsche Nationalbibliothek verzeichnet diese Publikation in der Deutschen Nationalbibliografie; detaillierte bibliografische Daten sind im Internet über http://www.d-nb.de abrufbar

Emmert, Simon:
Developing and Calibrating a Numerical Model for Microbially Enhanced Coal-Bed Methane Production, Universität Stuttgart. - Stuttgart: Institut für Wasser- und Umweltsystemmodellierung, 2021

(Mitteilungen Institut für Wasser- und Umweltsystemmodellierung, Universität Stuttgart: H. 279)
Zugl.: Stuttgart, Univ., Diss., 2021
ISBN 978-3-942036-83-2

NE: Institut für Wasser- und Umweltsystemmodellierung <Stuttgart>: Mitteilungen

Herausgegeben 2021 vom Eigenverlag des Instituts für Wasser- und Umweltsystem-modellierung

Druck: DCC Kästl e.K., Ostfildern

Acknowledgements

I would like to express my gratitude to all those who helped make this work and this thesis possible. Numerous people have shaped, supported, motivated, and helped me to develop the skills and mindset needed for this thesis. Thanks to all of you.

Zuerst danke ich meiner wunderbaren Frau Alex für den Rückhalt, die ständige Motivation, Geduld, gute Verpflegung und die Erinnerungen an die Tatsache, dass es neben der Arbeit auch noch ein Leben da draußen gibt. Ebenso danke ich meiner gesamten Familie für die tolle Unterstützung und Motivation in den letzten knapp 4 Jahren und darüber hinaus.

Ein besonderer Dank gilt meinem Hauptberichter Holger Class. Er hat mich seit der Bachelorarbeit, über die Masterarbeit bis hin zur Promotion betreut, mich stets voll unterstützt und mir ein unglaubliches Vertrauen entgegengebracht. Danke für die fachlich wie auch menschlich immer sehr wertvollen Ratschläge, Ideen und vor allem die Ruhe und Gelassenheit, die dich konstant umgibt.

Special thanks also to Robin Gerlach for his support, supervision and guidance. Especially regarding the biogeochemistry and writing, I have learned a lot from you. In addition, I would like to thank you for all the helpful discussions via Webex and also for the time when I got to visit Bozeman. It was a great start of my doctorate, and I am very grateful for being able to visit your lab, MSU, Bozeman, and the nature around.

Ebenso danke ich Oliver Röhrle für die Übernahme des Mitberichts, die fachliche Unterstützung und den "Startfunken" im 3. Semester, dass Forschung an der Uni spannend sein kann. Herrn Engesser danke ich für die Übernahme des Vorsitzes unter Corona-Bedingungen und die spannende Diskussion während der Prüfung.

Meinen weiteren "Chefs" Rainer Helmig und Bernd Flemisch danke ich für ihre offene, lockere Art und ihre immer vorhandene Hilfsbereitschaft. Ihr schafft ein unglaublich menschliches Klima und bringt einen fachlich enorm weiter! Danke für die vielen Diskussionen und Hilfestellungen. Gleichfalls danke ich Pru, Steffi und Beate für ihr allzeit offenes Ohr und die Hilfe im Umgang mit allen Bürokratie-Angelegenheiten. Michelle und David danke ich herzlich für ihren quasi 24/7 technischen Support.

I would also like to thank Al Cunningham for the discussions on this work and for the stay in Bozeman. It was a pleasure to stay with your family for Easter, plant trees on a Ranch, and thanks for the camping equipment and the advice regarding our Yellowstone trip.

A special thanks goes to Katie Davis for completing amazing experimental data that made this modelling work possible. Additionally, thank you for explaining the data and experiments to me over and over again, and for getting up early in the morning to discuss with me.

Ebenso danke ich Alisa Disam, Moira Peter und Yue Wang für ihre wertvollen Beiträge aus ihren Projekt-/Bachelor-/Masterarbeiten. Für die Betreuung meiner eigenen Masterarbeit und spannende Diskussionen, die wir bis heute führen, möchte ich außerdem Johannes Hommel danken.
Within my time at the IWS, I was fortunate enough to work with a number of friendly and always helpful colleagues. Thank you for the fun discussions, cakes, and coffee-breaks that sometimes even ended up in philosophical debates. It was a pleasure to work with you.

Zu guter Letzt danke ich der DFG für die Finanzierung dieses Projekts und allen deutschen Steuerzahler*innen für die Finanzierung der DFG. Hoffen wir, dass wir Stück für Stück mehr Erkenntnisse erlangen.

"Denn wir erkennen stückweise,
und wir weissagen stückweise;
wenn aber das Vollkommene kommt,
wird das, was stückweise ist, weggetan werden."
- 1. Kor. 13,9-10

Contents

List of Figures

List of Tables

Nomenclature

Selected Acronyms

+	indicates an amendment addition at a specific time
-	indicates no amendment addition at a specific time
CBM	coal-bed methane
Da	Damköhler number
EPS	extracellular polymeric substances
GB	Glass beads
GIA	global implicit or fully implicit approach
MECBM	microbially enhanced coal-bed methane
OS	Operator Splitting
PRB	Powder River Basin
REV	representative elementary volume
S-SNIA	strang sequential non-iterative approach
SA	sensitivity analysis
SNIA	sequential non-iterative approach

Abbreviations for phases and components

aa	acetoclastic archaea
ab	amendment and coal consuming bacteria
Am	Amendment
Bio	Microbial cells/Biofilm
cb	coal consuming bacteria
Cc	(bio)convertible fraction of coal
ha	hydrogenotrophic archaea
ma	methylotrophic archaea
sa	solid/trapped amendment

Greek Letters

Δt	time step	[s]
ΔG	Gibbs free energy	[kJ/mol]
$\lambda^{\kappa}_{attach}$	attachment or filtration coefficient of κ	[1/m]
$\lambda^{\varphi}_{detach}$	detachment coefficient of φ	[1/s]
μ	dynamic viscosity	[Pa s]
μ	Monod growth coefficient	[1/d]
μ_{max}	maximum growth coefficient	[1/d]
ϕ	porosity	[-]
ϱ	mass density	[kg/m^3]

ϱ_{mol}	molar density	[mol/m^3]
σ	surface tension between fluids	[N/m]
k_d	decay rate constant	[1/s]

Roman Letters

$D^{\kappa}_{\alpha,\mathrm{pm}}$	effective diffusion coefficient of component κ in phase α	[m^2/s]
A	area	[m^2]
C	Concentration	[kg/m^3]
$\mathbf{g}$	gravitational acceleration	[m/s^2]
H^{κ}_{w}	Henry coefficient of component κ in the wetting phase	[Pa]
$\mathbf{K}$	intrinsic permeability	[m^2]
k_r	relative permeability	[-]
K	Monod half saturation constant	[kg/m^3]
M	molecular mass	[kg/mol]
$E_{X_{\sim i}}$	Mean taken over all input factors but X_i	[-]
E_{X_i}	Mean taken over input factor X_i	[-]
$\mathbf{n}$	unit normal vector	[-]
p	pressure	[Pa]
p_{c}	capillary pressure	[Pa]
p_{e}	entry pressure	[Pa]
q^{κ}	molar sink/source term	[mol/(m^{3}s)]

r	radius	[m]
r_d	decay rate	[kg/m^{3}s]
r_g	growth rate	[kg/m^{3}s]
r^κ	retention rate of component κ	[mol/m^{3}s]
r^φ	detachment rate of component φ	[mol/m^{3}s]
S	saturation	[-]
S_e	effective wetting-phase saturation	[-]
S_i	first-order Sobol index of i	[-]
$S_{r\alpha}$	residual saturation of phase α	[-]
S_{Ti}	total-order Sobol index of i	[-]
T	end time, final time	[s]
t	time	[s]
$\mathbf{v}$	velocity vector	[m/s]
V_i	Variance based first-order effect	[-]
$V_{X_{\sim i}}$	Variance taken over all input factors but X_i	[-]
V_{X_i}	Variance taken over input factor X_i	[-]
V	volume	[m^3]
$\mathbf{x}$	spatial coordinate	[m]
X	mass fraction	[-]
x	mole fraction	[-]

X	biomass abbreviation (Monod kinetics)	
$Y_{P,S}$	Yield of product P from substrate S	[-]
$Y_{X,S}$	Yield of biomass X from substrate S	[-]
$Y^{P}_{X,S}$	Yield of biomass X from substrate S, while producing product P	[-]

Sub and superscripts

rα	residual phase (e.g. saturation)
n	non-wetting phase
0	initial / at time = 0
α	phase index (w: wetting, n: non-wetting, s: solid)
P	Product abbreviation (Monod kinetics)
pore	pore
S	Substrate abbreviation (Monod kinetics)
s	solid phase
w	wetting phase
κ	fluid component index
φ	solid component index

Abstract

With rising global primary energy consumption since the 19th century, new innovative ideas for energy production are needed. While renewable energies are taking over the electricity market e.g. in Germany and Europa, the global primary energy consumption is still based on fossil fuels. The relative share of coal and oil consumption of the current global energy mix is decreasing, while the natural gas share is increasing. One of the ways to contribute to a more sustainable utilization of our resources could be to enhance gas production from coal-beds with the help of microbes. While experimental investigations already demonstrate the potential of microbially enhanced coal-bed methane (MECBM) production on the lab scale, no in-depth mathematical and conceptual model including all sub-processes is reported in literature so far. With this study, we develop and present a conceptual food-web, included into a numerical model, that is calibrated and validated using batch experiments. The model is extended to model flow and transport features, test hypotheses, and compare against column experiments. Additionally, a sensitivity analysis of the model parameters as well as a preliminary study regarding operator-splitting techniques for the MECBM model are presented.

Batch calibration The presented mathematical and conceptual model comprises a food-web that includes two types of bacteria and three types of archaea representing members of the microbial community. Each microbial-community member is potentially interacting and competing with other members of the microbial community for substrate. Two out of nine experimental data sets are used to successfully calibrate the model. The calibrated model effectively predicts the methane concentrations within a 10 % range of deviation from the experimental results. A validation is performed with the results of the remaining batch experiments that were run with varied conditions. The hypotheses of amendment-induced stimulation of the microbial community members is supported by this study. Complex interactions between microbial activity,

substrate-specificity and bio-availability of coal for methane production can be captured and understood with the model.

Column studies The calibrated batch model provides the basis for including hydraulic flow and transport processes into mathematical models important for the design and implementation of more sustainable methods of harvesting methane from un-mineable coal beds. The model is extended to upflow reactor columns and compared to experimental studies including flow, transport and reactions of amendments as well as intermediate products. Filtration and retardation effects, biofilm decay, and attachment and detachment processes of microbial cells due to shear stress are implemented in the model for the column studies. These processes cannot be easily observed or investigated in experiments and the model provides a deeper understanding of the complex and strongly interacting processes involved in microbially enhanced coal-bed methane production. With this extended model, the entire process of enhancing methane production under flow conditions with microbial stimulation can be modelled, and hypotheses, derived from experiments, can be tested in the model.

Sensitivity analysis Three of the investigated cases from the column studies are used to perform a sensitivity analysis. The parameters of the sensitivity analysis are all grouped to vary each microbial reaction in the model and, where applicable, the retardation of amendment and attachment and detachment of microbial cells. Total methane production is evaluated over time as the model response of the sensitivity analysis. The model shows reasonable sensitivity values for the individual case studies that further support the findings of the previous column study. Interestingly, with changing physical processes for the different case studies, the parameter sensitivities are also shifted. An overview of sensitive parameters is presented in the form of a heatmap as a comparison of all three investigated case studies.

Operator splitting approaches Operator splitting techniques are a valuable tool when modelling large reactive-transport systems. The system of equations is usually split into different parts, which for the MECBM model are a transport part for all fluid phases and a reaction part. With this decoupling of the equations the solution schemes can be solved more easily however, a splitting error is introduced. A first study of two

different splitting approaches is presented. While accuracy and computational speed-up are in ranges as reported by other studies, the fully-implicit and fully-coupled reference model converges best with higher timestep sizes. However, more advanced splitting techniques could enhance the operator splitting approaches for MECBM models in the future and could become more relevant when modelling field-scale applications.

Zusammenfassung

Durch den seit dem 19. Jahrhundert weltweit steigenden Primärenergieverbrauch wächst auch der Bedarf an neuen innovativen Ideen der Energieerzeugung. Während der Strommarkt z.B. in Deutschland und Europa von erneuerbaren Energien erobert wird, basiert der globale Primärenergieverbrauch dagegen noch immer auf fossilen Brennstoffen. Dabei spielt der Anteil an Kohle und Öl eine zunehmend kleinere Rolle, während Erdgas einen wachsenden Anteil des derzeitigen globalen Energiemixes ausmacht. Eine Möglichkeit, die uns zur Verfügung stehenden Ressourcen nachhaltiger zu nutzen, könnte die mikrobiell angeregte Gasproduktion aus Kohleflözen sein.
Das Potenzial einer mikrobiell erhöhten Produktion von Methan aus Kohleflözen (MECBM) wurde bereits durch experimetelle Untersuchungen im Labormaßstab gezeigt. Über ein mathematisches und konzeptionelles Modell, welches alle Teilprozesse einschließt, wurde in der Literatur bislang jedoch nicht berichtet. Im Rahmen dieser Arbeit entwickeln wir eine konzeptionelle MECBM-Nahrungskette, die in ein numerisches Modell implementiert wird. Dieses Modell wird anhand von Batch-Experimenten kalibriert und validiert. Daran anschließend werden mit dem Modell verschiedene Hypothesen getestet und die Ergebnisse mit Säulenversuchen aus Laborexperimenten verglichen. Zusätzlich werden eine Sensitivitätsanalyse der Modellparameter sowie eine Voruntersuchung hinsichtlich Operator-Splitting-Techniken des MECBM-Modells vorgestellt.

Batch-Kalibrierung Das hier vorgestellte mathematische und konzeptionelle Modell umfasst eine Nahrungskette, in der die mikrobielle Gemeinschaft durch zwei funktionelle Gruppen von Bakterien und drei Gruppen von Archaeen abgebildet wird. Jedes Mitglied der mikrobiellen Gemeinschaft interagiert und konkurriert potenziell mit anderen Mitgliedern der mikrobiellen Gemeinschaft um Substrat. Zwei von neun vorliegenden experimentellen Datensätzen werden verwendet, um das Modell erfolgreich zu

kalibrieren. Mit dem kalibrierten Modell kann die Methankonzentrationen mit unter 10 % Abweichung zu den experimentellen Ergebnissen effektiv vorausgesagt werden. Durch diesen Vergleich mit den übrigen Batch-Laborexperimenten, welche unter variierenden Bedingungen durchgeführt wird, erfolgt die Validierung des Modells. Diese Studie stützt damit die Hypothese der substrat-induzierten Stimulation von Mitgliedern der mikrobiellen Gemeinschaft. Komplexe Wechselwirkungen zwischen mikrobieller Aktivität, Substratspezifität und Bioverfügbarkeit von Kohle für die Methanproduktion können mit dem Modell erfasst und analysiert werden.

Säulenstudie Das kalibrierte Batch-Modell wird um hydraulische Strömungs- und Transportprozesse erweitert. Diese Prozesse sind für den Entwurf und die Umsetzung von nachhaltigeren Methoden der Methangewinnung aus nicht-abbaubaren Kohleflözen wichtig. Das Modell wird daher auf Säulenversuche ausgedehnt und mit experimentellen Studien verglichen. Diese beinhalten nun Strömung, Transport und Reaktionen von Ausgangs- und Zwischenprodukten. Filtrations- und Retardierungseffekte, Absterben von Biofilm sowie Anlagerungs- und Ablöseprozesse von Mikroorganismen aufgrund von Scherbeanspruchung werden im Modell implementiert. Diese Prozesse können in Experimenten nicht ohne weiteres beobachtet oder untersucht werden. Das Modell liefert ein besseres Verständnis der komplexen und stark interagierenden Prozesse, die bei der mikrobiell erhöten Methanproduktion in Kohleflözen stattfinden. Mit diesem erweiterten Modell kann der gesamte Prozess der durch mikrobielle Stimulaton erhöhten Methanproduktion unter Strömungs- und Transportbedingungen modelliert werden. Darüberhinaus können aus Experimenten abgeleitete Hypothesen im Modell getestet werden.

Sensitivitätsanalyse Drei der untersuchten Fälle aus der Säulenstudien werden nun zur Durchführung einer Sensitivitätsanalyse verwendet. Die Parameter der Sensitivitätsanalyse werden gruppiert, um jede mikrobielle Reaktion im Modell und gegebenenfalls die Filrations- und Retardationseffekte sowie das Anlagern und Ablösen von Mikroorganismen zu variieren. Die gesamte Methanproduktion wird als Modellantwort der Sensitivitätsanalyse über die Zeit ausgewertet. Das Modell zeigt plausbile Sensitivitätswerte für die einzelnen Fallstudien, die jeweils mit den Ergebnissen aus der Säulenstudie übereinstimmen. Interessanterweise werden mit sich ändernden physikalischen Prozessen für die verschiedenen Fallstudien auch die Parameterempfindlichkeiten

verschoben. Eine Übersicht der sensitiven Parameter wird in Form einer Heatmap als Vergleich aller drei untersuchten Fallstudien dargestellt.

Operator splitting Ansätze Operator-Splitting-Techniken sind ein wertvolles Hilfsmittel bei der Modellierung großer reaktiver Transportsysteme. Das zu lösende Gleichungssystem wird beim Operator-Splitting in verschiedene Teile aufgeteilt. Für das MECBM-Modell handelt es sich um einen Transportteil für alle Fluidphasen und einen Reaktionsteil. Mit dieser Entkopplung der Gleichung lassen sich die einzelnen Gleichungssysteme schneller lösen, allerdings entsteht dabei ein Splitting-Fehler. Eine erste Untersuchung zweier verschiedener Operator-Splitting-Ansätze wird vorgestellt. Die Genauigkeit und Rechengeschwindigkeit dieser Ansätze liegen in Bereichen, wie sie auch in anderen Studien berichtet wurden. Dennoch konvergiert das voll-implizite und vollgekoppelte Referenzmodell ohne Operator-Splitting besser und mit größeren Zeitschritten. Fortschrittlichere Splitting-Techniken könnten jedoch in Zukunft die Operator-Splitting-Ansätze für MECBM verbessern.

1 Introduction

The rising global energy demand is calling for new ways of generating energy, while climate and environmental protection agencies and individuals are trying to keep the environmental impact at a minimum [Bruckner et al., 2014]. Global primary energy consumption has been increasing, with only minor stops caused by global crises, from 1800 until today [Smil, 2016, Dudley et al., 2018]. Even though renewable energies become more popular, natural gas, coal and crude oil made up 87% of the world's primary energy consumption in 2018 (natural gas 24.51%, coal 27.97%, crude oil 34.52%) [Dudley et al., 2018]. While the relative consumption of coal and crude oil has been decreasing gradually over the last decade, the consumption of natural gas has increased. Coal-bed methane (CBM) is part of the unconventional gas resources. Together with shale and tight gas, they are a growing part of the global energy mix, that has traditionally been considered too costly to produce [Birol et al., 2012]. Since easy exploration of coal gas is inhibited by low permeabilities, expensive drilling techniques and production enhancing processes were necessary. CBM could be harvested mainly in the Northern Hemisphere and in Australia as shown in Figure 1.1 by Strapoc et al. [2011]. It is harvested in the United States, Canada and Australia [Senthamaraikkannan et al., 2016b] already, and potentially in Germany [Birol et al., 2012]. Figure 1.1 also shows that up to 4 % of the methane production in the USA is estimated to be mainly due to biogenic methane production, while 10 % were from CBM wells in the year 2008. More recent data indicate that methane production in total has increased even further from approx. $765 \times 10^9\,\mathrm{m}^3$/year in 2009 to over $1053 \times 10^9\,\mathrm{m}^3$/year in 2018 [Dudley et al., 2018].

First studies present that instead of using high pressures, chemicals and other methane production enhancing techniques, shallow coal beds could be microbially stimulated to enhance methane production in a more natural way [Jones et al., 2010, Park and Liang, 2016]. This is called microbially enhanced coal-bed methane (MECBM) production.

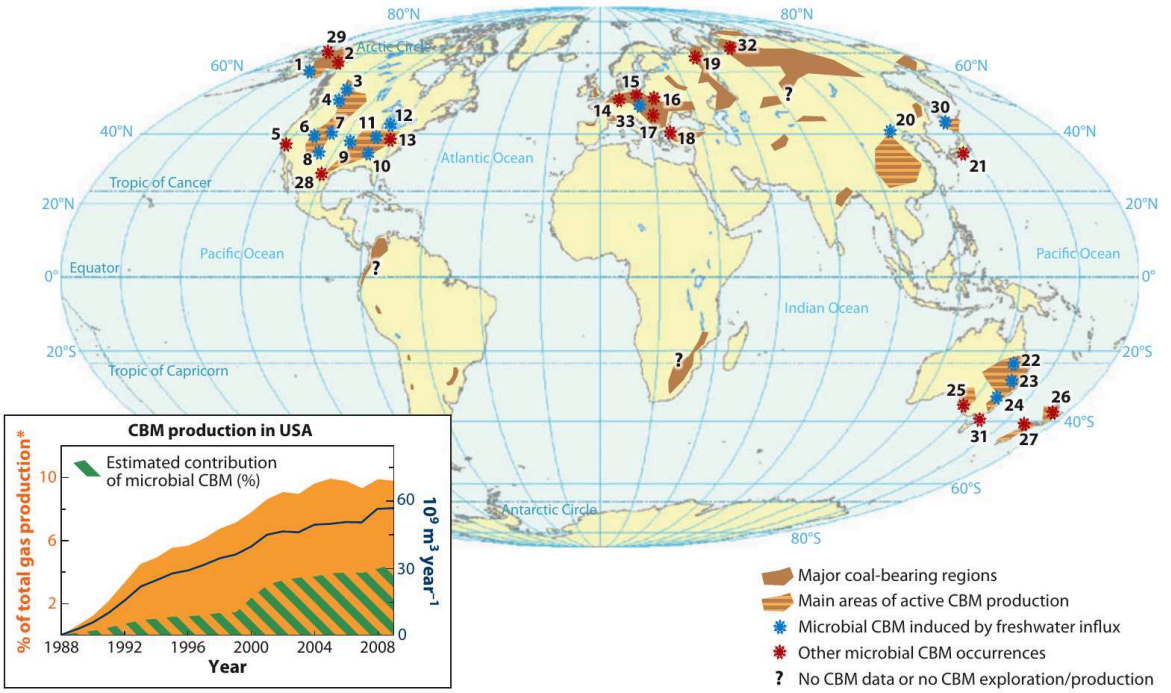

Figure 1.1: Coal bed methane production potential worldwide. The major coal-bearing regions are in the Northern Hemisphere. CBM production already is performed for some countries. The small Figure on the bottom left shows total methane production (blue) and the percentage of CBM production in the USA from 1988 to 2008. Republished with permission of ANNUAL REVIEWS INC. , from Strapoc et al. [2011]; permission conveyed through Copyright Clearance Center, Inc.

The idea behind MECBM production is that by providing the microbial community with substrate, the microbial conversion of coal and other substrates to methane is enhanced. However, little is known about the microbes, nutrients or the conditions favourable for MECBM production. With this thesis, we show a conceptual way of modelling the potential processes involved in enhancing methane production from coal beds with the help of microbes.

1.1 Bacteria, archaea and biofilms in porous media

Bacteria and archaea are both prokaryotes. They are generally set up simpler than eukaryotes and can, among other forms, exist as suspended, floating, or sessile cells [Cullimore, 1999]. Archaea differ from bacteria mainly by a slightly different cell structure, lipids, and their metabolism (e.g. methanogenesis). Many archaea have enzymes that help them survive under extreme conditions.

These microbial cells can attach to surfaces and are often surrounded by a matrix of extracellular polymeric substances (EPS), that protects the cells from their surrounding environment. Attached cells with surrounding EPS are often referred to as biofilm [Bryers, 2000]. In our context these cells can attach to a porous medium. Once attached, they can grow into a mature biofilm and either single cells or larger pieces can detach again and colonize the porous medium further downstream [De Beer and Stoodley, 2006].

1.2 Biogeochemical processes

Subsurface processes have been studied and developed, aiming at controlling biogeochemical reactions and processes in a favourable way. The applications range from groundwater remediation problems [Rittmann, 1993, Cunningham et al., 2003] over enhancing oil or gas productions [Bachmann et al., 2014, Geetha et al., 2018, Saravanan et al., 2020] to storage or release of gas, or mineral precipitation [Whiffin et al., 2007, Phillips et al., 2013, 2018, Cunningham et al., 2019]. While most studies focus on a single reactive process occurring mostly at interfaces between biofilm, fluid, and porous medium, this thesis presents a complex food-web with interacting and depending microbial cells and their biogeochemical reactions for MECBM production.

1.3 Coal beds

A porous medium typically consists of solid material containing pores or void spaces. Coal beds are usually dual porosity systems. This means, that there is the influence of micropores ($< 2\,\mathrm{nm}$) on the one hand which primarily affect gas adsorption [Harpalani and Zhao, 1991]. Jones et al. [1987] state that the coal with its micropores is known to have a very large internal surface area (up to $205\,000\,\mathrm{m}^2/\mathrm{s}$). On the other hand, there is the influence of macropores ($> 50\,\mathrm{nm}$) or so-called fractures. These bigger pores form cleats throughout the whole matrix and are accessible to fluid flow.
Since most of the experimental studies that serve as a basis for this work use crushed coal from the Powder River Basin (PRB), a rather homogeneous pore-size distribution is given. Many effects, e.g. cleats and preferential flow paths, which are of importance

for real coal beds, are assumed to have minor effects for this work, as all experimental studies used for comparison use crushed and cleaned coal. Since the same coal from the PRB is used in all studies, the coal is also assumed to be of the same rank and type.

1.4 Microbially enhanced coal-bed methane production

While unconventional methane production focused on shale and coal beds with mature coals and high thermogenic gas contents, it soon was obvious that low permeability and mineralization processes in fractures and cleats of the coal were hindering gas production [Birol et al., 2012]. To overcome this, either expensive drilling techniques are necessary or one moves to less mature coals with higher permeability and formation thickness. However, these formations are typically characterized by a lower gas content [Meslé et al., 2013]. The strategy with MECBM focuses on shallow coal beds with a smaller formation thickness, which can have biogenic methane production, as Magot et al. [2000] state that microbial growth is limited to temperatures below 80 °C.
Many studies in recent years observe methane release from coal mines and their drainage systems and focus on the microbial community [Dojka et al., 1998, Strapoc et al., 2008, Jones et al., 2010, Beckmann et al., 2011]. There, the release of methane is a potential hazard to mine workers or the climate, if the methane is released into the atmosphere. CBM has been harvested in the PRB since 1993 [Hower et al., 2003], and has shown to be primarily microbially generated [Barnhart et al., 2017]. Further studies on the characterization of methanogenic consortia in the PRB were performed by Flores et al. [2008] and Green et al. [2008], which, among others, lead to a series of experimental studies on biogenic methane production from PRB coal that this modelling work is based on [Barnhart et al., 2017, Davis et al., 2018a,b, 2019].
In this thesis, it is investigated how with small amendment additions of e.g. yeast or algae extract the microbial community is stimulated and produces additional gas from the coal and the amendments [Barnhart et al., 2017, Davis et al., 2018b]. Experimental studies have shown the applicability in the lab, while many questions remain. Numerical modelling can be used as an instrumental tool to test hypothesis that are not easily tested in experiment; however, a good scientific basis in form of profound and comparable experimental investigations is needed to establish such a model. So far only a few works for a numerical model regarding MECBM production have been publishedp

[Senthamaraikkannan et al., 2016b,a, Saurabh and Harpalani, 2018]. Most of these models focus on the acetoclastic methanogenesis or use one lumped reaction from the entire process of coal to methane conversion. Additionally, the transport processes are modelled at the same time for some studies [Senthamaraikkannan et al., 2016a]. While they produce reasonable results for their test cases, Saurabh and Harpalani [2018] state that "one shortcoming is apparent, available data in public domain." Because the available data in the public domain is indeed, not as manifold as one could wish, we think that with focusing this work on the studies by Barnhart et al. [2017] and Davis et al. [2018a, 2019] the dataset is large and fundamental enough for a conceptual and numerical model. This conceptual and numerical can be extended and adapted to other types of coal in the future.

1.5 Objectives of this thesis

The aim of this work is to develop a numerical model that is able to assist in evaluating and pursuing experimental studies for MECBM production. This thesis contributes to the goal by four objectives:

- development of a conceptual model for the reaction kinetics in batch systems;
- extension to upflow column-reactor systems involving flow and transport of components, amendment, and potentially microbial cells or biofilms;
- investigate the sensitivity of modelling parameters for the column reactors;
- operator-splitting approaches to investigate the robustness of the numerical model and to reduce the computational time of the numerical model.

The first and second objective are considered as straightforward since experimental data for comparison is available. The sensitivity analysis is performed in a lumped way to reduce parameters and modelling runtime, meaning that each reaction pathway is only changed by one factor. The robustness and computational time of the model are important for further studies, as the research code we present here is able to solve all the systems reliably. However, a large computational effort is observed for the more complex cases, as all components and processes are included and solved even though they might be of minor importance.

1.6 Structure of this thesis

An overview of the structure along the lines of the main objectives is presented here. A short introduction of the fundamentals for the microbial reaction system as well as for flow and transport in porous media is given in Chapter 2 and Chapter 3. As this work is based on experimental studies, the key findings of these experimental studies are recapitulated in Chapter 4. Chapter 5 describes the calibration and validation of the conceptual and numerical model with experimental batch-reactor data. Chapter 6 extends the previously validated system to model flow and transport for different scenarios using e.g. amendment retardation or partitioning, microbial cell attachment and detachment. A sensitivity analysis of the different column scenarios is presented in Chapter 7. Chapter 8 focuses on the robustness of the numerical model and how to reduce computational time using decoupling approaches. In the end, Chapter 9 concludes and summarizes the achievements of this thesis.

2 Biogeochemical fundamentals

Microbial communities are almost omnipresent, often interdependent, and specialized to survive in their environment [Bryers, 2000]. In many subsurface organic materials as e.g. coal, microbial species are found. In comparison to other organic materials, coal is not an easy substrate due to its complex structure [Park and Liang, 2016]. Nevertheless, many studies [Harris et al., 2008, Strapoc et al., 2008, Barnhart et al., 2017, Davis et al., 2018a,b, Beckmann et al., 2019, Lupton et al., 2020] show that methane can be biologically produced from coal and that apparently biogeochemical processes on coal are of importance for methane production from coal beds. This chapter focuses on the basics of microbial metabolisms and explains the processes involved in MECBM production.

2.1 Coal properties, bio-availability and adsorption

Coal is formed from the remainders of organic materials (e.g. plants) buried and compressed under sediments over a long time under high pressures and temperatures. The degree of coalification is described by the rank of the coal. For a lower ranked coal more plant structures can be observed in the coal, whereas for a higher ranked coal more carbon content is present as most plant materials have been metamorphosed [Taylor et al., 2009]. Under suitable conditions, the rank of the coal increases from peat and lignite over (sub-)bituminous coal to anthracite.
The coal investigated in this thesis is from the Powder River Basin and is characterized by Barnhart et al. [2017] to be of sub-bituminous rank. For MECBM production processes, it is of interest how much of the coal's carbon content is available for microbial conversion. Barnhart et al. [2017] show that 99.5 % of the coal energy content remained after long-term incubation of coal in batch studies, which leads to the assumption that

0.5 % of this coal is available for microbial conversion in the model.
As already mentioned in Section 1.3, coal is known to have a large surface area due to its high degree of micropores. This large surface area is important for ad- and desorption processes that can occur on coal. Adsorption is a physical process that is best described as an attraction of particles (atoms, ions or molecules) from a fluid phase to the surface of a solid phase (adsorbent). Ad- and desorption processes are commonly described by isotherms, where popular isotherms for coal beds are the Langmuir [Langmuir, 1917] or the Freundlich isotherm [Freundlich et al., 1906]. A previous study [Scholz, 2017] investigated the behaviour of adsorption isotherms for MECBM batch system and concludes, that under laboratory batch conditions, the modelling of ad- and desorption processes only shows a minimal effect. Adsorption could have an impact for column- and field-scale studies, but further experimental data is needed to model this quantitatively. At the current state, this is not of further interest for this thesis, but should be considered and investigated in future projects.

2.2 Microbial metabolism

2.2.1 Monod kinetics

Microbial growth rates mostly depend on a growth-limiting substrate concentration, which is usually modelled using Monod kinetics [Monod, 1942]. The growth coefficient μ, which depends on the concentration C_s of a growth-limiting substrate S, can be written as:

$$\mu = \mu_{max} \left(\frac{C_s}{K_s + C_s} \right), \tag{2.1}$$

where μ_{max} is the maximum growth coefficient and K_s is the Monod half saturation constant. It is defined as the concentration of substrate at which the growth coefficient equals half of the maximum rate [Chmiel et al., 2018]. Monod kinetics consist of two linear approximations: a zeroth order equation part and a first order part. When there is plenty of substrate available ($C_s >> K_s$) the Monod kinetics approach is dominated by the zeroth order equation:

$$\mu \approx \mu_{max}. \tag{2.2}$$

When $C_s << K_s$, the Monod kinetics are approximated as first order reaction rate:

$$\mu \approx \left(\frac{\mu_{max}}{K_s} \right) \cdot C_s. \tag{2.3}$$

2.2.2 Biomass growth and decay

Growth of microbes is defined as an increase in cell numbers rather than cell size. As long as microbes find suitable conditions, they grow at a rate described by the growth rate:

$$r_g = \mu_{max} \left(\frac{C_s}{K_s + C_s} \right) \cdot X, \tag{2.4}$$

with X being the biomass of cells.
The decay rate of microorganisms is assumed to be a first-order function of the biomass concentration:

$$r_d = k_d \cdot X, \tag{2.5}$$

where k_d is the decay rate constant.

2.2.3 Substrate utilization and product formation

To connect substrate consumption to biomass growth, a third variable, the so-called yield $Y^P_{X,S}$ is introduced. It expresses how much biomass X is produced per utilized mass of substrate S, while (where applicable) producing product P. The rate of substrate utilization is dependent on the microbial growth rate of this substrate, with the yield as proportionality constant:

$$\frac{dS}{dt} = \frac{r_g}{Y_{X,S}}. \tag{2.6}$$

Although dimensionless, the correct unit of the yield is “mass of biomass” per “mass of (limiting) substrate consumed”.
For product formation, the growth rate r_g from biomass and the yield $Y_{P,S}$ are used to described the formation of products by:

$$\frac{dP}{dt} = r_g \cdot \left(\frac{Y_{P,S}}{Y^P_{X,S}} \right). \tag{2.7}$$

2.3 Microorganisms and biofilms in porous media

Microorganisms in the context of MECBM production are the essential part for all biogeochemical reactions that occur. As previously mentioned in Chapter 1.1, the different microbial cells can form biofilms by producing EPS on porous media. While the process of the evolution of a biofilm itself is topic studied by e.g. Bryers [2000], we assume attached cells to immediately form a biofilm in the model. Biofilm in the context of this modelling work is described as part of the solid phases, even though the real biofilm species in itself are not solid or rigid bodies. However, the concept of a continuum can be applied to the biofilm species with the REV (representative elementary volume) description as explained in Section 3.1. We do not consider the individual microbial cells and EPS, but biofilms are described as an entity taking up a certain volume fraction of space per control volume.
As already mentioned in Chapter 1.1, the MECBM microbial community consists of bacteria and archaea. For a better approximation in the model, we derive from Davis et al. [2018a] that the bacterial community could potentially be separated into an amendment and a coal-converting part. Therefore, we operationally define two groups of bacteria depending on their substrate utilization ability. Archaea are separated into three different groups, following the three main methanogenic pathways [Davis et al., 2018b, Strapoc et al., 2011, Schink, 1997]. While the distinction between the two groups of bacteria is artificial, it allows the model to track growth of microbes based on amendment utilization and coal utilization separately. An overview of the interactions between the microbial species, in form of a flow chart, is given in Figure 2.1.

2.3.1 Bacteria*

Coal bacteria

We characterize one group as the "Coal Bacteria" (cb), which we consider to primarily feed on the bioconvertible fraction of coal. They produce acetate and hydrogen from the coal.

*Section 2.3.1 is taken from Section 3.1.1. of Emmert, Class, Davis, and Gerlach [2020a] and reprinted with permission from © 2020 Elsevier Inc.

Amendment and coal bacteria

The other group is the so-called "Amendment and Coal Bacteria" (ab), which feed on coal, but are also able to utilize the added substrate "amendment". From their substrates, they produce acetate, hydrogen and methyl groups.

2.3.2 Archaea[†]

Acetoclastic archaea

Acetoclastic archaea (aa) stand for a group of archaea that produce CH_4 from acetate using the acetoclastic pathway. The acetoclastic pathway is described as the conversion of acetic acid to CH_4 and CO_2, or from acetate to CH_4 and bicarbonate (HCO_3^-).

Hydrogenotrophic archaea

Hydrogenotrophic archaea (ha) represent a group of archaea producing CH_4 from hydrogen (as e^- donor) and CO_2 (as e^- acceptor) via the hydrogenotrophic pathway to CH_4 and H_2O.

Methylotrophic archaea

The methylotrophic archaea (ma) are the group of archaea that produce CH_4 from methyl groups, where, in principle, three methyl groups are reduced while one is oxidized to CO_2. Even though the methylotrophic pathway is included in the model for the amendment and coal consuming bacteria, the focus is on the acetoclastic and hydrogenotrophic pathways, as they appear to contribute more significantly to CH_4 production [White et al., 2000, Garcia et al., 2006].

[†]Section 2.3.2 is taken from Section 3.1.2. of Emmert, Class, Davis, and Gerlach [2020a] and reprinted with permission from © 2020 Elsevier Inc.

2.4 Biogeochemical processes for MECBM[‡]

The basic idea of the conceptual model itself is found in literature [Zinder, 1984, 1993, Park and Liang, 2016] and includes coal as a porous matrix and substrate, the microbial community in form of biomass, amendment as an additional substrate, as well as multiple intermediate products. Many experimental studies have been performed in order to characterize the microbial community [Jones et al., 2010, Strapoc et al., 2008, Meslé et al., 2013, Ritter et al., 2015]. This thesis focuses on the main reactive pathways and simplifies the microbial community to groups, which are distinguished by their substrate. One group consists of two types of microbes converting amendment and/or coal to intermediates. This first step is the hydrolysis of complex organic compounds to simpler and more bioavailable organic compounds, such as sugars or amino acids [Park and Liang, 2016]. The second step is fermentation, where complex organic compounds are being fermented to simpler intermediates, such as fatty acids, organic acids, alcohols, as well as the known precursors for methanogenesis acetate, hydrogen and CO_2 [Gupta and Gupta, 2014, Schink, 1997]. Other bacteria produce acetate, hydrogen and CO_2 from these intermediates [Schink, 1997].
The last step is methanogenesis described to be performed by highly specialized archaea using three principally different pathways, namely hydrogen, methyl and acetate reduction [Jones et al., 2010, Ritter et al., 2015]. A conceptual overview of all the processes considered here, in form of a flow chart, is given in Figure 2.1.
Microbial growth rates are implemented using Monod Kinetics, while the decay rates are considered to be first-order approximations. Component source and sink terms are calculated using biomass and component-dependent yield reaction terms for each microbial conversion as explained in detail in Section 2.4.1.

As already introduced in Section 2.1 for the microbial conversion of the coal, Barnhart et al. [2017] showed that 99.5 % of the coal energy content remained after the batch experiments. It is estimated from the CH_4 production and from coal energy content that 0.5 % of the coal is available for conversion by the microorganisms [Barnhart et al., 2017]. The microorganisms are assumed to consume the easily convertible components of the coal first and the yield coefficients are assumed to be similar to organic compounds with similar oxidation states under anaerobic conditions.

[‡]Section 2.4 is partially based on Section 2.2., Section 3, and Section 3.1. of Emmert, Class, Davis, and Gerlach [2020a] and reprinted with permission from © 2020 Elsevier Inc.

2.4.1 Energetics and bacterial growth[§]

In this section, the general energetics and kinetics of substrate utilization and bacterial growth are explained. According to McCarty [1972], equilibrium calculations are not sufficient to determine concentrations of substances in natural aquatic systems. Therefore, the dynamics of biological, chemical and physical processes must be considered. For each microbial process, three half-reactions as part of a redox-reaction pair, describing the process of interest, are considered, which generally represent an oxidation, reduction and biomass accumulation reaction, respectively. The half-reaction equations with their respective Gibbs free energy are taken from McCarty [1972]. One reaction system is explained in the following; all other reaction systems used in the model are given in the Appendix A. The half-reactions for a reaction system using coal, in which carbon has an approximate oxidation state of about zero (similar to carbon in glucose or acetate), normalized to the exchange of one e-, and their corresponding Gibbs free energy values (ΔG) in kJ/mol are:

$$\Delta\mathrm{G} = -41.924: \quad \frac{1}{24}\mathrm{C_6H_{12}O_6} + \frac{1}{4}\mathrm{H_2O} = \frac{1}{4}\mathrm{CO_2} + 1\mathrm{H^+} + 1\mathrm{e^-} \tag{2.8}$$

$$\Delta\mathrm{G} = 27.652: \quad \frac{1}{8}\mathrm{CO_2} + \frac{1}{8}\mathrm{HCO_3^-} + 1\mathrm{H^+} + 1\mathrm{e^-} = \frac{1}{8}\mathrm{CH_3COO^-} + \frac{3}{8}\mathrm{H_2O} \tag{2.9}$$

$$\Delta\mathrm{G} = 100.00: \quad \frac{1}{4}\mathrm{CO_2} + \frac{1}{20}\mathrm{NH_3} + 1\mathrm{H^+} + 1\mathrm{e^-} = \frac{1}{20}\mathrm{C_5H_7O_2N} + \frac{2}{5}\mathrm{H_2O} \tag{2.10}$$

These three equations are solved with three closing relations:

1. The sum of $\mathrm{e^-}$ has to be 0.
2. The sum of Gibbs free energy has to be 0 for the combined process.
3. Everything is normalized to one mole of substrate.

[§]Section 2.4.1 is taken from Section 3.1.3 of Emmert, Class, Davis, and Gerlach [2020a] and reprinted with permission from © 2020 Elsevier Inc.

The results are component-dependent yields as already described in Section 2.2.3. Solving the resulting system of three linear equations results in a biomass yield as well as a product yield for each reaction. These yields represent the energy balance for the reactions and provide the basis for the biogeochemical reactions.

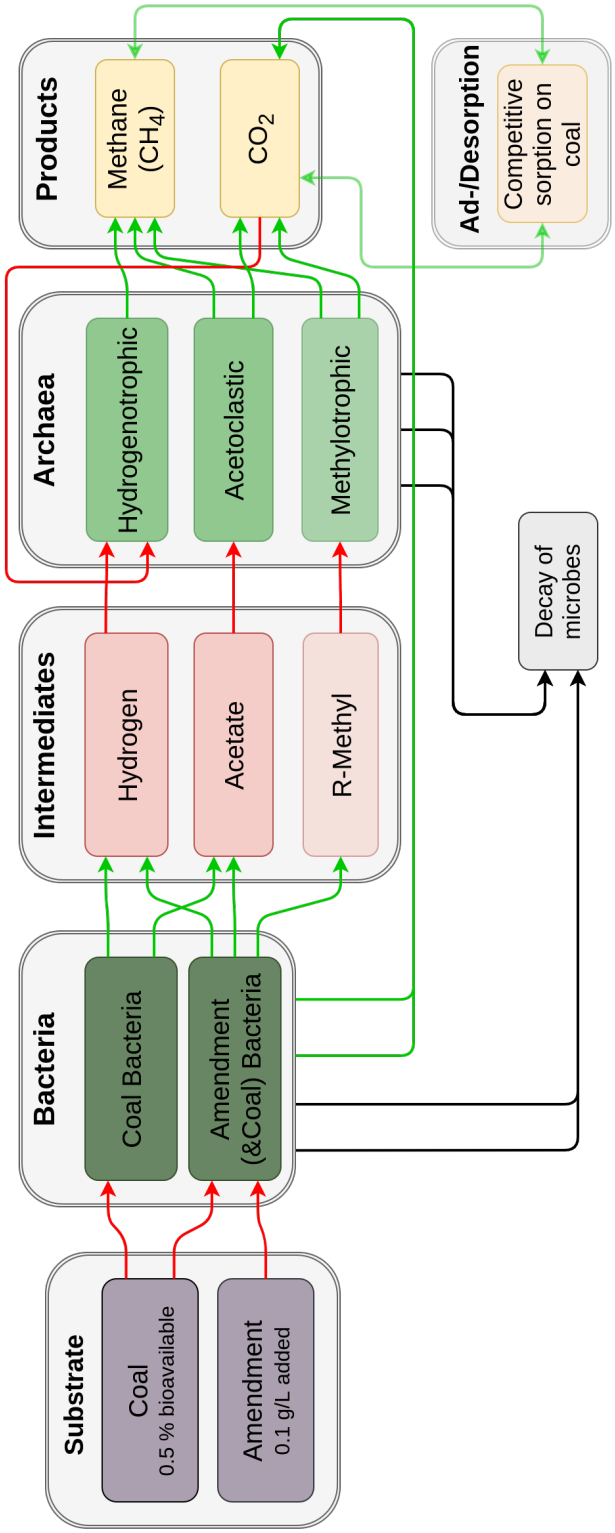

Figure 2.1: Schematic of the conceptual MECBM food web. The two substrates coal and amendment are considered for the two substrate-specific groups of bacteria which produce biomass, hydrogen, acetate and methyl groups. These intermediates are then assumed to be consumed by methanogenic archaea to produce biomass, methane and CO_2. Reprinted with permission from Emmert et al. [2020a], © 2020 Elsevier Inc.

3 Mathematical Model

This chapter provides an overview of the conceptual and mathematical model, used to represent the relevant processes involved in MECBM production. The idea of the conceptual model is already given in form of the flow chart in Figure 2.1 and explained in Section 2.4. We present a multiphase flow concept with bio-, and geochemical reactions within the porous medium. We assume the porous medium to consist of crushed coal grains, that make up a solid structure and are impermeable. Various microbial cells are possibly attached to the surface of this porous medium forming a biofilm and the remaining void space is occupied by up to two fluid phases. The wetting fluid phase is considered to be water, while the non-wetting fluid phase is assumed to consist primarily of methane. Substrates, intermediate, and end products are dissolved in the wetting phase and can also be present in the non-wetting phase, e.g. in the case of CO_2. More information on the basics of multiphase flow and corresponding modelling concepts can be found in Helmig et al. [1997] and Scheer et al. [2021].

3.1 Scale

Multiphase flow and transport as well as growth and decay of biomass can be described on various scales. The two relevant scales for the MECBM model are the micro and the macro or REV (representative elementary volume) scale [Bear, 2013, Helmig et al., 1997]. On the micro scale, we distinguish between grain structure, fluid phases, and e.g. biofilms, and we can resolve the individual features and interfaces. Resolving the micro scale details with imaging techniques and preparing it for a simulation results in many unknowns and expresses a high computational demand for the modelling framework [Blunt et al., 2013].

On the macro or REV scale, we average over the micro scale properties to obtain a REV that resembles the characteristics of the porous medium, as it is shown in Figure 3.1. Detailed information about pores are sacrificed and transferred into volume-averaged quantities, as e.g. porosity, permeability, and phase saturations. On this scale, it is assumed that Darcy's law is a valid simplification of the momentum balance equation. The definition of an REV is, that the characteristic quantities do not change when changing the size of the averaging volume [Bear, 2013, Helmig et al., 1997].

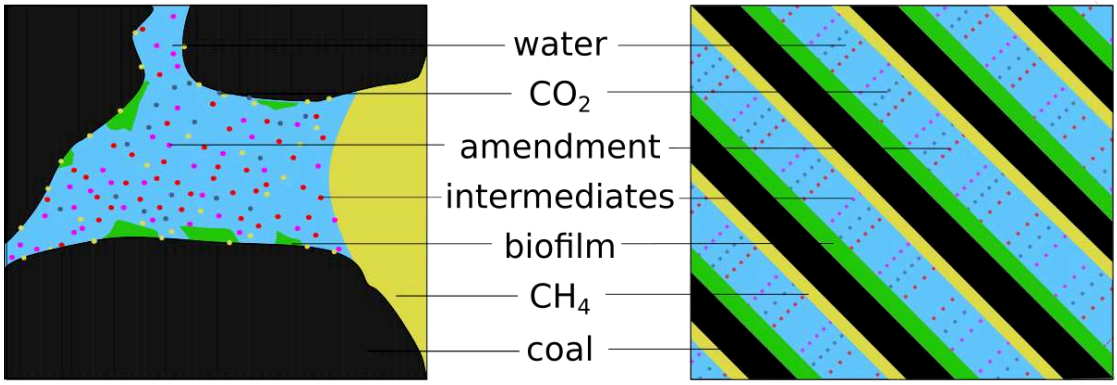

Figure 3.1: Schematic of the pore to REV scale representation used in the model concept. Scale/Amount not representative. Reprinted with permission from Emmert et al. [2020a], © 2020 Elsevier Inc.

3.2 Properties of porous media

While Rainer Helmig keeps postulating that "porous media are everywhere"* the question of how we define porous media has been discussed by many [Bear, 2013, Helmig et al., 1997]. In this chapter, the basic properties of porous media and how they are described in the context of this thesis is recapitulated.

*Prof. Dr.-Ing. Rainer Helmig, University of Stuttgart, Vernissage "Pretty Porous - Alles Porös" https://www.youtube.com/watch?v=CmeasmqiQDg Retrieved 2020-09-20

3.2.1 Porosity

The porosity ϕ on the REV scale is defined as:

$$\phi = \frac{V_{\text{pore}}}{V_{\text{total}}}, \quad 0 < \phi < 1, \tag{3.1}$$

where V_{pore} is the pore volume (or void volume) of the sample and V_{total} the entire volume of the REV. Mechanical deformation of the matrix is neglected, however biofilm growth, decay or consumption of coal can lead to a changing porosity for this study. Adapting the porosity when further solid phases (e.g. bioconvertible coal or biofilm) are present is done with:

$$\phi = \phi_0 - \sum \phi^{\varphi}, \tag{3.2}$$

where ϕ_0 is the initial porosity and ϕ^{φ} the volume fractions of the solid phases mentioned in Section 3.4.

3.2.2 Saturation

The pore space is filled by one or more fluid phases, which can be liquid or gaseous in our case. The amount of pore space filled by a fluid phase α is called S_α and defined as:

$$S_\alpha = \frac{V_\alpha}{V_{\text{pore}}}, \quad 0 < S_\alpha < 1, \quad \text{with } \sum_\alpha S_\alpha = 1. \tag{3.3}$$

If one phase replaces another phase in an REV, the remaining amount of the displaced phase is called residual saturation $S_{r\alpha}$.

3.2.3 Capillary pressure

We consider a system with two fluid phases in the pore space. This fluid-fluid interface is curved, as the wetting phase has a lower contact angle than the non-wetting phase. The common assumption of local thermodynamic equilibrium is assumed to be valid for low velocities according to Class et al. [2002]. The capillary pressure p_{c} is then defined as the pressure difference between two phases in equilibrium:

$$p_{\text{c}} = p_{\text{n}} - p_{\text{w}}. \tag{3.4}$$

On the micro-scale, p_c can be expressed by the Young-Laplace equation:

$$p_c = \frac{2\sigma \cos \alpha}{r}, \tag{3.5}$$

with σ as the surface tension between fluids, α the contact angle between wetting and solid phase, and r the radius of an idealized circular tube. On the REV scale, the micro-scale tubes concept of capillary pressure needs to be transferred to a relationship using REV quantities. This results in a relation between capillary pressure and saturation given e.g. by Brooks and Corey [1964], others would work equally well. Here p_c is calculated from the effective wetting-phase saturation S_e, the entry pressure p_e, and λ which is a parameter for the pore size distribution in this case:

$$p_c = p_e S_e^{-\frac{1}{\lambda}}, \tag{3.6}$$

where S_e is:

$$S_e = \frac{S_w - S_{rw}}{1 - S_{rw}}, \tag{3.7}$$

with S_{rw} as the residual wetting phase saturation that cannot be displaced by the other fluid phase.

3.2.4 Darcy's law

The flow of fluids within the porous medium is assumed to be creeping as described by Bear [2013], where the inertial forces are assumed to be much smaller than the viscous forces. The resulting momentum balance can be described by Darcy's law and allows solving for the filter, seepage or Darcy [Darcy, 1856] velocity $\boldsymbol{v}_\alpha$:

$$\boldsymbol{v}_\alpha = -\frac{k_{r\alpha}}{\mu_\alpha} \boldsymbol{K} \left(\nabla p_\alpha - \rho_\alpha \boldsymbol{g} \right), \tag{3.8}$$

for each phase α, with μ_α as the dynamic viscosity, p_α the fluid pressure, ρ_α the density, and $\boldsymbol{g}$ as the gravitational forces [Helmig et al., 1997]. The intrinsic permeability tensor $\boldsymbol{K}$ describes the friction coefficient of the porous medium and for multiphase systems the dimensionless relative permeability $k_{r\alpha}$ describes the additional resistance to the flow of one fluid phase due to the presence of another fluid phase.

Relative permeability When two or more phases are present on the micro scale, the resistance of flow is increased in comparison to a similar system with only one phase. This is described by $k_{r\alpha}$ on the REV scale. It scales the intrinsic permeability and is depending on the saturation for the wetting phase with

$$k_{\mathrm{rw}} = S_{\mathrm{e}}^{\frac{2+3\lambda}{\lambda}} \tag{3.9}$$

and the non-wetting phase with

$$k_{\mathrm{rn}} = (1 - S_{\mathrm{e}})^2 \left(1 - S_{\mathrm{e}}^{\frac{2+\lambda}{\lambda}}\right). \tag{3.10}$$

3.3 Phases and components

3.3.1 Phases

Relevant fluid phases in the context of MECBM are described as continua with distinct properties, e.g. density and viscosity. The phases are considered miscible, meaning that components from one phase can dissolve in the other phase. We consider a wetting phase consisting of primarily water, and a non-wetting phase which is primarily made up of CH_4. In addition to the fluid phases, we also consider up to seven solid phases. Namely, these solid phases are five different species of biofilm and the bioconvertible fraction of coal. The seventh solid phase is trapped or filtered amendment and is only used in two modelling scenarios.

3.3.2 Components

The fluid phases can consist of several components κ, that are distinct chemical species or groups of chemical species. The non-wetting fluid phase can consist of CH_4, CO_2 and H_2, the wetting fluid phase consists of brine (H_2O) and contains most of the dissolved components, which namely are amendment, acetate, hydrogen (H_2), methyl groups (CH_3), methane (CH_4), and carbon dioxide (CO_2).

For components with low concentrations that are solved in a phase that mostly consists of a main component, diffusive fluxes are described by Fick's law with binary diffusion

coefficients D_α^κ. For this multi-phasic system, so-called effective diffusion coefficients $D_{\alpha,e}^\kappa$, are used on the REV scale. These effective coefficients are calculated from the binary diffusion coefficient D_α^κ using the tortuosity τ, saturation and porosity after Bear [2013] to:

$$D_{\alpha,e}^\kappa = \tau S_\alpha \phi D_\alpha^\kappa. \tag{3.11}$$

We assume an ideal gas for the non-wetting phase except for the water and CO_2 components, where tabulated values are used [Wagner et al., 2000, Span and Wagner, 1996]. CO_2 is assumed to be present abundantly, thus carbonate alkalinity and pH can be assumed to be constant for the sake of simplicity in the model.

3.3.3 Mole fractions

The detailed composition of each phase is described by a mole fraction of the components, where each mole fraction x_α^κ is defined as:

$$x_\alpha^\kappa = \frac{n_\alpha^\kappa}{\sum_i n_\alpha^i}, \tag{3.12}$$

with n_α^κ as the number of moles of component κ in phase α.

When considering local thermodynamic equilibrium in a control volume, all components have an equal chemical activity and therefore, the phase composition can be derived from pressure, temperature and the following constraint on the sum of mole fractions in a phase:

$$\sum_\kappa x_\alpha^\kappa = 1, \tag{3.13}$$

after Class [2007].

The equilibrium mole fraction of component κ in the gas phase (n) is computed using Dalton's law under the assumption that the component vapour is in equilibrium with the liquid phase:

$$x_\mathrm{n}^\kappa = \frac{p_\mathrm{sat}^\kappa}{p_\mathrm{n}}, \tag{3.14}$$

with p_sat^κ as the component saturation vapour pressure.

Similarly, the mole fraction of component κ in the liquid phase (w) is calculated using Henry's law:

$$x_{\mathrm{w}}^{\kappa} = \frac{p_{\mathrm{n}}^{\kappa}}{H_{\mathrm{w}}^{\kappa}}, \tag{3.15}$$

where the component partial pressure p_{n}^{κ} is calculated using the mole fraction and the phase pressure: $p_{\mathrm{n}}^{\kappa} = x_{\mathrm{n}}^{\kappa} p_{\mathrm{n}}$, and the Henry coefficient for the dissolution of the component in water H_{w}^{κ}.

3.4 Balance equations

This section presents the balance equations that are used in this thesis. Where applicable, the generalization of the multiphase Darcy's law, described in Section 3.2.4, can be directly inserted into all mass balance equations. We will discuss mass balance equations for all components in the two phases as well as mass balance equations for all solid phases.

3.4.1 Mass balance equations for components in two-phase flow

The mass balance of a component κ for a two-phase flow system, can be written as

$$\sum_{\alpha} \left[\frac{\partial}{\partial t} \left(\phi \rho_{\mathrm{mol},\alpha} x_{\alpha}^{\kappa} S_{\alpha} \right) + \nabla \cdot \left(\rho_{\mathrm{mol},\alpha} x_{\alpha}^{\kappa} \mathbf{v}_{\alpha} \right) - \nabla \cdot \left(\rho_{\mathrm{mol},\alpha} \mathbf{D}_{\mathrm{pm},\alpha}^{\kappa} \nabla x_{\alpha}^{\kappa} \right) \right] = q^{\kappa} \quad \alpha \in \{\mathrm{n}; \mathrm{w}\}. \tag{3.16}$$

Here, t is time, ϕ porosity, $\rho_{\mathrm{mol},\alpha}$, S_{α}, and $\mathbf{v}_{\alpha}$ the molar density, saturation and the velocity of phase α respectively, x_{α}^{κ} the mole fraction of component κ and $\mathbf{D}_{\mathrm{pm},\alpha}^{\kappa}$ is the diffusion tensor in phase α. Sources and sinks due to biogeochemical reactions or external sources and sinks for component κ are captured by q^{κ}.
For the numerical case study with attaching and detaching microbial cells, the transported cells are handled as additional inactive tracer-like components and thereby transported with the Darcy velocity (see Eq. (3.8)).

3.4.2 Mass balance equations for solid phases

Conservation equations for biofilms, coal, and attached inactive amendment are considered to be rigid and are each consisting of a single component. Therefore, their mass balance consists only of a storage and a source term:

$$\frac{\partial}{\partial t}\left(\phi^{\varphi}\rho^{\varphi}\right) = q^{\varphi}, \quad \varphi \in \{\mathrm{Cc}; \mathrm{cb}; \mathrm{ab}; \mathrm{aa}; \mathrm{ha}; \mathrm{ma}; \mathrm{sa}\} \tag{3.17}$$

with φ indicating whether the convertible fraction of coal (Cc), the five biofilm components (cb, ab, aa, ha, ma) or solid amendment (sa) is used. Here, ϕ^{φ} is the volume fraction, ρ^{φ} mass density and q^{φ} is the source term due to biogeochemical reactions, growth, decay or attachment/detachment of the solid phase φ. Component source and sink terms are calculated using biomass and component-dependent yield reaction terms for each microbial conversion (see Section 2.4.1). The porosity and permeability of the system change depending on consumption of coal as well as on growth, decay, attachment, and detachment of microbial cells.

3.5 Attachment and detachment due to flow

Cell attachment and detachment might occur under flow conditions. In the same way, particles that are transported with the flow could be trapped, filtered and thereby retarded in the porous medium.

3.5.1 Retardation and filtration†

Modelling retardation and filtration processes in porous media can be considered on the micro or macro scale. Good overviews of deep-bed filtration and the corresponding mechanisms are given in Jegatheesan and Vigneswaran [2005], Rockhold et al. [2004], Molnar et al. [2015]. Since the model in this study is based on the REV concept, we will focus on the macro-scale description of retardation and filtration processes. Many numerical studies have been performed with respect to filtration processes and there are

†Section 3.5.1 is taken from Section 2.4.1 of Emmert, Davis, Gerlach, and Class [2020b] and reprinted with permission, published by CC BY 4.0 MDPI 2020.

different approaches and equations with different levels of complexity available. Since this study is a first step towards a more realistic description of the MECBM process and many different processes are of potential importance, we focus on a very basic description of filtration that is coherent in most filtration concepts.
We describe the particle retention rate of a particle κ as a rate r^κ added to the source term q^κ (see Eq. (3.16)) in Eq. (3.18):

$$r^\kappa = \lambda^\kappa_{attach} C^\kappa_w v_w, \tag{3.18}$$

where λ^κ_{attach} is the attachment or filtration coefficient of component κ, C^κ_w is the concentration of a component in the aqueous phase, which is calculated from $C^\kappa_w = x^\kappa_w \rho_{mol,w} M^\kappa$, and v_w is the aqueous phase velocity. λ^κ_{attach} is usually dependent on the structure of the porous medium, the flow properties and interactions between the particles. Many models, ranging from basic [Iwasaki et al., 1937, Tien et al., 1979] to more advanced [Liu et al., 1996] have been proposed; however, we use a simple form of Eq. (3.18) and do not account for more complex calculations of λ^κ_{attach} for now. The process of attachment or detachment is modelled by adding the rate r^κ to the equivalent solid source term q^φ which corresponds to κ. Thus, every component κ has an equivalent solid part φ.
Since we assume that the particles are not only attaching to the porous medium but can also be resuspended and transported with the mobile phases again, the process we model is rather a mixture between filtration and partitioning or retardation [Molnar et al., 2015].
In general, we assume that detachment is proportional to the shear stress. Shear stress is actually not represented in our macro-scale (REV-scale) model concept. Thus, it has to be considered on the macro-scale by an effective process that upscales the micro-scale effects. We use here the aqueous-phase potential gradient following Rittman's general model [Rittman, 1982] of biofilm shearing with Speitel Jr and DiGiano [1987]. Rittman model and parameters could be improved through further knowledge about the type of biofilm, however this is beyond the scope of this study, which is why we keep the variable parameters for fitting at a minimum and stay with this approach in Eq. (3.19):

$$r^\varphi = k^\varphi_{\text{detach}} \phi^\varphi \rho^\varphi \tag{3.19}$$

where we describe the rate of detachment r^{φ} of solid φ mainly with a detachment coefficient for this solid $k^{\varphi}_{\text{detach}}$. For the amendment, this detachment coefficient $k^{\varphi}_{\text{detach}}$ is defined in Eq. (3.20):

$$k^{\varphi}_{\text{detach}} = \lambda^{\varphi}_{\text{detach}} \left(\phi S_{\text{w}} \left|\nabla p_{\text{w}} - \rho_{\text{w}} \mathbf{g}\right|\right)^{0.58}. \tag{3.20}$$

Here, $\lambda^{\varphi}_{\text{detach}}$ is the detachment or resuspension coefficient of solid component φ due to shear stress.

3.5.2 Cell attachment and detachment[‡]

Cell attachment in porous media is a different process than retardation or filtration of amendments. However, the mechanistic description is similar in the way the equations are used in the model. Therefore, when modelling cell attachment, we also use Eq. (3.18) with a different $\lambda^{\kappa}_{attach}$ than for the amendment, as the cell attachment mechanisms of suspended cells κ might be different depending on the type of cell. However, we do not have further experimental information on the cell types and model all microbial cells with the same estimated and calibrated $\lambda^{\kappa}_{attach}$.
For cell detachment, we also use Eq. (3.19), but calculate the detachment coefficient with an extended relation derived from Ebigbo et al. [2010]:

$$k^{\varphi}_{\text{detach}} = \lambda^{\varphi}_{detach} \left(\phi S_{w} \left|\nabla p_{w} - \rho_{w} \mathbf{g}\right|\right)^{0.58} + \frac{\phi^{\varphi}}{\phi} \mu^{\varphi}_{\text{g}}, \tag{3.21}$$

where the volume fraction of the respective biofilm ϕ^{φ} is set in relation to the porosity ϕ and the growth rate μ^{φ}_{g} of the biofilm φ in addition to detachment as defined in Eq. (3.20).

[‡]Section 3.5.2 is taken from Section 2.4.2 of Emmert, Davis, Gerlach, and Class [2020b] and reprinted with permission, published by CC BY 4.0 MDPI 2020.

3.6 Numerical model and solution strategies

The numerical model explained in the previous sections with its mass transport and reaction system needs to be discretized and solved. The employed numerical schemes for space and time discretization are briefly presented in this section. The model itself is implemented in the numerical software framework DuMu^{x} [Flemisch et al., 2011, Koch et al., 2020], which is an open-source simulator for flow and transport processes in porous media. DuMu^{x} has its focus on multi-phase and multi-component flow systems as well as on model coupling of potentially different physical domains. It is based on DUNE [Bastian et al., 2008b,a, 2020], which provides easy access to changing grids, linear algebra abstractions, solvers, and parallel computing. The system is using a cell-centred finite volume approach with the two-point flux approximation for discretization in space. The scheme is consistent for so-called K-orthogonal grids, which is always the case in this study. An implicit backward Euler method is used as time discretization for the batch and column scenarios presented in Chapters 5 and 6. All equations are solved in a monolithic, fully-coupled and fully-implicit way.

Many reactive-transport models do not use a fully-implicit approach, but use so-called operator-splitting methods to sequentially solve different parts of the equations. It is beyond the scope of this thesis to provide an in-depth review of current reactive transport modelling. However, e.g. Steefel et al. [2015] present a good review on the past and current development of reactive transport modelling research topics and software frameworks. More general discussions on the principles of reactive transport modelling are explained e.g. in Kirkner and Reeves [1988] and Lichtner [1996]. Only for the numerical investigation regarding decoupling processes, we briefly investigate operator-splitting methods in the context of other discretization schemes. The differences between them are explained below.

3.6.1 Fully implicit approach

The conservation equations for the model are solved using a fully-implicit method, meaning we use a so-called global implicit approach (GIA) to solve e.g. mass transport and chemistry in one step, with the help of Newton's method as linearization technique and the construction of a Jacobian matrix. For time discretization we are using an

implicit backward Euler scheme. GIA is mass conservative and does not need any iterative procedures, as all interactions are described by a single set of equations. A major drawback of GIA is that all unknowns are approximated in a single step, creating large coupled system that are computationally expensive to solve. Additionally, chemical reactions typically introduce further non-linearities, which increase the degree of non-linearity. Therefore, GIA is typically assumed to be less efficient than e.g. decoupled schemes when modelling systems with multiple phases and components that are not strongly interacting.

3.6.2 Operator splitting approaches

A computationally decoupled formulation is different from the previously described GIA approach in the way the equations are set up and solved. For an operator splitting (OS) approach, the system of equations is usually split into different parts. This can be a transport part for all fluid phases and a reaction part for all phases. We can define an operator notation for the transport and reaction part of a given set of components with concentrations C used for simplicity as follows:

$$\begin{aligned} \frac{\partial C(t)}{\partial t} &= \mathcal{L}(C(t)) + \mathcal{R}(C(t)), \\ \text{with } t \in [0,T], \quad C(0) &= C_0, \end{aligned} \tag{3.22}$$

with $\mathcal{L}$ being the spatial operator representing the advection and diffusion part, and $\mathcal{R}$ representing all chemical reactions from Equation (3.16). So far, Equation (3.22) is representing the same component balance as Equation (3.16). The spatial and reaction operator were introduced to split the calculation. Additionally, the transport part can be split into a phase composition and phase transport part.
The simplest OS approach without iterations is the sequential non-iterative approach (SNIA), which for one timestep consists of a transport step followed by a reaction step, using the transported concentrations.

First-order splitting

When considering Equation (3.22) with first-order splitting (also named Lie-Trotter splitting), the transport problem is solved on the time subintervals $[t^n, t^{n+1}]$, where $n = 0, 1, ...N-1$, $t^0 = 0$ and $t^N = T$. Now the algorithm is:

$$\frac{\partial c_t(t)}{\partial t} = \mathcal{L}(c_t(t)), \quad \text{with } t \in [t^n, t^{n+1}] \quad \text{and } c_t(t^n) = c_t^n, \tag{3.23}$$

where the initial condition is $c_t^n = C_0$. With the solution of the transport part, the reaction operator follows with:

$$\frac{\partial c_r(t)}{\partial t} = \mathcal{R}(c_r(t)), \quad \text{with } t \in [t^n, t^{n+1}] \quad \text{and } c_r(t^n) = c_t(t^{n+1}), \tag{3.24}$$

and the approximate split solution at time $t = t^{n+1}$ is then defined as $c_t^{n+1} = c_r(t^{n+1})$.

Strang splitting

Another SNIA approach is the Strang splitting after Strang [1968], which is reported to be a second-order accurate splitting algorithm. It is performed by first solving a half-step of the transport problem with the timestep $\Delta t/2$ as:

$$\frac{\partial c_t^*(t)}{\partial t} = \mathcal{L}(c_t(t)), \quad \text{with } t \in [t^n, t^{n+1/2}] \quad \text{and } c_t(t^n) = c_t^n, \tag{3.25}$$

which is then followed by a full reaction step with Δt:

$$\frac{\partial c_r(t)}{\partial t} = \mathcal{R}(c_r(t)), \quad \text{with } t \in [t^n, t^{n+1}] \quad \text{and } c_r(t^n) = c_t(t^{n+1/2}), \tag{3.26}$$

and followed by another transport half-step with

$$\frac{\partial c_t(t)}{\partial t} = \mathcal{L}(c_t(t)), \quad \text{with } t \in [t^{n+1/2}, t^{n+1}] \quad \text{and } c_t(t^{n+1/2}) = c_r(t^{n+1}), \tag{3.27}$$

where $t^{n+1/2} = t + 0.5\Delta t$ and the approximate split solution at time $t = t^{n+1}$ is then defined as $c_t^{n+1} = c_t(t^{n+1})$.

Sequential iterative approach

A common approach to reduce the splitting error introduced by the decoupling of component transport and chemical reactions is the sequential iterative approach (SIA). The two models for the operators as described in Equation (3.22) are iterated and coupled via source/sink terms, updating each iterative cycle [Hundsdorfer and Verwer, 1995]. The iteration is performed until a convergence criterion is reached. However, the iterative procedure is not unconditionally stable, due to the explicit coupling. This can lead to convergence issues, which are commonly overcome or inhibited by small splitting timesteps as described in Fahs et al. [2008]. While a study by Wang [2019] showed that standard SIA is not applicable for a MECBM model, others [Carrayrou et al., 2004] conclude that a standard SIA scheme should not be used for such systems, as it can lead to convergence and stability issues while OS errors are not completely removed. Therefore, Carrayrou et al. [2004] introduce new symmetric approaches for SIA that show better convergence rates, which are not further investigated here.

3.6.3 Damköhler numbers and characteristic timescales

Modelling decoupled transport and reactions is prone to introduce OS errors, that are attributed to the different spatial and temporal scales of the transport and the reaction processes. For this study, the spatial discretization is chosen with a very high spatial discretization of 80 cells over the height of the column for all investigations. Therefore, only the temporal scales of transport and reaction are investigated in terms of OS error in the following.
To describe the relation of chemical reactions versus transport, the Damköhler numbers are introduced. First-order Damköhler numbers describe the relation of the reaction rate to the advective mass-transport rate by:

$$Da = \frac{\text{reaction rate}}{\text{mass-transport rate}}. \tag{3.28}$$

Depending on the nature of the system, advective or diffusive Damköhler numbers can be calculated according to Bahr and Rubin [1987], that either depend on the characteristic advective or diffusive timescales in relation to the reaction timescales. The

resulting Damköhler numbers are always dependent on the definition of the corresponding time and length scales. For this study, the characteristic length scale l can either be assumed to be grid dependent and defined as the mesh size or as the distance covered by component transport over one timestep: $l = v\Delta t$. Since we can not refine our mesh any further, the latter approach is used. The characteristic advective timescale t_a is defined as

$$t_a = \frac{l}{v}, \tag{3.29}$$

where v is the velocity, which corresponds to the wetting-phase velocity for this case, as most components are transported in the wetting phase.
Since Damköhler numbers are only investigated for the column scenario, which is assumed to be primarily advection-driven, the diffusive timescale is not evaluated for now. The characteristic reactions' timescale t_r is defined as

$$t_r = \frac{1}{\bar{c}^\kappa}, \tag{3.30}$$

with $\bar{c}^\kappa$ as the effective rate of chemical reaction of species κ. With these, the Damköhler number used for transport in this thesis is now defined after Eq. (3.28) as

$$Da = \frac{t_a}{t_r} = \frac{l\bar{c}^\kappa}{v}. \tag{3.31}$$

Eq. (3.31) can now be used to evaluate if the reactions or the transport are dominating. However, the exact determination of the Damköhler numbers is often not straightforward. For an application, as the column setup, the reactions are often time and space dependent, which leads to different Damköhler numbers along the column. Additionally, each component reaction might have its own Damköhler number which varies over time. Many literature studies evaluate the maximum Damköhler number occurring over the entire model region and all reactions [Carrayrou et al., 2004, Hron, 2015, Steefel et al., 2015]. For this study, the Damköhler numbers are only investigated per component as a post-processing step and could be implemented e.g. as a time-stepping criterion for future work.

4 Experiments at MSU Bozeman*

Multiple experimental studies have been performed regarding the stimulation of coal-to-methane conversion, the microbial community of coal-beds, as well as the effect of different types and concentrations of added amendments [Barnhart et al., 2017, Davis et al., 2018a,b]. These studies show that amendments are able to stimulate coal-dependent methane production [Barnhart et al., 2017] and that different microbial communities in coal-beds might have an influence on methane production, while coal treatments for enhancing the coal's bio-availability can also have an effect [Davis and Gerlach, 2018]. The latest studies by Davis et al. [2018a,b] show that organic amendments increase the biogenic conversion of coal to methane. However, the increase is not proportional to the amendment concentrations [Davis et al., 2018a,b]. Adding small amounts of amendments increases the rate of biogenic methane production while also increasing to some extent the total amount of produced methane.
The experimental studies leading to this modelling thesis, were performed at Montana State University in Bozeman, MT, USA. All experimental studies focus on the production of methane from coal and amendments, and use the same coal and inoculum of previously enriched Flowers-Goodale coal-bed microbial consortium [Barnhart et al., 2016]. This ensures that an easy transfer of parameters and gained knowledge from one study to another is possible.

4.1 Batch experiments

All batch experiments were set up in 26 ml Balch tubes and received either 1 g of ground coal or glass beads and 10 mL total liquid volume. The inoculum consisted of

*Chapter 4, and Section 4.1 are based on Sections 2. and 2.1 of Emmert, Class, Davis, and Gerlach [2020a] and reprinted with permission from .

1 mL of a previously enriched Flowers-Goodale coal-bed microbial consortium [Barnhart et al., 2016]. These inoculated systems possible amendment, as additional substrate, was added on possibly three different times during the study. Amendment additions occurred on Day 0, 76 and 117 for this study. The amendment, a Chlorella microalgae species, was added in form of a 1 mL suspension resulting in a 0.1 g/L amendment concentration in the Balch tubes. The Balch tubes were sealed, mixed regularly and the gas was sampled approx. every 2 weeks. The experimental results of are given in Davis et al. [2018a] and are used for comparison with the respective numerical results in Chapter 5.

4.2 Column experiments[†]

The column studies are based on Davis et al. [2019] and the same ratio of coal to amendment, as for the batch studies, was used. The inoculum again consisted of a previously enriched Flowers-Goodale coal-bed microbial consortium [Barnhart et al., 2016]. Davis et al. [2019] investigated methane production under continuous-flow conditions in four column reactors. All columns were packed with coal initially and inoculated with microbial consortia prepared equivalently to the batch experimental studies by Davis et al. [2018a] and numerical studies by Emmert et al. [2020a]. In the following, a "+" stands for amendment addition and a "−" for no amendment addition at Day 0 or Day 61. "Coal" indicates that the column was operated with coal as porous medium, where we assume 0.5% of the carbon in the coal to be available for bioconversion to methane [Emmert et al., 2020a]. Two reactors (Coal^{++} and Coal^{+-}) were amended initially with algal biomass, while the other reactors remained unamended. Out of those two, only Coal^{++} was amended again on Day 61. The reactors with amendment additions on Day 0 produced methane continuously at a similar rate, regardless of whether they were amended a second time or not. Two other reactors (Coal^{-+} and Coal^{--}) did not receive amendment on Day 0, but Coal^{-+} received an amendment addition on Day 61. The unamended reactor (Coal^{--}) never produced gas, while the reactor that was only amended on Day 61 (Coal^{-+}) showed delayed and little methane production over the duration of the experiment. The latter two reactors will not be investigated in this

[†]Section 4.2 is based on Section 2.2 from Emmert, Davis, Gerlach, and Class [2020b], published by CC BY 4.0 MDPI 2020..

thesis as the available data are too sparse to improve the model in a meaningful way at this point.
With these experimental results, and taking into account ^{13}C gas analysis, Davis et al. [2019] conclude that methane generation in the column is primarily from coal-to-gas conversion with minimal contributions to gas production from amendment-to-gas conversion. This leads to two primary hypotheses being investigated using the developed numerical model.

- Hypothesis 1 states that not all amendment is transported into or through the column but might have been trapped in the inlet region of the column during the injection. This could lead to the second amendment addition effectively not reaching the column at all, and thereby explaining the almost identical behaviour of reactors $Coal^{++}$ and $Coal^{+-}$.
- Hypothesis 2 states that with flow and transport occurring in the column, microbial cells need to attach to the coal surface and grow. This process is slower than in the batch experiments reported in Davis et al. [2018a] and Emmert et al. [2020a].

5 Batch calibration and validation*

The experimental results from Davis et al. [2018a] are compared against the numerical model here, as already described in Section 4.1. Since we model a batch system, the goal is to calibrate and validate the conceptual model (see Figure 2.1) and the reaction system as explained in Section 2.2.3. The detailed equations and all their parameters are given in Tables in Appendix A. Flow and transport are included in the equations as described in Chapter 3, but are not needed for this setup.

5.1 Results

A numerical calibration of the reaction system is performed at first in Section 5.1.1. The model with fitted reaction system is then put to a test and a validation is achieved in Section 5.1.2. The results show that the calibration and validation of the model are performed successfully by applying the fundamentals explained in Chapters 2 and 3.

5.1.1 Calibration

The calibration uses methane production data from two series of batch experiments [Davis et al., 2018a,b]; other batch results serve as data for the subsequent validation of the calibrated model in Section 5.1.2. The amendment-dependent parameters are calibrated from a setup with glass beads, formation water and three amendment additions over time (red in Figure 5.1). Then, the coal-dependent parameters are calibrated independently of another setup with only coal and formation water (black in Figure 5.1).

*Chapter 5 is based on Sections 5, 6, and 7 from Emmert, Class, Davis, and Gerlach [2020a] and reprinted with permission from

Calibrated parameters are the yield coefficients of each microbial species, as well as the growth rates of the microbes. When fitting the parameters, it is important to understand that most parameters listed in Tables B.3, B.4, B.5, B.6 are either pre-calculated using the yield reactions described in Section 2.4.1 or based on literature values. Some parameters are chosen as being fixed, while others, e.g. the growth rates of the microbes, with a higher uncertainty were included as variables in the calibration. The parameters as well as their theoretical ranges are listed in Tables B.3, B.4, B.5, B.6. The calibration itself is performed with the help of PEST (Model-Independent Parameter Estimation and Uncertainty Analysis) [Doherty, 2015].
It is important to note that certain parameters are correlated. This issue is addressed by strictly evaluating parameter values, and if a calibration result shows to be at the maximum or minimum range of one parameter, we investigate this behaviour separately and reevaluate the model fit again. With this approach we try to achieve a reasonable model fit, as judged by a Mean Absolute Error (MAE), while being aware that the correlations between the parameters might be addressed more thoroughly through improved knowledge regarding the processes involved.

The metrics chosen here to assess the overall match of the simulation results to the experimental data is the Mean Absolute Error. It is the average magnitude of the errors when the absolute differences between the experimental and simulation results are used and have equal weight. The advantage over the commonly used Root Mean Square Error (RMSE) is that the interpretation of the MAE is straightforward, as it describes the average error only and that it allows for varying test sample sizes, whereas the RMSE varies with the variability within the distribution of error magnitudes, with the square root of the number of errors, as well as the magnitude of the average-error (MAE) [J. Willmott and Matsuura, 2005]. The calibration itself is performed using both the RMSE and the MAE, as J. Willmott and Matsuura [2005], Chai and Draxler [2014] state a combination of both metrics is beneficial to assess model performance.

The calibration results are compared to the experimental data in Figure 5.1. All other model predictions are compared to the experimental results in Figures 5.2, 5.3 and 5.4. ExpGB^{+++} marks the experimental results of a glass bead case (GB) with amendment additions on day 0, 76 and 117, while e.g. DuMu^{x} coal^{---} stands for a simulation run that contains coal but does not receive amendments over time ($^{---}$) at any of the three possible addition times. In general, a "+" indicates an amendment addition, whereas a "−" indicates no amendment addition at the three possible addition times.

This naming scheme is adapted from Davis et al. [2018a], where also an overview of amendment additions and samples is given in Figure 1 [Davis et al., 2018a].

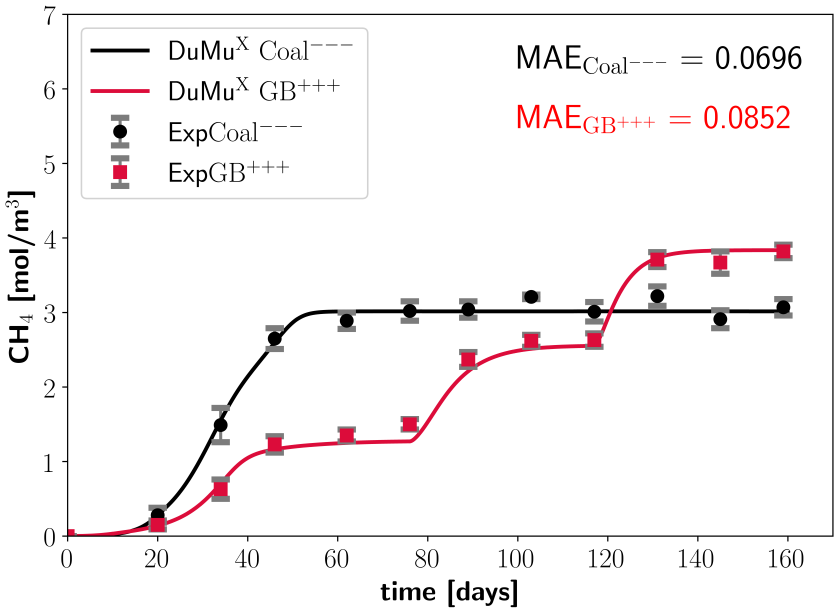

Figure 5.1: Calibration of simulation model to glass beads and coal scenarios. The plots show methane concentration of the experimental batch systems compared to the simulation results (DuMu^{x}) over time. It shows the two data-sets used for calibration: One system with only coal and no amendment (coal^{---}) added over time and the other set with glass beads and three amendment additions (GB^{+++}). Reprinted with permission from Emmert et al. [2020a], © 2020 Elsevier Inc.

The calibration of the model to the experimental data yields a MAE of 0.0852 mol/m^3 for the GB^{+++} case with a maximum methane concentration of 3.84 mol/m^3 (see Figure 5.2). The coal^{---} case shows a slightly lower MAE of 0.0696 mol/m^3 with a maximum methane concentration of 3.01 mol/m^3 (see Figure 5.3). Compared to the standard deviations from the experiment of 0.125 mol/m^3 for coal^{---} and 0.0944 mol/m^3 for GB^{+++} the MAEs for both cases are considered low as they smaller than the corresponding experimental standard deviations. These results also correspond to an averaged relative error of 2.22 % or 2.31 % respectively for the calibration, when comparing the MAE to the maximum methane concentration. Given such low errors, in comparison to the experimental standard deviations, we consider the calibration of the model successful.

5.1.2 Validation

Figure 5.2 shows the comparison for the glass beads with different amendment addition strategies. The increase after the amendment additions is captured well, as the experimental data as well as the simulation data coincide. However, the simulation appears to underestimate the methane concentration towards the end of the experiments. The MAE is slightly higher at 0.141 mol/m^3 for the GB^{++-} case, and 0.212 mol/m^3 for GB^{+--}, compared with an experimental standard deviation of 0.0868 mol/m^3. Given a total production of only 1.28 mol/m^3 for GB^{+--}, an MAE of 0.212 mol/m^3 is considered large and on the brink of being acceptable (16.58 % relative error), while the standard deviation in the experiments was only 0.078 mol/m^3.
These larger MAEs seem to be the result of an underprediction of methane production in the simulations, which can be attributed to additional methane production in the experiments associated with the inoculum addition. Small amounts of methane (up to 0.68 mol/m^3) appear to be generated in GB^{---} experiments as shown in Davis et al. [2018a], Figure 2(b).; Davis et al. demonstrate that the inoculum itself potentially adds small amounts of organic compounds in the form of soluble organics or biomass, which can ultimately be converted into methane. For most scenarios, this additional amount of methane is small but in the glass bead only or only one-time amended glass bead systems (e.g. in GB^{+--}) it appears to have a large enough influence to decrease the model fit resulting in fairly large MAEs. Regarding the GB^{++-} case, it is evident that the results match quite well visually. Here, the largest variation is seen in the experimental data between day 125 and the end. Such fluctuations in the experimental data are not captured by the model. The MAE is 0.141 mol/m^3 with a total production of 2.56 mol/m^3, which yields a relative error of 5.51 %; again, there is slightly higher methane production observed in the experiments than predicted by the model, possibly due to the discussed introduction (carryover) of organic material with the inoculum as discussed in Davis et al. [2018a].

Figure 5.3 shows the coal cases with late amendment additions. The MAE of the initial coal fit is 0.0696 mol/m^3 and remains small at only 0.125 mol/m^3 and 0.161 mol/m^3 respectively for the combined cases of coal and amendment treatments (coal^{-+-} and coal^{-++}). Standard deviations of the experimental results are 0.149 mol/m^3 for both cases. Comparing these with the MAE as well as the relative averaged errors over time, the results show very good agreement. Coal^{-+-} has an error of 2.91 % for a maximum

production of 4.29 mol/m^3 and coal^{-++} of 2.89 % with 5.57 mol/m^3 maximum production. Given that the combined process (amendment-stimulated conversion of coal to methane) was not used for calibration, the model reproduces the outcome of the combined process very well.

Figure 5.4 shows the coal cases with initial amendment additions. Here, the mismatch between the experimental results and the simulation is obvious and the MAE is significantly higher than in the previously shown results. This is mainly caused by an initial underestimation and an overestimation of the methane concentration at early times (between Day 0 and Day 50) in the simulation compared to the experimental results. The coal^{+--} case still produces significant amounts of methane and matches the maximum production with 4.29 mol/m^3 to the experimental results. However, the initial deviation compared to the experiments leads to an overall MAE of 0.173 mol/m^3 which is still below the standard deviation of the experiments with 0.304 mol/m^3. Nevertheless, coal^{++-} and coal^{+++} show the conceptually expected increase of methane, while the experimental results show some spreading. On Day 136, the experimental coal^{++-} system exhibits higher methane concentrations than the experimental system with an additional amendment addition (coal^{+++}). As in Figure 5.3, the increase in methane production, after the 2nd and 3rd amendment addition is calculated by the model to be faster than the experimental results indicate. Here, the combined process is slightly overestimating the methane production. However, the overall output of the model is still very close to the experiments. Even with the non-intuitive results after Day 136 discussed above, the model still has MAEs in the range of the averaged standard deviations of the experiments with an MAE of 0.315 mol/m^3 compared to an averaged standard deviation of 0.416 mol/m^3 for coal^{++-}, as well as 0.317 mol/m^3 compared to 0.427 mol/m^3 for the coal^{+++} case. The maximum observed methane productions are 4.29 mol/m^3, 5.57 mol/m^3 and 6.85 mol/m^3 with relative errors of 4.03 %, 5.65 % and 4.63 % for coal^{+--}, coal^{++-}, and coal^{+++} respectively.

Comparing the output of the model to the experimental data, the combined setups (Figure 5.3 and 5.4) can serve as a validation case for our model. If the assumptions regarding the food web hold true, both the individual and the combined test setups should produce results which are within the range of the experimental error. This behaviour is indeed observed for 8 out of 9 data sets, however a systematic difference is observed for the setups with glass beads and amendment only. While the distinct increases, and therefore the main features are captured, the predicted max. amount of

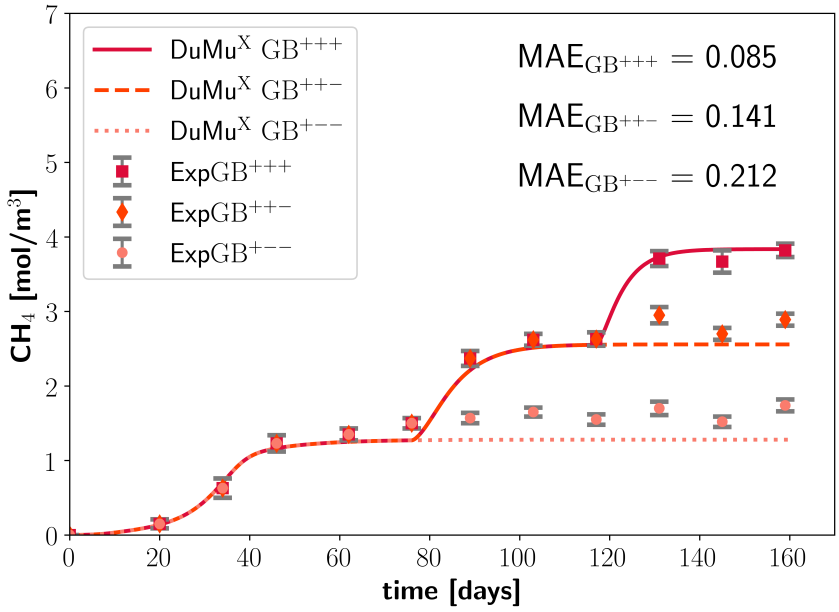

Figure 5.2: Glass beads plus amendment comparison. The plot compares the calibrated model against the experimental results for a system with glass beads and up to three different amendment additions. Reprinted with permission from Emmert et al. [2020a], © 2020 Elsevier Inc.

methane produced in all glass bead setups is lower than observed in the experiments (see Figure 5.2). This behaviour can potentially be attributed to organic carbon available for conversion to methane in the inoculum as shown in Davis et al. [2018a], Figure 2(b). Therein, Davis et al. suggest: "It is unlikely that all of this carbon was converted to CH_4 or IC [inorganic carbon], but it cannot be completely ruled out as a potential carbon source for methane or IC production" [Davis et al., 2018a]. As discussed above the effect of the inoculum as an additional process is not implemented. This was not done here since inoculum was added to all treatments that produced methane and it had not been clear at the time of model conception that methane production from the inoculum was going to occur.

Incomplete mixing resulting in diffusion-controlled conversion of organics to methane as a possible reason for this slow continued methane production is unlikely as the Balch tubes were shaken regularly. With at least parts of the continued methane production being clearly attributed to the inoculum [Davis et al., 2018a], implementation of diffusion-limited processes into the model was not pursued here since it would have introduced additional complexity into the model, which was not experimentally justified.

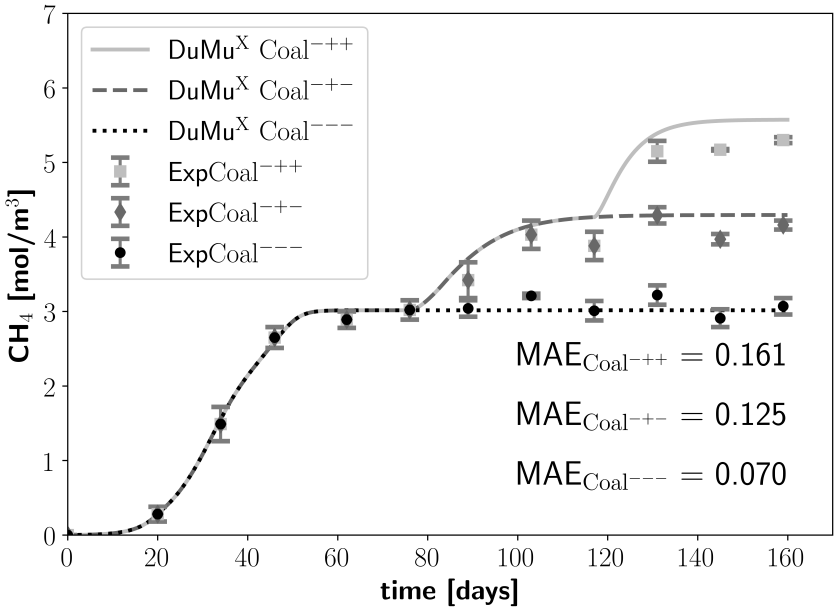

Figure 5.3: Comparison between model and experiment: initially only coal with amendment additions starting from Day 76. Reprinted with permission from Emmert et al. [2020a], © 2020 Elsevier Inc.

The setups initially with coal only and amendment additions after Day 76 (Figure 5.3) show very good agreement, with MAEs almost identical to the calibrated glass-beads fit. The second and third increases due to amendment additions level out at the experimentally observed methane concentrations; however the maximum methane concentration is reached slightly earlier in the simulation compared to the experiments. This is not too surprising since the processes are calibrated separately and are independent of each other as long as enough substrate is available. The effect where different microbes might compete for the same substrate is only observed when most of the amendment or coal is already consumed, which in our cases is only the case towards the end of the experiments.

The combined setups with coal and amendment additions starting at the beginning of the experiments (Figure 5.4) show visible differences in the plot which are confirmed by greater MAE values. While the MAE of coal^{+--} is in the range of the previous MAEs of other predictions, MAEs for coal^{+++} and coal^{++-} show to be the largest over the entire data set. This can be attributed partially to the mismatches of the initial increase in methane production during the first 60 days, but especially the large

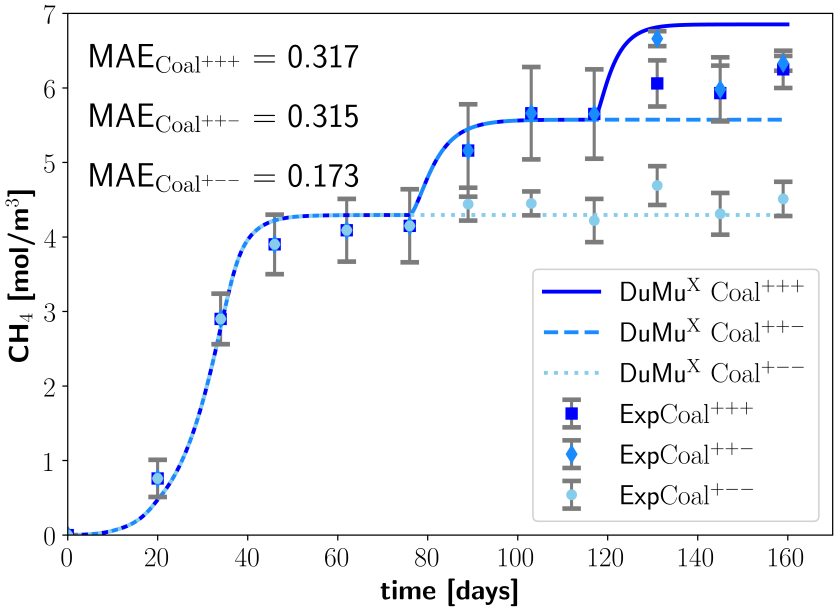

Figure 5.4: Comparison between model and experiment: coal and amendment additions starting on Day 0. Reprinted with permission from Emmert et al. [2020a], © 2020 Elsevier Inc.

MAEs of coal^{+++} and coal^{++-} are due to the values after Day 120. A faster increase in methane production is especially visible for the second and third amendment addition, which is consistent with the results from Figure 5.3.

For the other two setups, the experimental standard deviations are already greater and the values of the two different experimental setups almost coincide. These experimental results are discussed in detail in Davis et al. [2018a] and the possible reasons can not be addressed by a mathematical model of the type used here. However, the simulation shows the expected behaviour of a third (coal^{+++}), yet slightly smaller increase than the first and second increase or no increase for no additional amendment addition respectively (coal^{++-} and coal^{+--}).

With these results, the model reflects well the behaviour of the experimental systems and indicates that the general assumptions, the reaction kinetics, and the included microbiological pathways can be considered successfully validated. This strongly supports the hypothesis of a coal and amendment utilizing part of the microbial community being stimulated by the amendment additions, which results in an increase in biomass and an accelerated conversion of the bioavailable fraction of coal to products available to

methanogenic archaea. As mentioned above, further work related to the possible effect of adsorption for this experimental setup is recommended. In general, the results show that the numerical model is capable of capturing the relevant processes for MECBM production.

5.2 Discussion

As mentioned above, the hypothesis of substrate-specific microbes involved in MECBM production is strongly supported by this calibration and validation study. The parameters for the two different processes were calibrated independently, and with the calibrated parameters the model is able to reproduce the combined results. In the absence of tools allowing for monitoring of carbon flux from coal and amendment separately through these coal converting consortia, a quantitative assessment and evaluation of substrate-specific activities can only be achieved with mathematical/numerical tools.

The model assumes that 0.5 % of the coal is available for the microbes to be converted. This assumption is taken from Barnhart et al. [2017] and was based on the coal energy content before and after batch studies. Changing the fraction of bioavailable coal to a value other than 0.5 % would have no basis in the literature and leads to an overestimation of the methane production or when attempting to refit the model with these values, exceeds the physically plausible ranges of the parameters in many cases.

Moreover, the question of the correct or representative coal-composition remains. As mentioned in Section 2.4.1, the oxidation state of the coal from the PRB is calculated to be around -1 when taking the coal values from the latest studies in Davis et al. [2019]. Yet, when calculating the parameter's ranges, we use Gibbs-free-energy calculations based on glucose. The microbes only convert a small easily bioavailable fraction of the coal, while other parts of the coal are not converted. When assuming this, the difference between the amendment and the coal is relevant. The amendment in the experiments consists of algae [Davis et al., 2018a], which are also assumed to behave like glucose for the Gibbs-free-energy calculations. Hence, the yields of biomass relative to coal and amendment are equal, but the total amount and availability of the amendment is assumed to be higher, as the structure and composition of the amendment is already similar to microbial biomass. However, the two different substrates coal and

amendment are similar according to the thermodynamic reaction kinetics, yet different in the way the microbes are able to access and utilize them. Minor mismatches between simulations and experimental batch results show room for improvement regarding the conceptual model or the experiments including a need for uncertainty assessment as well as for a sensitivity analyses of all parameters used in the model. Especially for the glass bead cases, continuous methane production is observed in the experiment, but not in the model. Even though this increases the MAE, we want to reiterate that the overall fit is considered good with the model predictions remaining in the range of the standard deviation of the experimental results. Acknowledging that experimental results, even if they show a low standard deviation, still have underlying uncertainty gives us further confidence in the model, as this uncertainty puts the modelling results in the same range of deviation as the experimental results. Further studies could focus on quantifying this uncertainty with the aim of understanding the processes involved. However, adding more complexity to a model, without further detailed knowledge of the processes involved would not improve our current understanding of MECBM production.
This heavily parametrized model is able to produce plausible results because literature values and Gibbs free energy calculations according to McCarty [1972] provide narrow ranges for each parameter. Without these ranges based on a-priori knowledge, many parameters would be heavily correlated and the best fit could potentially result in parameters that are out of their physically meaningful range. This shows that for a system like the MECBM model, the set-up, and parameter values, have to be chosen based on independent experimentation and well-founded calculations. Additionally, a step-wise calibration and setup of the model, as proposed here, is advised.

The implementation of the model within the software framework DuMu^{x} [Koch et al., 2020] allows for modelling flow, transport, and reactions. DuMu^{x} is able to solve flow, transport and bio-geochemical reactions fully implicitly. Flow and transport capabilities were not tested in this part of the study, only the reactions were calibrated and validated. Therefore, it is required to include this validation of the conceptual approach and the kinetics of the reactions in well-controlled flow experiments, such as the column experiments of Davis et al. [2019], as it is done in Chapter 6.

5.3 Conclusions

MECBM production on the field scale involves strong interactions of microbial activity with flow and transport processes, thus featuring additional complexity introduced by the bio-geochemical processes. This chapter demonstrates the need for a solid understanding of the basic metabolic pathways as they were implemented qualitatively in a proposed food web and investigated quantitatively using a systematic comparison with experimental results.

The hypothesis of amendment-stimulated growth of coal-degrading microbes is strongly supported by this study. The model was calibrated using conceptually substrate specific microbes, and the simulation results match the experimental data well. This chapter lays a foundation for understanding the interaction between microbes, nutrients, and the coal matrix. The coal bio-availability was estimated for this study according to experimental data and proves to be sufficient for the numerical model. Many detailed calculations and experimental investigations were necessary to set up a numerical model capable of modelling this. Including complex "machines" like microbes into mathematical models involves numerous parameters with influence on their behaviour, which are hard or impossible to accurately estimate in their entirety [Scheibe and Yabusaki, 1998, Zhao et al., 2011].

The model will be extended in the following chapters to continuous flow studies, which involves additional interactions with flow and transport. Reactive transport can be modelled and the model can be used to test hypotheses not easily tested using experiments. This involves the basic assumptions of the coal's bio-availability, the amendment transport and possibly retardation. This mathematical and conceptual model shows the importance of specific substrate utilization by microbes in the subsurface and provides a tool for further investigations in the field of MECBM production.

6 Investigation of column studies*

The numerical batch model from Chapter 5 with the fundamental processes of microbial growth and the governing calibrated reactions can be extended to simulate column and field-case studies. By focusing on the modelling of upflow column reactors and comparing the simulation results against experimental data [Davis et al., 2019], this chapter is taking the next step from Chapter 5. The goal is to improve insight into relevant processes involved in MECBM on the column scale. Therefore, the numerical model is set up with different scenarios to test various hypotheses. The scenarios include (i) using the batch reaction kinetics with flow and transport, (ii) using the same model with changed boundary conditions to model inlet clogging, (iii) an extension of the model to capture retardation of the particulate amendment added to the columns, and (iv) cell attachment and detachment processes are investigated. Substantial work has been done in the field of modelling filtration Jegatheesan and Vigneswaran [2005], Rockhold et al. [2004], Molnar et al. [2015]; however most studies consider only a single fluid phase with respect to filtration. Therefore, the filtration equations are only used for the aqueous phase and its components. Also, the porous medium (coal) and biofilm as well as possibly suspended microbial cells can interact and add additional complexity to the model. This model can account for effects of additional decay or transport of microbes through shear stress, induced by the flow in the porous medium. Attachment and detachment of microbes or substrate is implemented as well.

As we will show, there are different mechanisms that can be implemented in the model to account for experimental observations, and to best fit the experimental data, a combination of these mechanisms is required. For example, we consider increased biofilm inactivation and decay as well as the retardation of amendment in the porous column, and we can show that in this case a combination of cell attachment and detachment with amendment retardation produces the best results. With this chapter, we show

*Chapter 6 is based on Emmert, Davis, Gerlach, and Class [2020b] and reprinted with permission from CC BY 4.0 MDPI 2020.

the clear advantage of the model in being able to measure methane production in total, while at the same time monitoring concentrations of substrates and intermediate products in the column, which is not easily done in experiments.

6.1 Materials and methods

This section has its focus on the description of the numerical model and the relevant processes involved in column-scale MECBM production. The conceptual model as well as the reaction kinetics are defined in Chapter 5. For this chapter, we advance the batch model to a fully-coupled reactive transport model. The components are transported with the fluid phases and converted by the reactions, which take place "inside" the biofilm. This biofilm is generally attached to the porous matrix and is able to grow and to decay. All these processes occur on the pore scale; however, we treat them in an averaged sense on the scale of a Representative Elementary Volume (REV), as previously discussed in Hommel et al. [2018], and apply them using REV-scale parameters and equations that describe the porous medium with its interactions between solid matrix, biofilm, components and fluids. We do not model component transport or flow inside the biofilm but rather keep the biofilms rigid on the porous matrix so that they potentially interact with flow and transport. Porosity and permeability are updated accordingly.

The general conservation equations and the filtration, retardation, attachment, and detachment equations are explained in Chapter 3. In the following Section, the changes made to the model different scenarios are recapitulated and explained shortly.

6.1.1 Numerical model

With our numerical setup, we can now model flow and transport through a lab-scale column. The modelled column is a simplified abstraction of the experimental setup from Davis et al. [2019] without inlet and outlet regions. It is 0.139 m in height, has a diameter of 0.0525 m, and consists of an inflow boundary at the bottom and an outflow (fixed pressure) at the top while lateral boundaries are Neumann no-flow. We are using a fully coupled and fully implicit discretization in time and space, and

everything is solved monolithically with the help of DuMu^{x} . In detail, we use a cell-centered finite-volume scheme in space and the implicit Euler method is applied for time. The resulting system is linearized using the Newton-Raphson method and solved using BiCGStab [Van der Vorst, 1992]. The dune-foamgrid module Sander et al. [2017] is used to generate a one-dimensional abstraction of the three-dimensional column for modelling with 80 grid cells.
Depending on the modelling setup, the inflow boundary conditions are adapted over time, resulting in four different modelling cases:

- Case 1: Homogeneously distributed biofilm with pulse-like amendment additions.
- Case 2: Homogeneously distributed biofilm with stretched-out amendment additions (inlet clogging).
- Case 3: Homogeneously distributed biofilm with amendment additions, filtration and amendment retardation effects.
- Case 4: Injected microbial cells with amendment additions, filtration and amendment retardation effects.

The different modelling cases with their respective parameters, added amendment and/or biofilm, are also illustrated in Figure 6.1. A constant water injection representing the experimental flow rate of 0.005 mL/min (8.33×10^{-11} m^3/s) is applied for all modelling cases at the inflow boundary. The amendment additions might occur on Day 0 and Day 61. If there is only one amendment addition on Day 0, it is depicted with the dashed lines that mostly are covered by the two amendment addition case which is represented by solid lines. The biofilm addition for Case 4 only occurs once on Day 0, while biofilm is assumed to be present homogeneously throughout the column for all other Cases.

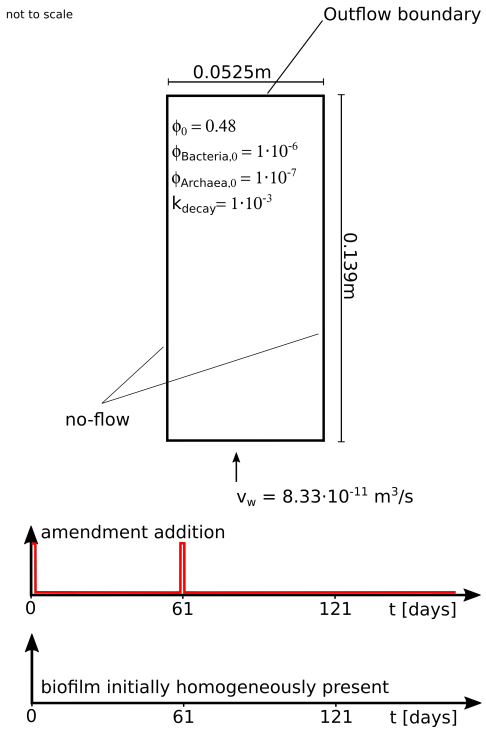

(a) Setup and parameters for Case 1.

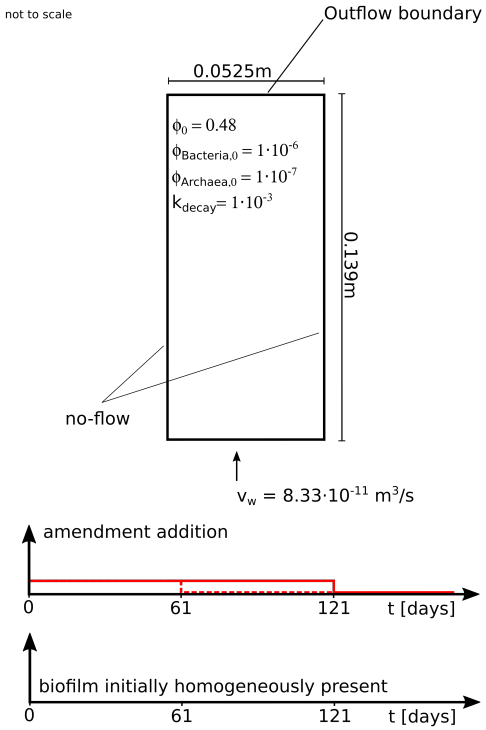

(b) Setup and parameters for Case 2.

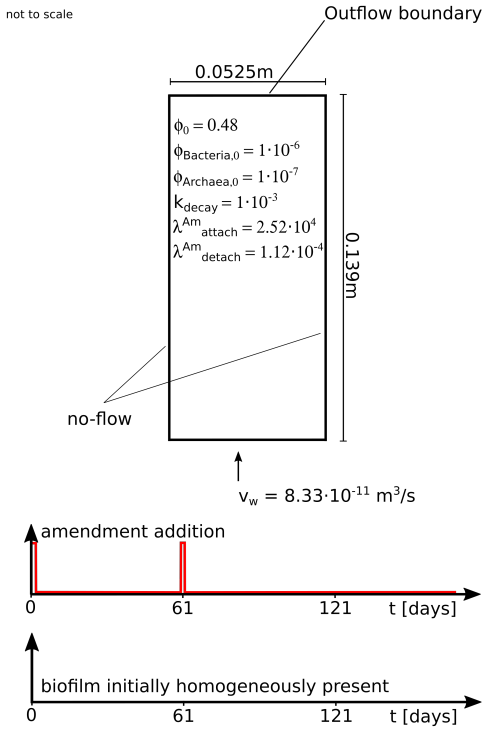

(c) Setup and parameters for Case 3.

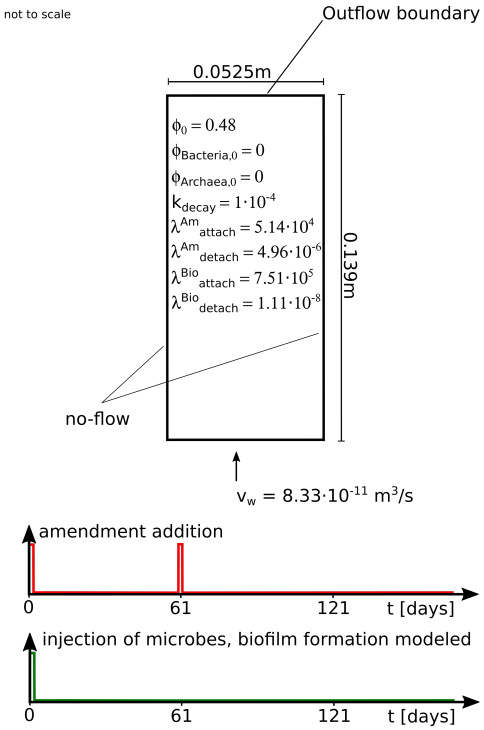

(d) Setup and parameters for Case 4.

Figure 6.1: Visualization of the model setup for the different cases and relevant the corresponding relevant parameters for all cases. The inclusion of retardation of amendment, as well as attaching and detaching microbial cells, involves additional attachment and detachment parameters. All unchanged Parameters are given in Table D.1. Reproduced with permission from Emmert et al. [2020b], CC BY 4.0 MDPI 2020.

With these cases, we investigate the different hypotheses introduced in Chapter 4. Case 1 serves as a reference for what a well-established flow simulator coupled to the batch-reaction system (with minor modifications in the biofilm distribution) computes as a result. Case 2 builds on the post-experimental observation that the inlet region of the column potentially was clogged with amendment or biofilm [Davis et al., 2019]. To translate this into the model, we assume that the amendment is not added as a single pulse, but each amendment addition is stretched out over 61 days. This means we inject the same total amount of amendment, but in small continuous portions over 61 or 121 days and assume no retardation inside column. Case 3 addresses the same experimental observation as Case 2 with respect to the clogging in the inlet region; however, in this case a filtration model is implemented for clogging or retardation of the amendment inside the column. Case 4 is, computationally, the most challenging case, as we now implement microbial cell attachment and detachment, while also using the amendment filtration from Case 3. This introduces additional complexity to the model, but we consider it to be the most realistic scenario since in the experiments the inoculum was also injected. All other modelling parameters used are given in Table 6.1.

Table 6.1: Parameters for the simulation cases. Reproduced with permission from Emmert et al. [2020b], CC BY 4.0 MDPI 2020.

Parameter	**Value**	**Unit**
Column length	0.139	$[m]$
Column diameter	0.0525	$[m]$
Porous medium porosity	0.48	$[-]$
Flow rate	0.005	$[ml/min]$
Decay rate coefficient	$1 \cdot 10^{-4}$	$[d^{-1}]$
Amendment attachment coefficient Case 3 $\lambda^{Am}_{attach,C3}$	$2.52 \cdot 10^{4}$	$[m^{-1}]$
Amendment detachment coefficient Case 3 $\lambda^{Am}_{detach,C3}$	$1.12 \cdot 10^{-4}$	$[s^{-1}]$
Amendment attachment coefficient Case 4 $\lambda^{Am}_{attach,C4}$	$5.14 \cdot 10^{4}$	$[m^{-1}]$
Amendment detachment coefficient Case 4 $\lambda^{Am}_{detach,C4}$	$4.96 \cdot 10^{-6}$	$[s^{-1}]$
Cell attachment coefficient Case 4 $\lambda^{Bio}_{attach,C4}$	$7.51 \cdot 10^{5}$	$[m^{-1}]$
Cell detachment coefficient Case 4 $\lambda^{Bio}_{detach,C4}$	$1.11 \cdot 10^{-8}$	$[s^{-1}]$

6.1.2 Processes

This numerical study aims at reproducing experiments by Davis et al. [2019]; however, the calibration of the model is not straightforward because the experimental data are

not as abundant as in the batch studies performed previously by the same group [Davis et al., 2018a]. Multiple processes occur simultaneously, hence the experimental evidence does not always allow unique conclusions. With different simulation scenarios we use the flexibility of the model to analyse the processes and to contribute to the discussion, thus improving the understanding of the processes that occur.
Processes that might have an impact on the methane production include changes in the reaction system due to the flow, amendment retardation in the sense of inlet clogging or filtration and thereby retardation effects in the column, cell attachment and detachment due to flow as well as combinations of all mentioned processes. The previous sections describe very basic approaches to model these processes. We note that we intend to keep the complexity of the processes as simple as possible, even though more sophisticated and more parametrized approaches might be available in certain cases. Therefore, when it comes to changes of the reaction system due to the flow, we assume that an observed decrease in production rates, in comparison with batch systems, could be modelled in different ways. One option would be to consider a reduced activity of the biofilm. This can be achieved in the model by reducing the volume fractions of initial biofilm, reducing growth rates or increasing decay rates. Another mechanism for achieving reduced production rates could include incomplete mixing in the columns, i.e. substrates are not available equally well as in the batch systems. In any case, the coupled flow, transport, and reaction model inherently accounts for a reduction of concentrations due to transport. Of course, one might, for example, furthermore decrease reaction yields. We note here that we are well aware of the complexity that our model has, and, given the limited amount of experimental data, we restrict ourselves to including only those mechanisms which we think are most relevant. Eventually, we try to model the changes in methane production mainly with biofilm properties, i.e. detachment, decay due to shear stress or less active biofilm; and we assume thereby that the same reactions as obtained from the batch systems now coupled to flow and transport can represent the effect on the total methane production.

Biofilm modifications due to flow

In this study, different modelling setups with and without cell attachment or detachment are investigated. Shear stress, induced by flow through the column, might have an impact on the biofilm, as parts of the biofilm can detach and potentially decay.

Additionally, biofilms might not grow as abundantly due to dilution of required components. For modelling setups that do not account for cell attachment or detachment (Cases 1, 2, and 3), the decay rate of biofilm is increased by an order of magnitude from 10^{-4} d^{-1} to 10^{-3} d^{-1}. This is assumed to account for some potential inactivation or additional decay under flow conditions relative to batch experiments. This is performed for these cases to better match the first 50 days of the numerical study to the experimental results. Additionally, the active biofilm volume fraction initially present along the entire column is reduced by up to an order of magnitude.

6.2 Results

We describe the four different cases introduced in Section 6.1.1 individually here. The model is compared only to two experimental setups with an initial amendment addition. As previously described, the other experimental results showed minimal or no methane production and are not included in the comparison study here.
The experimental data (see e.g. Figure 6.2a) show a relatively continuous increase in cumulative methane production from the column starting from Day 25 or 30 and increases to 0.0017 mol or 0.0015 mol for Exp Coal^{++} (blue dots) or Exp Coal^{+-} (black dots). Even though a second amendment addition was performed on Day 61 for Exp Coal^{++} , the experimental data do not show a substantial increase in methane production after Day 61 compared to Exp Coal^{+-} .
We evaluate the model until Day 200 for all modelling cases and assess the agreement with the available experimental data. However, for the amendment retardation as well as for the cell attachment and detachment cases, additional figures with up to 600 or 1050 days are provided. This is done, as not all amendment and coal is consumed at the end of the 200-day study. Therefore, methane production from the column has not stopped either, and we want to investigate the model response over the entire theoretical time of methane production. In addition to the methane production over time, the substrate availability is plotted. Substrate availability means that the relative abundance of the two main substrates (coal and amendment) is investigated for each study. To facilitate the comparison, their local concentration or volume fraction at each point in the column is summed over the entire column and plotted as percentage of what is maximally available during the simulation. However, information on where in the column the substrate is still available cannot be presented for this type of plot.

The parameters used for simulations are given in Table 6.1. Where applicable, modifications to the biofilm decay rate and initial distribution are explained in Section 6.1.2. All reaction kinetics and processes are from the validated batch model defined in Emmert et al. [2020a].

6.2.1 Case 1: Homogeneously distributed biofilm, pulse-like amendment

The first modelling case is using the batch kinetics with minor adjustments in the biofilm decay rate and initial biofilm presence. The results of the cumulative methane production at the top of the column are shown in Figure 6.2a. The blue curve shows methane production for the DuMu^{x} Coal^{++} case as a result of the model. Methane production is first detectable in the columns on Day 24 and a gradual increase can be seen from Day 30 until approximately Day 80. After that, methane production levels out at 0.0015 mol.
The black curve shows methane production for the DuMu^{x} Coal^{+-} case and is identical to the DuMu^{x} Coal^{++} case for the first 61 days. Since there is no second amendment addition on Day 61, the methane production of DuMu^{x} Coal^{+-} slows down after Day 61 and levels out after Day 100 at 0.0012 mol.
Figure 6.2b shows the two main substrates, coal and amendment, available in the column over time in a normalized way. The coal is given with the black curves for DuMu^{x} Coal^{++} and DuMu^{x} Coal^{+-} . The two setups coincide and their behaviour is very similar for this case. We see an only slow conversion of coal for the first 30 days, after that the microbial community has grown sufficiently to rapidly consume the coal. After Day 55 the conversion of coal slows down, as less substrate is available for the biofilm, before all coal has been consumed on Day 70.
Amendment on the other hand is injected for DuMu^{x} Coal^{++} on Day 0 and Day 61. The peak amendment concentration occurs at the second amendment addition on Day 61 for this column. Therefore, when normalizing amendment concentrations, the initially available amendment fraction is only at 81%. The added amendment is consumed and transported slowly until Day 35. From then on, the amendment is also transported out of the column unused. Therefore, the fraction of available amendment decreases faster now. On Day 61, the second amendment addition occurred and the maximum amount of amendment is present in the column. The decrease of amendment occurs as fast as

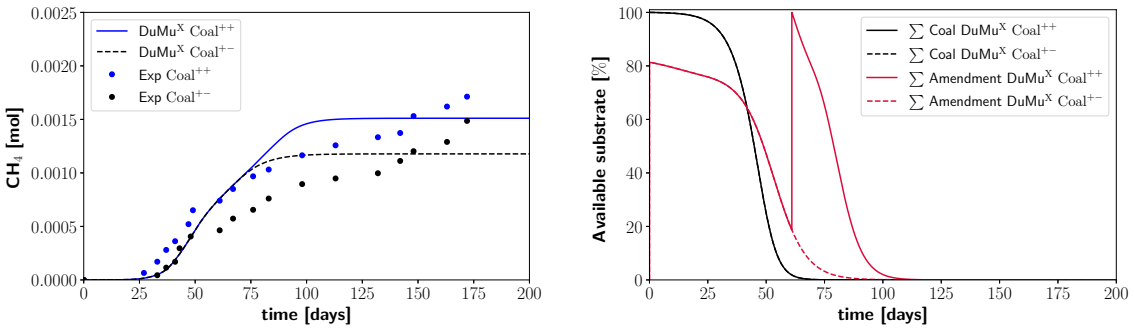

(a) Methane production. (b) Substrate availability.

Figure 6.2: Results of Case 1 with homogeneously distributed biofilm and pulse-like amendment additions on Day 0 and Day 60. (**a**) shows methane production of the column over time of the DuMu^x model compared to the experimental results. Blue is the scenario with two amendment additions (Coal^{++}), black with only one addition (Coal^{+-}). (**b**) shows the corresponding substrate availability for coal (black) and amendment (red). For the plot, substrate is summed over the entire column and plotted as percentage of what is maximally available during the simulation. Here DuMu^x Coal^{++} is depicted with a solid line and DuMu^x Coal^{+-} with a dashed line. Reproduced with permission from Emmert et al. [2020b], CC BY 4.0 MDPI 2020.

from Day 50 to Day 61, which is mainly attributed to the conversion of newly added amendment to intermediate products by the coal and amendment consuming bacteria in the biofilm and partially to the remaining amendment and its intermediate products from the first amendment additions. On Day 80, the second amendment addition starts being washed out of the column, while the conversion of amendment to intermediate products still occurs. This leads to a steeper slope of amendment availability, before levelling out at approximately Day 90. All substrate (coal and amendment) is consumed after Day 110.

When comparing Figure 6.2a and Figure 6.2b, it is visible that the initial increase in methane production is primarily driven by the conversion of coal and amendment. With the coal being consumed everywhere along the column and running out after Day 60, we also see a less steep slope in the methane production in Figure 6.2a. Now, mostly amendment is converted and the slope in the methane-production curve stays the same before it levels out around Day 80.

The overall match to the experimental results is reasonable for the first 75 days, as the modelling curve and the experimental data coincide in Figure 6.2a. However, after Day 75, a distinct difference between DuMu^{x} Coal^{++} and DuMu^{x} Coal^{+-} is visible for the modelling study, where the methane production of DuMu^{x} Coal^{+-} levels out, while the methane production of DuMu^{x} Coal^{++} increases further due to the second amendment addition. This is in contrast to the experimental studies Coal^{++} and Coal^{+-} , that behave similar to one another. Also, the cessation of methane production predicted by the model is not seen in the experiment. The cessation of methane production in the model is explained with all available substrate being consumed. Without substrate for the microbes, no further methane generation is possible in the model.

6.2.2 Case 2: Homogeneously distributed biofilm, continuous amendment injection

The second modelling case is using the same setup as the first case, but now the amendment is not injected as a pulse, but rather the injection is stretched out over 61 days. This aims at imitating a clogging or localized retention of the amendment at the inlet, that might have happened during the experiment [Davis et al., 2019]. The results of the cumulative methane production are shown in Figure 6.3a. The blue curve shows methane production for the DuMu^{x} Coal^{++} Case as a result of the model. The first detectable methane production of the column is on Day 26 and a gradual increase can be observed until approximately Day 80, after which methane production levels out at 0.0023 mol.

The black curve shows methane production for the DuMu^{x} Coal^{+-} Case and is identical to the DuMu^{x} Coal^{++} Case for the first 61 days. As before, DuMu^{x} Coal^{+-} ceases production after 100 days at approx. 0.0014 mol.

Figure 6.3b shows the two main substrates (coal and amendment) available in the column over time in a normalized way. Coal is given with the black curves for DuMu^{x} Coal^{++} and DuMu^{x} Coal^{+-} . The two setups coincide and behave in the same way for this case. The consumption of coal is almost identical to Case 1, as the initial coal and biofilm distribution is the same.

Only the amendment injection is varied, which leads to minimal changes of the coal consumption because parts of the bacteria can grow on coal and amendment. Amendment is injected for the DuMu^{x} Coal^{++} Case on Day 0 and Day 61. We see a quasi-linear

increase of methane for the first 54 days before more amendment is consumed and washed out than is being injected. After this peak on Day 54, a large part of the amendment is being washed out of the column, while at the same time being consumed for the next 25 days. On Day 80, approximately 40% of the amendment is available in the column, but since the microbes along the entire column have grown with the continuous feeding, the newly added amendment does not reach the end of the column anymore, but is being consumed in the influent region of the DuMu^{x} Coal^{++} column. This combination of amendment injection and consumption in the column leads to the slower decrease of available amendment until Day 121. On Day 121, the continuous amendment addition stops and the remaining amendment is consumed within a short time. On Day 150, no substrate (coal and amendment) is left in the column.
For the DuMu^{x} Coal^{+-} study, amendment is only injected continuously from Day 0 to Day 61. Therefore, the curves of DuMu^{x} Coal^{++} and DuMu^{x} Coal^{+-} coincide for the first 61 days. After this, the available amount of amendment for the DuMu^{x} Coal^{+-} study decreases rapidly for the same reasons given above. The microbial community has grown and consumes the remaining amendment completely by Day 80.

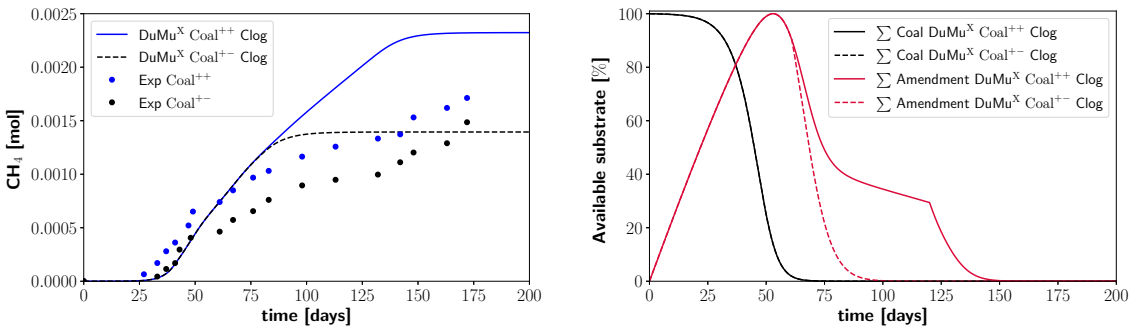

(a) Methane production (b) Substrate availability

Figure 6.3: Results of Case 2 with homogeneously distributed biofilm and stretched out amendment additions. (**a**) shows methane production of the columns over time of the DuMu^{x} model compared to the experimental results. Blue is the scenario with two amendment additions (Coal^{++}), black with only one addition (Coal^{+-}). (**b**) shows the corresponding substrate availability for coal (black) and amendment (red). For the plot the substrate is summed over the entire column and plotted as percentage of what is maximally available during the simulation. Here Coal^{++} is depicted with a solid line and Coal^{+-} with a dashed line. Reproduced with permission from Emmert et al. [2020b], CC BY 4.0 MDPI 2020.

When comparing Figure 6.3a and Figure 6.3b next to each other, the initial increase in methane production is primarily driven by the conversion of coal and amendment. With the coal being consumed everywhere along the column and running out after Day 60, we again see a less steep slope in the methane production in Figure 6.3a after Day 60. Now, mostly amendment is converted and the slope of the methane-production curve stays the same before it levels out.
A reasonable match to the experimental results is given for the first 60 days, as the modelling curve and the experimental data coincide in Figure 6.3a. However, after Day 60, both modelling studies show a larger methane increase than the experimental results. $DuMu^x$ $Coal^{++}$ and $DuMu^x$ $Coal^{+-}$ level out due to substrate depletion after 140 or 100 days respectively, whereas the experimental studies do not exhibit such a behaviour.

6.2.3 Case 3: Homogeneously distributed biofilm, amendment retardation

The third modelling case has the same homogeneous biofilm distribution along the column as Cases 1 and 2, and uses a pulse-like amendment injection. In contrast to Cases 1 and 2, it uses a filtration law to model amendment retardation and partitioning as described in Eq. (3.18). The results of the cumulative methane production at the top of the column are shown in Figure 6.4a and 6.4c to show all the modelling data. The blue curve shows the predicted methane production for the $DuMu^x$ $Coal^{++}$ Case. The first methane production at the end of the column is on Day 21 and a gradual increase can be seen from Day 30 until approximately Day 60. After that, methane production rates slow down temporarily until Day 470 (Figure 6.4c) due to the amendment being released along the column in regions where no large portions of amendment and coal consuming bacteria are present yet. With more amendment being released further downstream the column, amendment and coal converting bacteria can grow and produce more intermediate products, which in turn leads to a re-increase in methane production. After Day 470 a final increase can be observed, before the methane production levels out at 0.003 mol.
The black curve shows methane production for $DuMu^x$ $Coal^{+-}$ and is identical to $DuMu^x$ $Coal^{++}$ for the first 61 days. $DuMu^x$ $Coal^{+-}$ shows a slower increase in methane production from Day 61 until approximately Day 550. Most trapped amendment has

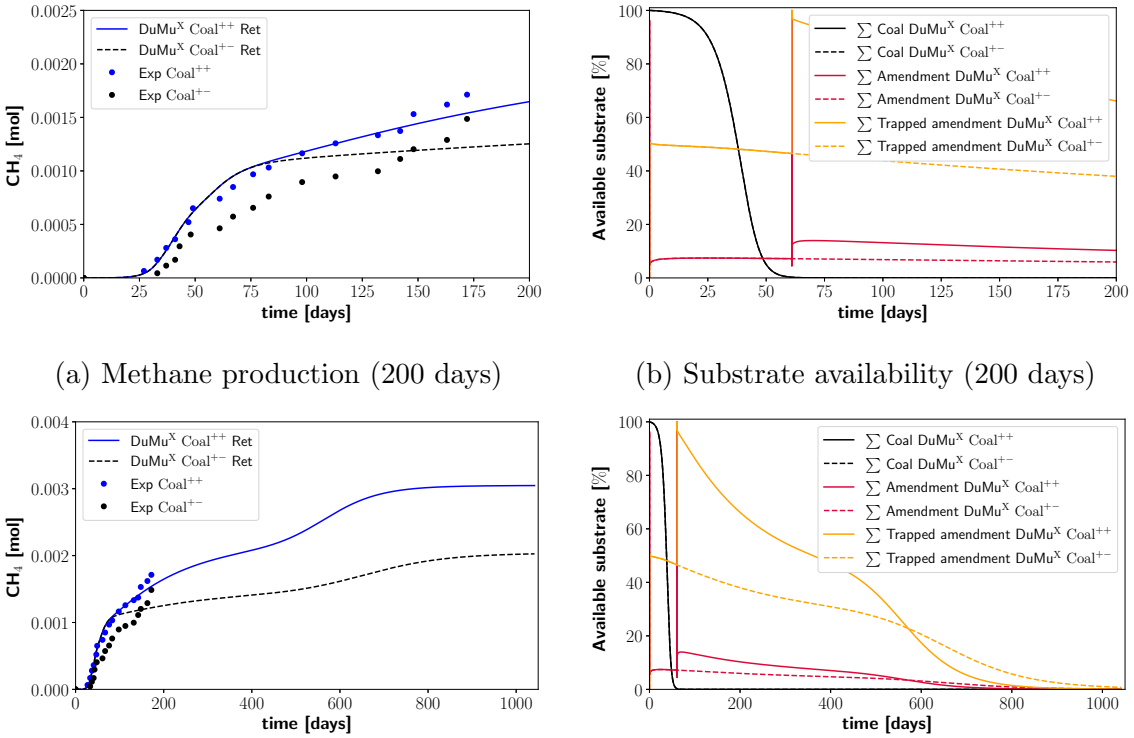

(a) Methane production (200 days)

(b) Substrate availability (200 days)

(c) Methane production (1050 days)

(d) Substrate availability (1050 days)

Figure 6.4: Results of Case 3 with homogeneously distributed biofilm and filtration and retardation effects of amendment. (**a**) shows methane production of the columns over time of the DuMu^x model compared to the experimental results. Blue is the scenario with two amendment additions, black with only one addition. (**b**) shows the corresponding substrate availability for coal (black), amendment (red), and trapped amendment (orange). For the plot the substrate is summed over the entire column and plotted as percentage of what is maximally present during the simulation. (**c**) and (**d**) show the same results as (**a**) and (**b**) until all substrate is consumed after 1050 days. Reproduced with permission from Emmert et al. [2020b], CC BY 4.0 MDPI 2020.

already been released from the first part of the column and the bacteria converting both coal and amendment have not grown enough in the second part yet. Therefore, most released amendment is transported further downstream, leads to new growth of amendment and coal consuming bacteria and to the production of some intermediates along the column. With the bacteria established in the second part of the column, the further released amendment parts are now being mostly converted and the last stretch of the methane production increases again to a total production of 0.002 mol.

Figure 6.4b and 6.4d show the two main substrates (coal and amendment) available in the column over time in a normalized way. Coal is given with the black curves for DuMu^{x} Coal^{++} and DuMu^{x} Coal^{+-} . The two setups coincide and behave in the same way for this setup. The consumption of coal is now even faster than in Cases 1 and 2, as the initial coal and biofilm distribution is the same, but amendment is added as pulse, is trapped and then released continuously. This amendment retardation leads to a more continuous release of amendment, which boosts the growth of microbes that convert both amendment and coal. Therefore, the consumption of the bioavailable portion of coal is completed 10 days earlier than in Cases 1 and 2.

Bioavailable amendment (red) is added for the DuMu^{x} Coal^{++} Case on Day 0 and Day 61. With the amendment filtration processes described in Eq. (3.18), most amendment is trapped in the first part of the column initially. We see that the trapped amendment (orange) starts at almost 50%, while the active and bioavailable amendment is at only 5% for the first 61 days. Both the trapped and the bioavailable amendment decrease over the first 61 days, before the second amendment addition increases the amendment levels to the highest level during this modelling scenario, (i.e. 100%) for the trapped amendment, and 12% for the active amendment. The pulse-like addition leads to more than 80% trapping of the amendment in a short time. This reduces the porosity and the porosity reduction leads to a larger release of trapped amendment as the velocities and shear forces increase. The amendment is now transported further downstream to the next grid cells in the model and trapped there again. Due to this trapping and release from one computational grid cell to the next, maximum positive and negative peaks in the amendment availability curves occur here on Day 61. The maximum amount of trapped amendment is present on Day 61 and continuously releases bioavailable amendment until approximately Day 450, before it has all been released back by Day 800. This in turn leads to a relatively constant bioavailable amendment fraction in the column of up to 15% of what is maximally available in the column following Day 61. This fraction decreases slowly over the next 400 days and this bioavailable amendment is consumed by the microbes and vanishes completely after Day 800.

For the DuMu^{x} Coal^{+-} study, amendment is only injected continuously from Day 0 to Day 61. Therefore, the curves of DuMu^{x} Coal^{++} and DuMu^{x} Coal^{+-} coincide for the first 61 days, after which the available amount of amendment for the DuMu^{x} Coal^{+-} study continues to decrease slowly until Day 800. The trapped amendment starts to decrease at a continuous rate until Day 600. From Day 600 until Day 1050, the amend-

ment is released a little faster, as the biofilm grows, reduces porosity and thereby increases detachment rates. Almost all trapped amendment is released after 1000 days.

A comparison of Figures 6.4c and 6.4d indicates that the increases in methane production are directly correlated to the release of trapped amendment and subsequent consumption of bioavailable amendment. Mostly, amendment is converted after all coal is already consumed. The second amendment injection for DuMu^{x} Coal^{++} leads to a larger methane production in Figure 6.4c compared to DuMu^{x} Coal^{+-} , while Figure 6.4d shows that the second amendment injection results in a faster release of trapped amendment and in turn to a faster consumption of all available amendment in total. This makes sense when we consider that with the additional substrate a larger volume fraction along the column is occupied by microbes. Through the increased growth of microbes, a self-enhancing effect can be observed that reduces the porosity, increases the shear stress, which in turn releases more trapped amendment and ultimately enhances the growth of microbes and methane production again.
The DuMu^{x} Coal^{+-} Case seems to predict slightly higher methane production than experimentally observed for the first 150 days, followed by a slightly lower methane production after Day 150. Overall, the methane production curves match the experimental results very well. Nevertheless, one has to be careful, as most of the methane generation and production in the model is attributed to the amendment after Day 50, which is not in line with the findings of Davis et al. [2019].

6.2.4 Case 4: Injected microbial cells, amendment retardation

The fourth modelling case does not assume any initial biofilm inside the column, but uses a pulse injection of microbes followed by a pulse-like amendment addition. Cell attachment and detachment are modelled using Eq.'s (3.18) and (3.21), while amendment retardation is modelled using Eq.'s (3.18) and (3.20).

The results of the cumulative methane production in the column are shown in Figure 6.5a and 6.5c. The blue curve shows methane production for the DuMu^{x} Coal^{++} Case as a result of the model. The first methane production of the column is on Day 18 and a gradual increase can be seen from Day 21 until approximately Day 130. After that, methane production rates decrease temporarily until Day 210 (Figure 6.5c). At this time, we can observe a small kink in the curve which is related to a numerical issue.

In order to understand this, one needs to keep in mind that the model can handle two fluid phases as long as they can subsist. At this point in time, the gaseous phase at the top of the column, where the pressure is the lowest, is at the brink of disappearance. This is because not enough methane is coming from the column towards the outlet of the column anymore. The model switches primary variables [Class et al., 2002] back and forth, which leads to a discrete change in the calculation of fluxes out of the column. Essentially, the effect of this phase change is observed in methane being held back in the column for a short time, after which it is released like in a small pulse when the gaseous phase can eventually subsist again at the boundary. After this time, a short plateau with very limited methane production is observed from Day 210 until Day 250. Then, after Day 250, methane production increases again before it gradually levels out at a maximum production of 0.0019 mol on Day 550.
The black curve shows methane production for DuMu^{x} Coal^{+-} and is identical to DuMu^{x} Coal^{++} for the first 61 days. DuMu^{x} Coal^{+-} also shows a slower methane production increase from Day 61 until approximately Day 210 when the methane production levels out at 0.0014 mol.

Figure 6.5b and 6.5d show the two main substrates (coal and amendment) available in the column over time in a normalized way. Coal shown in black for DuMu^{x} Coal^{++} and DuMu^{x} Coal^{+-} . The two setups coincide and behave in the same way for this setup. The available coal fraction decreases fast from 100% to 92% during the first 15 days, before utilization slows down until Day 100 when 91% of the bioavailable coal fraction are still present in the system. Coal is then consumed faster again and decreases to 60% by Day 300, before it is consumed even faster until it is depleted by Day 500.
The bioavailable amendment (red) is added on Day 0 and 61 for DuMu^{x} Coal^{++} and starts at 2% for amendment on Day 0. The bioavailable amendment reaches a peak on Day 25 at 4% before it decreases to 2% again by Day 61. With the second amendment addition a short spike to 100% is observed, before the available amendment starts to be transported along the column until Day 80. It then gradually decreases from 5% until Day 200.
The trapped amendment (orange) for DuMu^{x} Coal^{++} decreases as well, but starts initially with 80% trapped amendment. A gradual decrease to 20% is observed before the second amendment addition, and the maximum amount of trapped amendment on Day 61. Trapped amendment is released gradually until approximately Day 300, after which the remaining trapped part stays almost constant and decreases very slowly.

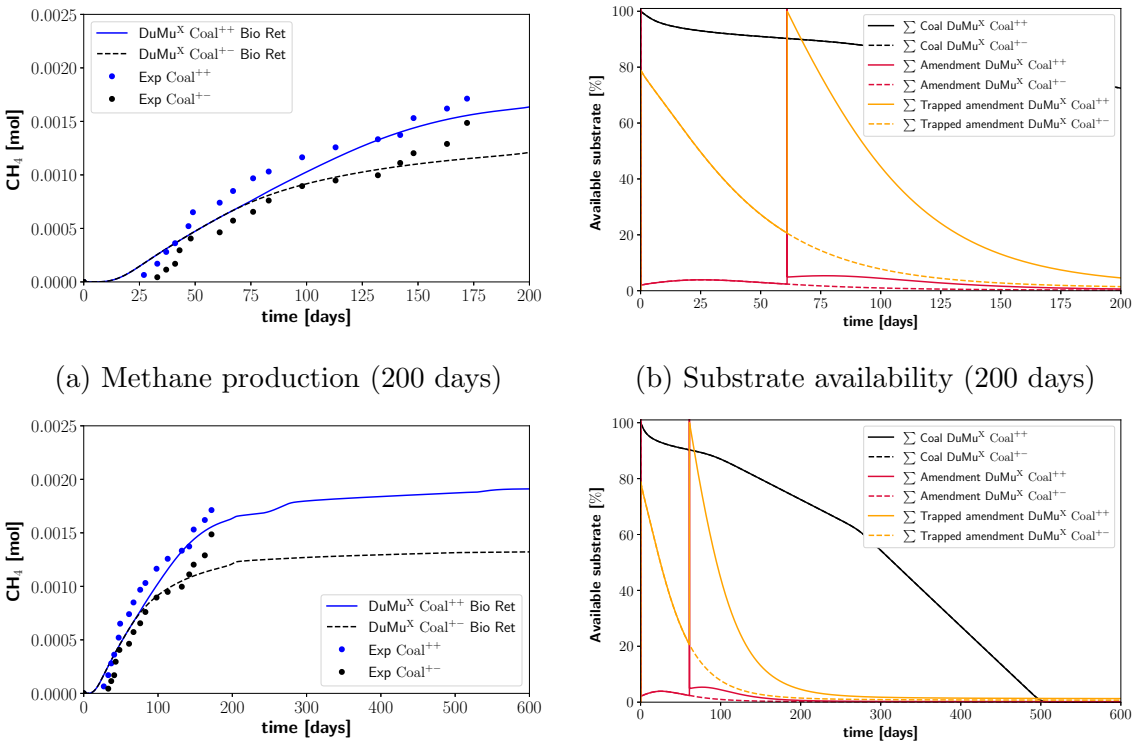

(a) Methane production (200 days)

(b) Substrate availability (200 days)

(c) Methane production (600 days)

(d) Substrate availability (600 days)

Figure 6.5: Results of Case 4 considering injection and retardation of injected microbial cells and amendment (**a**) shows methane production in the columns over time of the DuMu^x model compared to the experimental results. Blue is the scenario with two amendment additions, black with only one addition. (**b**) shows the corresponding substrate availability for coal (black), amendment (red), and inactive trapped amendment (orange). For the plot, the substrate is summed over the entire column and plotted as percentage of what is maximally present during the simulation. (**c**) and (**d**) show the same results as (**a**) and (**b**) and predict the behaviour of the column systems out to 600 days. Reproduced with permission from Emmert et al. [2020b], CC BY 4.0 MDPI 2020.

Amendment availability for DuMu^x Coal^{+-} is the same as described before and decreases after Day 61. Bioavailable amendment vanishes almost completely after Day 200. The trapped amendment for DuMu^x Coal^{+-} deviates on Day 61 from what is described for DuMu^x Coal^{++} . Here, the trapped amendment part is being released continuously and therefore decreases until Day 200.

The overall match to the experimental results is given for DuMu^x Coal^{++} and DuMu^x Coal^{+-} as the curves match the experimental results for the first 150 days. The DuMu^x Coal^{+-} Case shows a lower methane production than the experiment after Day 150.

For Case 3 the methane production curves of the model coincide with the experimental data points. Coal consumption rates appear to be in line with the findings of Davis et al. [2019].

6.3 Biofilm evolution along the column

In modelling Case 4, explained in Section 6.2.4, the microbial cells are injected at the beginning of the simulation and can attach and detach along the column. Due to the presence of coal and the injection of amendment, the bacterial groups grow and detach further downstream. If coal or amendment are not present at a location in the column the biofilm decays. Therefore, the consumption of coal and the presence of amendment are essential for the bacteria. Archaea are dependent on the presence of the bacteria, as the bacteria convert coal and amendment to intermediate products, which are converted to methane by the archaea. Therefore, the archaea can only establish if bacteria produce intermediate products upstream of the archaea or at the same location.
Since the biofilm is not present homogeneously along the column anymore and intermediate products can not necessarily be converted where they are produced, attachment and detachment of microbial cells is essential for modelling Case 4. In the following we will present a snapshot of the biofilm distribution combined with the bioavailable fraction of coal on Day 185 and 365.

6.3.1 Biofilm evolution on Day 185

Figure 6.6 shows the distribution of bacteria and bioavailable fraction of coal on the left and the distribution of archaea in the right plot (on the x-axis) on Day 185. The inlet region is at the bottom y-axis, and the outlet on the top. In the left plot of Figure 6.6, the bioavailable fraction of coal (black) is consumed completely for the first 30% column height. The volume fraction of coal-consuming bacteria (green) is higher at the inlet region and decreases to almost 0 at 10% of the column height. From 15% to 35% of the column the volume fraction of coal bacteria is greater again. Amendment and coal bacteria (purple) show high volume fractions for the first 10% of the column, before they decrease and are not present anymore in significant numbers starting at approximately 20% of the column height.

Amendment- plus coal-utilizing bacteria establish themselves quickly due to amendment availability and consume most of the bioavailable coal out to approximately 10% of the column height before coal-only-consuming bacteria can establish themselves. Hence, a low volume fraction of coal bacteria is observed for this part of the column. With the available amendment being consumed within the first 10% of the column, the amendment- plus coal-consuming bacteria did not establish as well after that, and the coal consuming bacteria volume fraction is able to increase from 15% to 35% of the column height. The bioavailable coal is consumed where there are bacteria, which can be seen at 35% of the column, where the increase in coal consuming bacteria coincides with a decrease in a volume fraction of bioavailable coal.
The right plot of Figure 6.6 shows the three types of archaea along the column. They all have their highest value at the inlet or within the first 5% of the column. As previously explained, they depend on the bacteria and it is visible, that they are only present where the bacteria are present, too. Methylotrophic archaea are assumed to only feed from amendment in Emmert et al. [2020a], and therefore depend on the amendment and coal consuming bacteria. A similar peak that is observed for the amendment and coal consuming bacteria is also visible for the methylotrophic archaea. The model predicts acetoclastic archaea to establish themselves further downstream than most other archaeal groups, since they consume the acetate produced by the coal-and amendment-consuming bacteria.

6.3.2 Biofilm evolution on Day 365

Figure 6.7 shows the distribution of bacteria and bioavailable fraction of coal on the left and the distribution of archaea in the right plot on Day 365. The inlet region is at the bottom of the y-axis, and the outlet on the top. In the left plot of Figure 6.7, the bioavailable fraction of coal is predicted to be consumed completely in the first 70% of the column. The volume fraction of coal bacteria in the first 30% of the column is similar to what was described for Day 185 in Figure 6.6 and remains at approximately the same level for the first 70% of the column. The model predicts the volume fraction of amendment- plus coal-consuming bacteria to peak within the first 20% of the column but to remain low for the remainder of the column.
The right plot of Figure 6.7 shows the three types of archaea along the column. They all have their highest value within the first 10% of the column, and look similar to

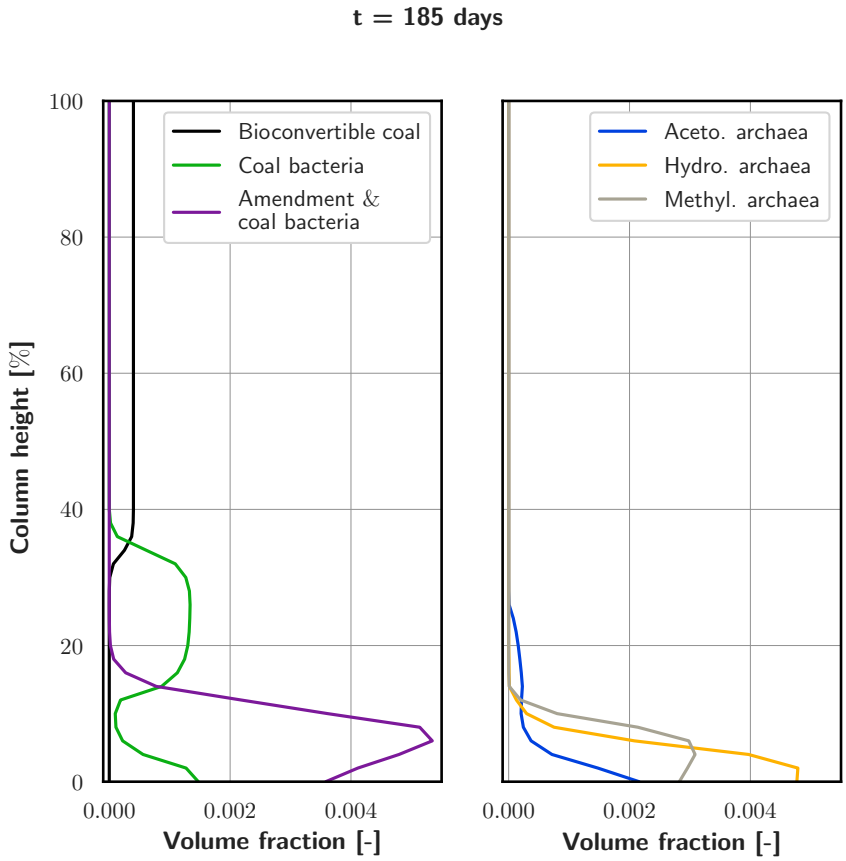

Figure 6.6: Distribution of microbial cells and bioavailable coal throughout the column (y-axis) on Day 185 as predicted for Case 4. The left plot shows the volume fraction of two types of bacteria and bioavailable coal, while the right plot shows the volume fraction of three archaeal groups. Reproduced with permission from Emmert et al. [2020b], CC BY 4.0 MDPI 2020.

the distributions predicted in Section 6.3.1 only with slightly lower values due to decay and detachment. For acetoclastic archaea small increases in the volume fraction can be observed between 40% and 75% of the column height with a number of smaller peaks throughout the remainder of the column. These peaks are a physical process, however it is numerically triggered. With attaching and detaching cells along the column, the numerical solver tolerance of 10^{-8} leads to minimal increases and decreases of volume fractions along the column. With more acetate being produced and transported downstream, the previously very limited number of microbial cells grow rapidly. We then observe a self-enhancing effect, as more biofilm is able to convert more of the acetate that passes along. This is only obvious for the fast growing acetoclastic

archaea in Figure 6.7, but also there are indeed smaller peaks for the hydrogenotrophic and methylotrophic archaea (these are not visible in Figure 6.7). Hydrogenotrophic archaea exhibit a second increase in volume fraction between 30% and 55% of the column height.

These increases in volume fraction of the archaea can be attributed to the bacterial conversion of coal into intermediates (acetate and hydrogen), which support growth of the archaea downstream of the bacteria. This indicates the importance of interactions between the different microbial species and why the attachment and detachment processes along the column are important.

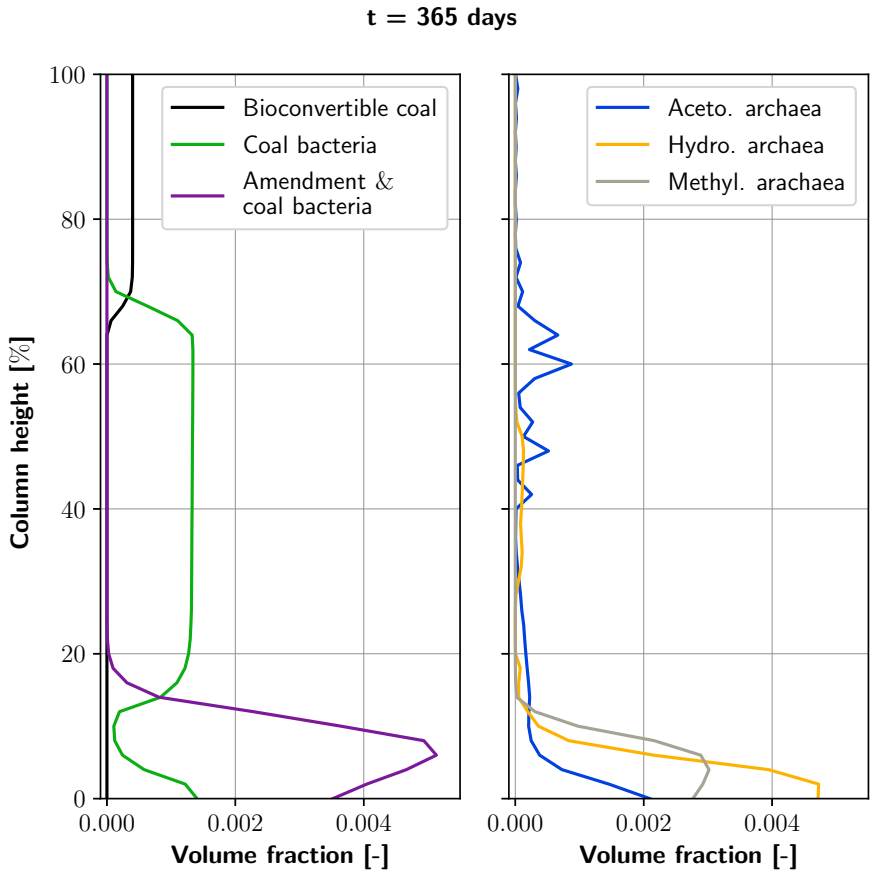

Figure 6.7: Distribution of microbial cells and bioavailable coal throughout the column on Day 365 as predicted for Case 4. The left plot shows the volume fraction of two types of bacteria and bioavailable coal, while the right plot shows the volume fraction of three archaeal groups. Reproduced with permission from Emmert et al. [2020b], CC BY 4.0 MDPI 2020.

6.4 Discussion

The focus of this study was on combining a previously validated batch reaction model Emmert et al. [2020a] with a well established flow and transport model Koch et al. [2020], solving all equations fully implicitly and monolithically. We have strong confidence in the reliability of the flow model since it has been validated repeatedly in different benchmarking studies Class et al. [2009], Flemisch et al. [2011, 2018]. Some studies indicate that biofilms might change their composition or behaviour under the influence of flow and transport [Besemer et al., 2007, Rochex et al., 2008], while others even report seasonal cycles [Lyautey et al., 2005]. Regarding biofilm in porous media, Kim et al. [2010] mention that "Darcy's velocity influenced the superficial morphology of biofilm and initial time of clogging, whereas substrate concentration affected the biofilm density and the rate of clogging". However, a study by Fang et al. [2017] reports that there is no significant change in communities' richness or diversity for river beds with static or dynamic conditions. As we model processes in porous media taking a step from a batch system to a flow-through column, we assume a difference in biofilm behaviour for our systems due to either flow velocity or the different substrate concentrations due to transport of components as reported by Kim et al. [2010]. Therefore, this study uses four different modelling cases to investigate various mechanisms in a comparison between one another, and, as importantly, in a comparison between the model and the available experimental data. It is an important detail to mention that the experimental study provides hints on the conversion from coal and amendment to intermediate products and to methane. Davis et al. [2019] found that most of the measured methane production in the experiment can be attributed to the coal.

Therefore, special attention has to be given not only to the methane production, but also to how the substrates (coal and amendment) are consumed along the column.
The first modelling case, as shown in Section 6.2.1 and Figure 6.2, is the first step when moving from a batch system to a flow reactor. Other studies indicate that batch kinetics can not be simply applied to flow studies in biofilm-affected systems without consideration of decreases in reaction rates due to substrate gradients inside the pores, diffusion limitations, and non-homogeneous flow conditions Grösbacher et al. [2018]. Therefore, the assumption of reducing the initially present biofilm volume fraction is a crude, but effective treatment when one assumes that the biofilm activity decreases due to substrate gradients and diffusion limitations in flow systems containing attached

microorganisms when moving biofilms from a batch reactor to a flow reactor. At first glance, the modelling results fit the methane production curves reasonably well, and they show that at least for the initial 100 days a model with such assumptions could theoretically produce a result that reflects the general behaviour of the experiment. We argue, however, that this could build false confidence, as the methane production clearly levels out in the model after 100 days, and the substrate consumption, with all bioavailable coal being converted after 60 days, does not reflect the experimental data.

With the first case not representing the results adequately, we want to discuss in the following Hypothesis 1 (see Sec. 4.2) that postulates a clogged inlet and, consequently, retardation of the amendment. The modelling scenarios for Cases 2 and 3 are investigating this hypothesis. The second modelling case as shown in Section 6.2.2 and Figure 6.3 is based on the observation by Davis et al. [2019] that a large amount of amendment or biofilm accumulated in the inlet region of the column. This could lead to a behaviour of amendment addition that is best described in the model by a continuous addition instead of the pulse-like fashion assumed for Case 1. In this scenario, the methane-production data show a more continuous and larger increase for the first 150 days of the modelling study. Also, the substrate-consumption study shows a more realistic outcome with slowly increasing and then decreasing amendment consumption. However, all bioavailable coal is again predicted to be consumed within the first 75 days. So even though this hard-coded change of the inlet conditions seems to enhance the model fit visually for the methane production, it still fails to match the observation of methane generation primarily from coal over the 200-day period as described in Davis et al. [2019]. With these results, we do not consider Hypothesis 1 fully justified, even though the changes in the model lead to a higher and more continuous methane production than in Case 1.

The first two cases clearly consumed all bioavailable coal within the first 75 days, and thereby do not fit the experimental results as described in Davis et al. [2019]. However, it is interesting to see that with a few basic assumptions the overall trend of methane production can be matched, even though major drawbacks regarding the substrates (coal and amendment) remain.

Hence, the third modelling case implemented a new feature in form of a filtration or retardation equation. It is shown in Section 6.2.3 and Figure 6.4, that this retention of the amendment helps in establishing a continuous methane production over a period

of up to 1000 days. The trapped amendment is not available to the microbes, and thus represents a local storage or retardation. Therefore, only small portions of amendment are available in the column at all times and the microbial community uses most of the amendment, whereas without trapping, e.g. as in modelling Cases 1 and 2, the amendment is partially washed out of the column. The trapping of amendment supports continuous growth of the microbes along the column which in turn helps in converting most of the added amendment to methane. With continuous release of amendment, coal and amendment bacteria grow more continuously and convert coal and amendment. Therefore, this modelling case produces the most cumulative methane as the microbes are continuously fed by the amendment and the coal as long as it is available. All the bioavailable coal along the column is consumed within approximately 50 days, which is the shortest period for all modelling cases. However, with the already established and active biofilm in the column, the model fails to match the observation by Davis et al. [2019] of slow coal conversion until the end of the experimental study. This prediction can be explained by the continuous feeding of the biofilm with amendment due to repeated retardation and release of the amendment based on changes in shear stress due to biofilm growth implemented with Eq. (3.20). The biofilm grows faster due to the changed availability of the amendment and as a result consumes the coal faster. This is derived from a comparison of coal consumptions from Figures 6.2b, 6.3b, and 6.4b. The model predicts the coal to be consumed up to 10 days earlier for Case 3 in comparison to Cases 1 and 2. Figure 6.4b additionally shows that amendment is mostly available at a low concentration for the microbes, whereas peaks in amendment concentration are visible for Cases 1 and 2. If at one point in the column, all bioavailable coal is converted, but amendment is still being released, the amendment is being transported downstream to support further biofilm growth. The implementation of Hypothesis 1 for Case 3 seems to approximate the results of the experimental study better than Case 2. Regarding the modelling, it also introduces additional degrees of freedom, as retardation of amendment can be adapted and fitted to the experimental results. With these findings, Hypothesis 1 is still not fully confirmed, but the implementation of amendment retardation yields a result that supports continuous growth of the microbial community by constantly releasing small portions of amendment over a long period of time. Namely, amendment is modelled to be present in the column for approximately 1000 days in Case 3, while it vanishes after approximately 150 days in Case 2. However, this implementation of Hypothesis 1 is not in line with what Davis et al. [2019] observed in the experiments, that primarily coal is converted. Thus, we have to conclude that

we can not explain the results with Hypothesis 1 alone. Therefore, Hypothesis 2 needs to be evaluated and discussed.

The fourth and last modelling case models the retardation and release of amendment as in Case 3 and additionally implements a microbial cell injection combined with cell attachment and detachment. This means, that the biofilm is not initially homogeneously distributed everywhere along the column anymore, but is now subject to constant changes due to flow and transport. In other words, this investigates the combination of Hypotheses 1 and 2. This model adds significantly more complexity, as cell attachment and detachment are – among others – again dependent on the velocity, the pressure gradient, and the porosity in the column. While the first 200 days of modelling match the experimental data visually in Figure 6.5, a few remarkable changes occur: Methane production at the end of the column occurs earlier than for all other cases. Since we model the cells now as being injected, and, as soon as the cells attach, assume a fully established biofilm, the volume fractions of biofilm in the influent region of the column are larger than for the other cases. All other cases only had a relatively small volume fraction of biofilm present in the beginning. If substrate arrives, biofilms need to grow and establish their food network first, before they produce large amounts of intermediates and end products. Therefore, the conversion of coal and amendment starts right away and an initial increase in methane production (Figure 6.5a) as well as a small but early decrease in coal availability can be observed (Figure 6.5d). After this, the microbial cells gradually detach, transport downstream, and reattach to form new biofilm. This leads to the continuous methane generation in the column, and the continuous decrease in coal consumption.
For Case 4, $DuMu^{x}$ $Coal^{+-}$ basically shows depletion of amendment around Day 300 and the subsequent continued methane generation can be attributed to the conversion of coal by the enriched biomass while still consuming parts of the coal until Day 500. Coal and amendment are the primary substrates, which are converted to intermediate products by two types of bacteria. The intermediate products are then converted to methane. What is observed here is that on the one hand, the bacteria are growing along the column because coal is continuously available. The bacteria produce intermediate products from the bioavailable coal and amendment, and these products are then transported along the column. As soon as the available amendment vanishes, the intermediate products are produced no longer in sufficient amounts. The archaea are also establishing along the column and in the beginning find reasonable amounts

of intermediate products as their substrate. With less intermediate products being available along the column, the archaea slowly decay as their substrate becomes less and less available. As soon as the archaea are not well established downstream of the intermediates-producing bacteria anymore, the methane generation in the column decreases. This is explained in more detail in Appendix 6.3 and Figures 6.6 and 6.7. With the bacteria still active, the coal is converted in the model, nevertheless.
Similar behaviour can be observed for $DuMu^{x}$ $Coal^{++}$, except for a small patch of archaea that manages to attach and grow downstream of intermediates-producing archaea. Due to this, the archaea can grow up again, detach and attach further downstream to produce additional methane from Day 250 on.

The resulting methane production as well as the substrate consumption are now in line with the findings of Davis et al. [2019]. The results show that cell attachment and biofilm detachment have significant effects on the model output. However, the model output still does not match the experimental data in every detail. With this case, we have shown that different processes interact in the model and while Hypothesis 1 alone was not able to explain the experimental findings, the combination of Hypotheses 1 and 2 leads to a model result that captures the key elements of the experimental study. This study provides a description of the possible processes without going into too much detail and without putting a focus on the fitting of many parameters that do not have experimental justification with the available data. Still, a basic approach of attachment and detachment for microbial cells was implemented using Eq. (3.20) with a Rittman's exponent of "0.58" which obviously would deserve fitting in a future joint numerical and experimental study, where also the attachment and detachment processes related to MECBM production should be addressed in detail.
Concluding this part of the discussion, we note that the presented attachment and detachment equations and parameters should be handled with care. What we present is a first step that shows the direction for future modelling and experimental investigations.

Finally, let us briefly comment on adsorption. It is known that small amounts of the newly generated methane might adsorb to the coal and thus we should expect the model to slightly overestimate the methane produced from the column. The model can easily account for adsorption. Still, we refrained from doing so since we do not have reliable data to quantify adsorbed methane under the pressure conditions we have in the flow-through experiment.

6.5 Conclusions

Processes related to microbially enhanced coal-bed methane are extremely complex and strongly interacting. In this study, we introduce a numerical model that couples a previously validated batch-reaction system fully implicitly to a well-established flow and transport solver. This model was used to test various hypotheses on mechanisms that affect MECBM production in flow-through columns.

Two hypotheses, see Chapter 4, were investigated by using four modelling cases implementing different assumptions regarding possible mechanisms. Hypothesis 1 states that not all amendment is transported into or through the column but might have been trapped in the inlet region of the column during the injection. Hypothesis 2 states that with flow and transport occurring in the column, microbial cells need to attach to the coal surface and grow. The results show that batch kinetics coupled to flow and transport in upflow column reactors might yield reasonable results for an initial time period; but this approach fails to match the experimental data in the long and indicates that further processes need to be considered in the coupling of MECBM reactions in flow through porous media.

In one case, we implemented inlet clogging, in another one retardation of amendment in the model. It is shown that methane production is prolonged and matches the experimental methane production results better than in the first case. However, a closer look at substrate consumption indicates drawbacks of this approach, mainly since a homogeneous biofilm distribution yields coal and amendment consumptions that are not in line with experimental findings from Davis et al. [2019]. Therefore, Hypothesis 1 alone is not sufficient to explain the presented results.

The last approach in this study uses attachment and detachment of microbial cells and new biofilm growth combined with retardation effects for the amendment. In essence, this one appears to be the most realistic of the four approaches evaluated here. The methane production matches the experimental results well and substrate consumption predictions are in line with experimental data from ^{13}C labelled studies. With this combination of Hypothesis 1 and Hypothesis 2, the experimental findings of Davis et al. [2019] can be explained reasonably well, indicating that both amendment retardation and microbial cell attachment and detachment are relevant. We refrain from further "tuning" of parameters for this study. A scientific value beyond merely

an expected better match to the experimental data can only be achieved with another joint experimental and numerical effort, which produces additional data.

To conclude further, we have shown that the numerical model can substantially aid in testing hypotheses and providing a basis for discussions; for example, specifically for this problem, the effects of attachment and detachment of cells as well as amendment retardation are of importance. The model allows to analyse the complex interacting processes in detail. The discussion has demonstrated that there are a number of interesting effects which cannot be distinguished in sufficient detail in experiments, since even simple column experiments on processes of this complexity have a black-box character. Therefore, we suggest that further modelling can consider these processes and focus on the fine-tuning of the processes and parameters such as e.g. the Rittman's exponent, $\lambda^{\kappa}_{attach}$, and $\lambda^{\kappa}_{detach}$. Of course, this should be accompanied by further experimental evidence. The model, as it exists now, allows for the evaluation of the listed and possibly other parameters which subsequently might become the focus of future experimental work. We should note as well that not all the effects observed in the model need to be necessarily a physically relevant phenomenon. We advise here some care and, in particular, further work on cell attachment, biofilm detachment, cell re-attachment and re-growth, as well as amendment retardation could improve knowledge and predictions of MECBM production in unmineable coal beds. More sophisticated modelling approaches regarding filtration and attachment-detachment processes are available and could be optimized to compare against new experimental column-scale results. Also, the assumption that the biofilms are all fully active once the cells are attached can be discussed in the future, since a lag-phase or something similar with low production in the beginning is usually observed for biofilms.

7 Sensitivity analysis of column studies

Many parameters are used when modelling MECBM production processes. To investigate the importance of the different parameters and their uncertainty in modelling, a sensitivity analysis (SA) is performed. SA, according to Saltelli et al. [2004], shows how the variation in the output of a model is related to different sources of uncertainty or variation in the inputs. It is accepted as a fundamental part of good modelling practice in environmental modelling. With the help of a SA, (i) important modelling factors can be prioritized, (ii) models can be validated, and (iii) factors that do not provide large contributions can be fixed and thereby eliminated.
In this study, we use the software tool SALib [Herman and Usher, 2017] to set up and evaluate the sensitivity of input parameters on the methane production output for column Cases 1, 3, and 4 from Chapter 6. The input parameters considered for this SA are the microbial reaction kinetics (e.g. microbial growth rates or yields) and, where applicable, the attachment and detachment factors for amendment and microbial cells. A reduction of input parameters is performed, before starting the SA to decrease the necessary amount of model runs. With this decreased set of parameters, more than 20 000 model runs are performed. For the Markov Chain Monte Carlo (MCMC) approach that SALib uses, this amount of model runs is considered few. However, the total CPU time was over 2.5 months and more runs did not seem feasible. Each microbial conversion process mentioned in Chapter 2 and displayed in Figure 2.1 is only approximated by one factor that is varied with $\pm 5\,\%$ during the SA. This results in SA factors as e.g. FAcAm, that is a single-varied factor influencing the production of acetate (Ac) from amendment (Am). It includes all yields and growth rates for this process and scales them. In addition to the microbially dependent parameters, the amendment deposition (filtration) and resuspension parameters (Cases 3 and 4), as

well as the microbial attachment and detachment parameters (only Case 4) are varied where applicable. The three different cases are investigated individually first, and transformed into a sensitivity heatmap later. The heatmap allows an easy comparison of parameter sensitivities for the different test cases.

7.1 Sensitivity analysis theory

This is a general introduction to sensitivity indices. For the sensitivity analysis, the MECBM model with all its details is taken as black-box model with input factors that can have an effect on the output. The effect of each factor, parameter or combinations of parameters is evaluated in sensitivity indices. These indices can be evaluated in several forms, and the focus of this study is on the first-order Sobol indices and total-order Sobol indices [Sobol, 2001].

7.1.1 First-order Sobol indices

The so-called first-order Sobol indices measure the contribution to the output variance by one model input alone. Therefore, a model Y, with factors X_i, in the form of $Y = f(X_1, X_2, ...X_k)$ shows a variance based first order effect V_i of:

$$V_i = V_{X_i}(E_{X_{\sim i}}(Y|X_i)), \tag{7.1}$$

with V_{X_i} and E_{X_i} as variance or mean taken over X_i, and $V_{X_{\sim i}}$ or $E_{X_{\sim i}}$ taken over all factors but X_i.

A first-order Sobol index S_i captures the "main effect" of its parameter by

$$S_i = \frac{V_i}{V(Y)}, \tag{7.2}$$

with $V(Y)$ being the unconditional variance of Y, when all factors X_i are able to vary. $S_i = 1$ would imply that all variance of Y is only driven by X_i. The first-order Sobol indices are assumed to be additive.

7.1.2 Total-order Sobol indices

The total-order Sobol index S_{Ti} measures the contribution to the output variance caused by a model input, including both its first-order effects (the input varying alone) and all higher-order interactions with other factors [Herman and Usher, 2017]. It is calculated as:

$$S_{Ti} = \frac{E_{X_{\sim i}}(V_{Xi}(Y|X_{\sim i}))}{V(Y)}. \tag{7.3}$$

However, the total-order indices are not necessarily additive anymore, due to their higher order interactions with other parameters being account for in S_{Ti}, meaning that $\sum_{i=1}^{d} S_{Ti} \geq 1$. Since the MECBM model and its parameters are highly interacting, first-order Sobol indices have shown to be lower than total-order Sobol indices. Herman and Usher [2017] state that total-order Sobol indices should be used for evaluation if higher-order interactions between the model inputs are present and first-order Sobol indices are significantly lower than total-order Sobol indices. Therefore, only total-order Sobol indices are discussed in the following.

7.2 Results of sensitivity analysis

The results for the individual sensitivity analysis of each test case is given in the following sections. The total-order Sobol indices are plotted over time for each factor that is changed in the respective modelling case. A large total-order Sobol index, indicates that the parameter has a large influence on the output of the model at that time, or in other words: is potentially of importance with respect to the methane production. A lower value indicates that the changes of the input parameter do not have a large influence on the outcome of the model result. Note, that the results of this SA could look different and lead to other Sobol indices, when analysed for other output data or for a longer timespan.

7.2.1 Sensitivity analysis results for Case 1

The SA for Case 1 of the column studies is an investigation where only the microbial production yields and growth rates are varied as input parameters and the effect on the output of methane production is analysed in Figure 7.1 over time.

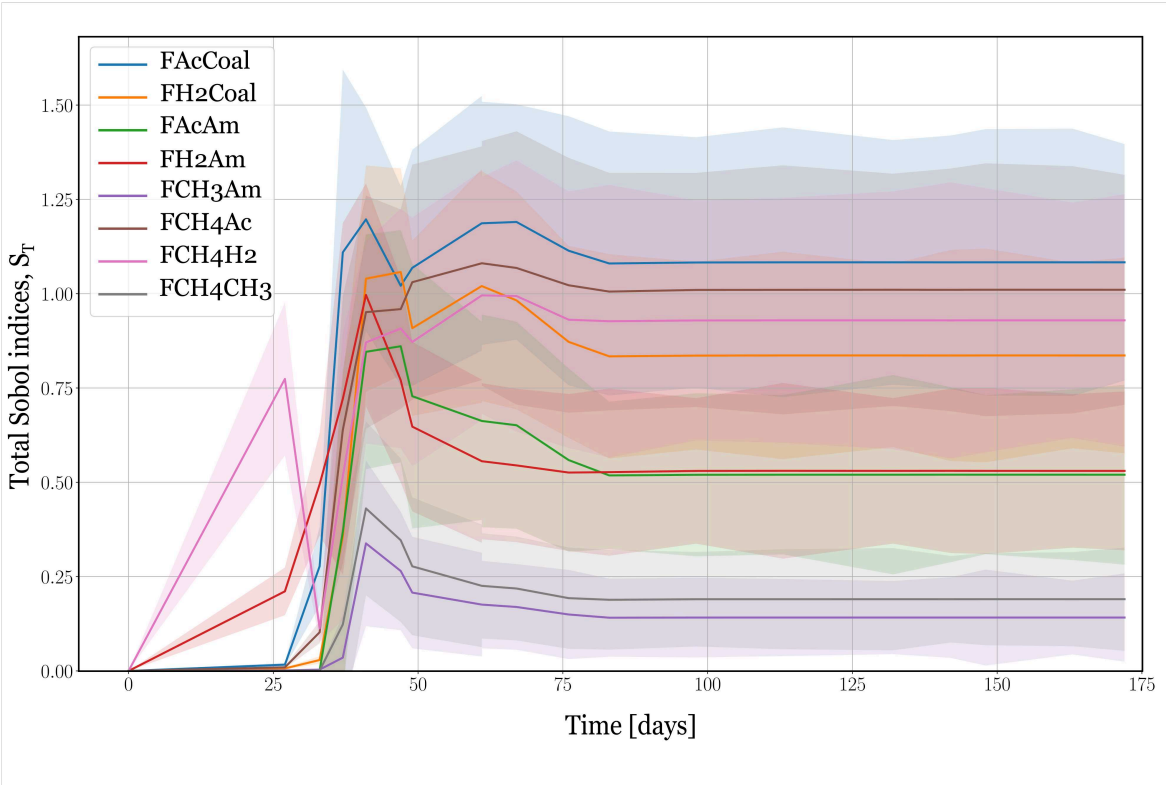

Figure 7.1: Result of the sensitivity analysis results for Case 1, with only microbial factors varied with ±5 %. The total-order Sobol indices for all varied parameters are shown over 172 days. The Sobol indices and their confidence intervals are computed for methane production output at the end of the column.

The eight different parameters are all part of the conceptual model process shown in Figure 2.1 and enhance or decrease certain reactions in total. As shown in Figure 7.1, total-order Sobol indices of FH2Am (red) and FCH4H2 (pink) increase to 0.21 and 0.77 for the first 27 days, while all other parameters do not show significant values. This is expected, as the system does not produce significant amounts of methane for the first 20 days and thereby the overall small methane production seems to be dominated by conversion of amendment to hydrogen via factor FH2Am and the subsequent conversion of hydrogen to methane via factor FCH4H2.

After Day 27, all other parameters show increased total-order Sobol indices, indicating that changes in the input of those parameters now also have an influence on the model output. While FH2Am continues to increase to a Sobol index 0.99 until Day 41, FCH4H2 decreases rapidly on Day 33 and then rises again with all other parameters until Day 41. Most parameters range between 0.5 and 1.2 for the rest of the period, with FAcCoal and FCH4Ac taking the largest Sobol indices, indicating that now also the conversion from coal to acetate and acetate to methane is of importance. It is interesting to see that FCH3Am and FCH4CH3 always stay below a Sobol index of 0.45, and thereby play a relatively minor role with respect to the total model output.

From Day 41 until Day 83, only small changes in Sobol indices are visible for most parameters, whereas after Day 83 no significant changes occur any more. The apparent peak of Sobol indices between Days 41 and 49 can be attributed to the way the model output is generated. During this time, the maximum increase in methane production was observed during the modelling studies. Since there is two initial substrates (coal and amendment) and three archaeal ways of producing methane, all varied parameters can lead to large changes in the model output during this period and clearly important or unimportant parameter can be estimated as they all have influences. Additionally, the sum of Sobol indices is well above 1, showing that higher-order interactions between the parameters have a large influence on the model output.

7.2.2 Sensitivity analysis results for Case 3

The SA for Case 3 is a study, where in addition to the parameters regarding the microbial reactions, filtration or retardation processes of amendment are modelled. They are implemented using deposition and resuspension functions of amendment and are, among physical parameters as e.g. pressure, dependent on either a deposition and a resuspension parameter, which are now also added to the SA to be varied. Therefore, not only the microbial production yields and growth rates from Case 1, but also the effect of amendment retardation, has an influence on the output of the model in Figure 7.2.

The initially important Sobol indices for this case are FCH4H2, FAcCoal and FCH4Ac, with values of 0.42, 0.35 and 0.15 on Day 27. The increase of FAcCoal and FCH4Ac is correlated and indicates the importance of the conversion from coal to acetate and

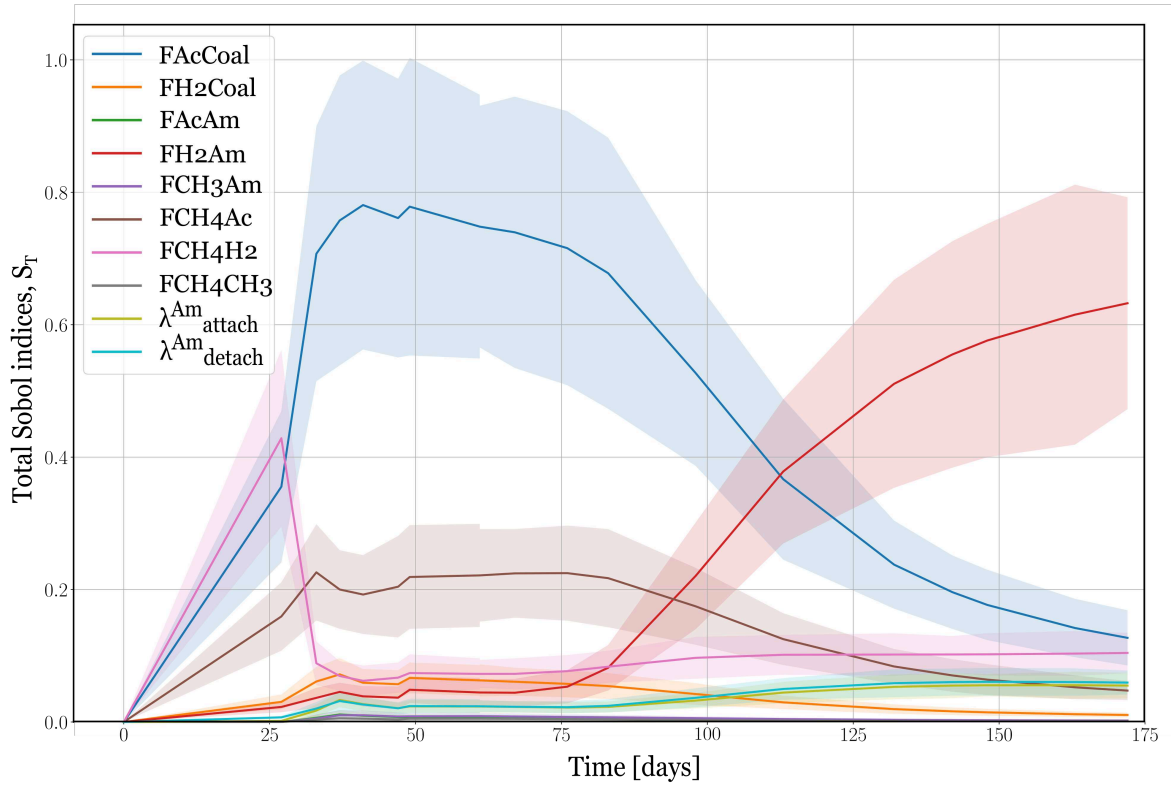

Figure 7.2: Result of the sensitivity analysis results for Case 3, with variation in the microbial factors and amendment deposition and resuspension factors (filtration like behaviour), all varied with ±5 %. The total-order Sobol indices for all varied parameters are shown over 172 days. The Sobol indices and their confidence intervals are computed for methane production output at the end of the column.

methane in the end. Apparently, FCH4H2 is a sensitive parameter in the beginning, as hydrogen is produced in the initial stage through either coal (via FH2Coal) or amendment (via FH2Am) and subsequently converted to substantial amounts of methane as indicated by the large Sobol index of FCH4H2. The hydrogen producing factors FH2Coal or FH2Am show a minimal increase on Day 27, but seem to not have a large influence at that time.

With the initial stage finished after Day 27, the following days until Day 83 show a different picture. Now FAcCoal seems to be dominating with constantly high Sobol indices at around 0.75. FCH4Ac stays at a Sobol index of above 0.2 and is in line with the high Sobol index of FAcCoal. The combination of those two parameters indicates a large influence of the acetoclastic pathway for methane production with acetate production from coal. The previously high Sobol index of FCH4H2 now decreases to values

of 0.1 or below, indicating that the conversion of hydrogen to methane does not have large effects on the model output any more at this stage.

The last stretch from Day 83 until the end of the 172-day study now exhibits one more characteristic change. FAcCoal's Sobol index decreases slowly to 0.12 at Day 172, while FH2Am increases from below 0.1 on Day 83 to over 0.6 at Day 172. The Sobol indices of all other parameters stay at relatively low values of around or below 0.1. This significant change of values for FAcCoal and FH2Am can be explained with the shift of bacteria from primarily converting coal to now converting amendment. FAcCoal shows to lose importance with respect to the methane production after Day 83, which is explained by most of the bioavailable coal along the column being consumed (see Figure 6.4b). Therefore, varying FAcCoal as an input does not have a large effect at that time any more. In contrast to this, amendment is now being trapped within the column for this case. As it is constantly released in small portions, the amendment and coal consuming bacteria now primarily consume the small portions of available amendment. With this, the increase of the FH2Am Sobol indices is explained. Consequently, the Sobol indices of amendment deposition and resuspension factors $\lambda^{\mathrm{Am}}_{\mathrm{attach}}$ and $\lambda^{\mathrm{Am}}_{\mathrm{detach}}$ each increase from 0.02 on Day 83 to approximately 0.06 on Day 172.
As an overall trend, the factors FAcCoal and FH2Am seem to dominate the system, closely followed by FCH4Ac and FCH4H2 which are successors of the first two factors and naturally depend on them. Interestingly, the amendment deposition and resuspension parameters show no large influence in the beginning and stay at a low level, but increase in importance towards the end. This is in line with the findings from Chapter 6 and indicates, that the system is dominated by the homogeneously distributed biofilm along the column for the first approx. 80 to 100 days independent of amendment retardation effects.

7.2.3 Sensitivity analysis results for Case 4

The SA for Case 4 combines the previous studies and adds attachment and detachment of microbial cells. Therefore, the parameters available for variation in the SA are the microbial reactions, filtration or retardation processes of amendment as well as attachment and detachment of microbial cells. The newly added attachment and detachment functions for microbial cells are dependent on the physical setup and use e.g. the local pressure gradient and porosity to determine the rate of attachment or detachment. Additionally, to the physical parameters, each function also uses one attachment or detachment parameter that can be varied in the SA. The influence of all these parameters on the methane production over time is given in Figure 7.3.

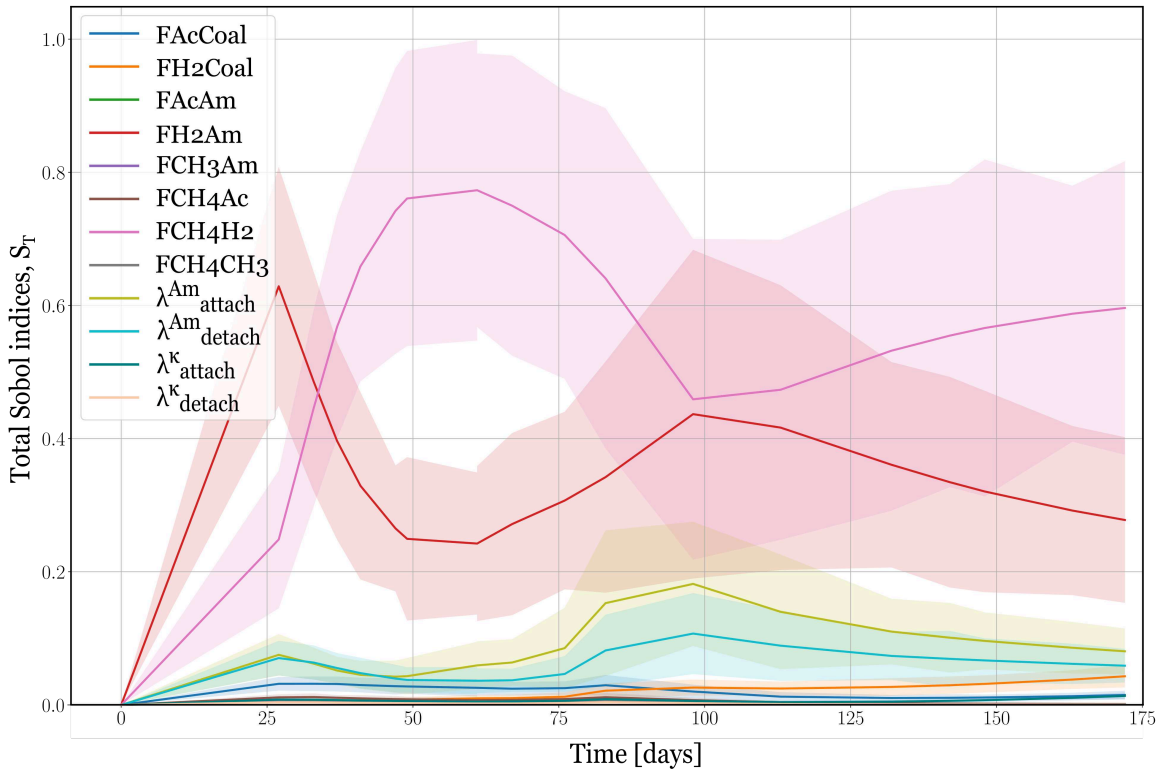

Figure 7.3: Result of the sensitivity analysis results for Case 4, with microbial factors, amendment deposition and retardation (filtration) factors, and microbial cell attachment and detachment factors, all varied with ±5 %. The total-order Sobol indices for all varied parameters are shown over 172 days. The Sobol indices and their confidence intervals are computed for methane production output at the end of the column.

The initially important Sobol indices for Case 4 are FH2Am and FCH4H2, with values of 0.62 and 0.24 on Day 27. The increase of FH2Am and FCH4H2 is correlated and indicates that initially most methane is produced from hydrogen, which in turn is produced from added amendment. While most other parameters do not show any significant Sobol indices on Day 27, $\lambda^{\mathrm{Am}}_{\mathrm{attach}}$ and $\lambda^{\mathrm{Am}}_{\mathrm{detach}}$ show a Sobol index of around 0.07, and FAcCoal of 0.03, all indicating that the output of the model is mainly governed by FH2Am and FCH4H2 and only partially by the deposition and resuspension ($\lambda^{\mathrm{Am}}_{\mathrm{attach}}$ and $\lambda^{\mathrm{Am}}_{\mathrm{detach}}$) or the conversion of coal to acetate.

As already observed for the other test cases, Sobol indices of FH2Am decrease after Day 27 to values below 0.25 after Day 49. In contrast to this, the Sobol indices of FCH4H2 continuously increase until Day 61 to a value above 0.77. With such a high value in relation to the lower values of all other parameters, FCH4H2 is dominating the system's response during that time. This trend is partially reversed from Day 61 until Day 98 for FCH4H2 and FH2Am again. The two parameters increase or decrease to almost the same Sobol index of approx. 0.45. Also, the deposition and resuspension parameters of amendment increase from Day 47 until Day 98 to Sobol indices of 0.18 for $\lambda^{\mathrm{Am}}_{\mathrm{attach}}$ and 0.1 for $\lambda^{\mathrm{Am}}_{\mathrm{detach}}$. With gaining influence on the model output of $\lambda^{\mathrm{Am}}_{\mathrm{attach}}$ and $\lambda^{\mathrm{Am}}_{\mathrm{detach}}$, also FH2Am gains importance, since $\lambda^{\mathrm{Am}}_{\mathrm{attach}}$ and $\lambda^{\mathrm{Am}}_{\mathrm{detach}}$ significantly determine how much amendment is available for conversion along the column. Therefore, when $\lambda^{\mathrm{Am}}_{\mathrm{attach}}$ and $\lambda^{\mathrm{Am}}_{\mathrm{detach}}$ increase, FH2Am is able to convert more amendment to hydrogen and thereby influences the methane production in the end.
The last stretch from Day 98 until the end of the 172-day study, FCH4H2's Sobol index increases again to 0.6, while FH2Am continuously decreases to 0.27 on Day 15. FCH4H2 and FH2Am are theoretically directly correlated, as they are in the same chain of conversion from amendment over hydrogen to methane. Therefore, it is reasonable that they are both of importance, but interesting to see that they are in a way competing for importance with respect to the model output measured in Sobol indices. The previously mentioned parameters $\lambda^{\mathrm{Am}}_{\mathrm{attach}}$ and $\lambda^{\mathrm{Am}}_{\mathrm{detach}}$ decrease gradually to Sobol indices of 0.08 and 0.05 on Day 172. All other parameters, except for FH2Coal, stay relatively unimportant with Sobol indices below 0.01 over the entire study. FH2Coal shows a slight increase towards the end of the study, but remains in a range that is close to 0. This is similar to FAcCoal during the first 50 days. No clear derivation or interpretation for those two parameters is performed at this stage, since the other parameters seem to dominate the system.

7.2.4 Sensitivity heatmap for Cases 1, 3, and 4

With a sensitivity heatmap it is intended to display similarities or differences in the importance of each parameter for the different test cases. As described in the previous sections, each parameter's Sobol index might vary over time for each test case. The individual Sobol indices of the parameters are now transformed and averaged over the entire time period to a single value for each parameter. These values are then plotted and colour-graded in Figure 7.4 with the three different investigated cases on the y-axis and the varied parameters on the x-axis. The colour-grading is achieved by normalizing the averaged total-order Sobol indices S_T with the sum over all S_{Ti} in the following way:

$$-\log_{10}(S_T/\sum_i S_{T,i})^{-1}. \tag{7.4}$$

The form of Equation (7.4) yields a positive value for all normalized values that are between 0 and theoretically 1. The higher the value, the more important is the corresponding parameter. The colour scale goes from light yellow (0 / unimportant) to dark red (3.5 / important). Only values of parameters that are also varied in this setup receive a coloured rectangle, so e.g. $\lambda^{\kappa}_{\text{attach}}$, which is the parameter for the deposition of microbial cells in the column, is only a parameter for Case 4 and is thereby left blank for Cases 1 and 3. Since the individual factors for each case are already discussed in previous sections, the key findings are only recapitulated here. For more details and the evolution of each parameter over time, please have look at the corresponding section.

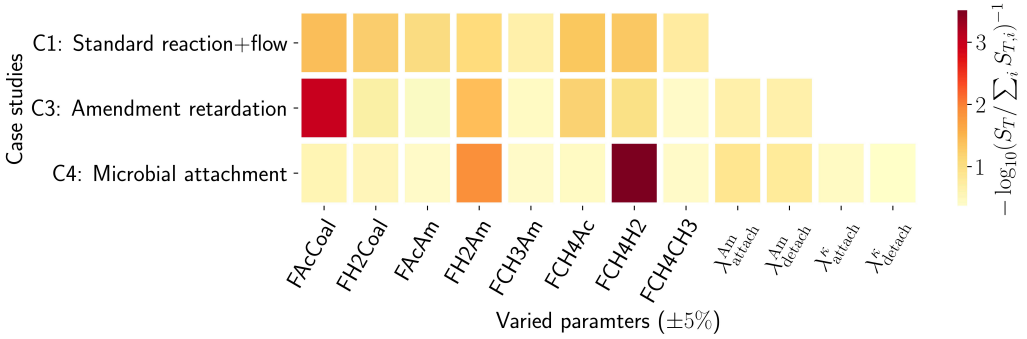

Figure 7.4: Sensitivity heatmap, ranging from not very sensitive (light yellow) to very sensitive (dark red) for three of the four column case studies. The parameters are each varied with ±5% of their pre-calculated value and only plotted where applicable. The colour grading is achieved by scaling the total-order Sobol indices.

The sensitivities for each case study are dimensionless and can range from 0 to up to 3.5 in their transformed and scaled version, in this study. As the untransformed values sum up to 1, each case study either has few very large (red) values and more lower (light yellow) values, or not so many lower values and more mid-sized (orange) values distributed over all parameters. Case 1, with only the reaction parameters allowed varying, shows almost equal importance of all parameters with Sobol values between 1 and 1.4. Only FCH3Am and FCH4CH3, which have values of 0.65 and 0.71, are an exception here, indicating that these parameters are unimportant in relation to the others. For the remaining parameters it is observed, that FAcCoal, FCH4Ac, and FCH4H2 are slightly more important.

A different picture is shown for Case 2, where for now in addition to the reaction parameters also deposition and resuspension of amendment are parameters. Here, FAcCoal seems to dominate with a value of 2.99, closely followed by FH2Am and FCH4Ac with 1.4 and 1.18, respectively. As already explained in Section 7.2.2, the conversion of primarily coal in the beginning and later the amendment leads to this result. FCH4H2 shows to be slightly more important with a value of 0.96, than the remaining parameters that stay below 0.6 for this case.
The last case is the study where microbial cells are allowed to attach and detach along the column with two new parameters $\lambda^{\kappa}_{\text{attach}}$ and $\lambda^{\kappa}_{\text{detach}}$. All previously mentioned parameters from amendment retardation and the reaction kinetics are varied, too. Case 4 now is dominated clearly by FCH4H2 and FH2Am with values of 3.5 and 1.9. This indicates a clear favourable pathway in the food-web (Figure 2.1), following the hydrogenotrophic pathway for methanogenesis from the conversion of amendment, for this case study. However, it has to be noted that for sake of computational, time only 172 days are evaluated and other parameters could become more important after that. With these two parameters taking such large values, the remaining parameters naturally have lower values. The amendment attachment and resuspension parameters $\lambda^{\text{Am}}_{\text{attach}}$ and $\lambda^{\text{Am}}_{\text{detach}}$ show values of 0.88 and 0.77, and are ranked third and fourth for this case study.

This SA and the heatmap was performed to illustrate similarities or contrasts in sensitivity for the different test cases. Only one clear similarity is obvious at first sight: FCH3Am and FCH4CH3 show to be relatively unimportant with respect to the model output for all cases. While no other set of parameters shows the same behaviour for all cases, different combinations of parameters show to be of importance for each case

study. We see e.g. for Case 4, that parameters FH2Am and FCH4H2 are linked, a similar link can be observed for Case 3 with FAcCoal and FCH4Ac, and partially also with FH2Am and FCH4H2, even though the link is not as strong there. Only for Case 1, an almost uniform importance of all parameters is observed. All other cases show distinct increases in certain parameters.
The evolution of $\lambda^{\mathrm{Am}}_{\mathrm{attach}}$ and $\lambda^{\mathrm{Am}}_{\mathrm{detach}}$ for Case 3 and Case 4 is interesting, too. $\lambda^{\mathrm{Am}}_{\mathrm{attach}}$ and $\lambda^{\mathrm{Am}}_{\mathrm{detach}}$ were introduced for Case 3 and showed to be of minor importance there. This can be attributed to the fact, that the biofilm is assumed to be distributed homogeneously along the column. Added amendment is transported, potentially filtered and directly converted as soon as it is released again. Therefore, the model output is much more dependent on the conversion of amendment (FH2Am) and not so much on the deposition and resuspension. However, for Case 4, $\lambda^{\mathrm{Am}}_{\mathrm{attach}}$ and $\lambda^{\mathrm{Am}}_{\mathrm{detach}}$ show to be of more importance. The difference here is that the microbial cells are now also injected and transported. Therefore, the biofilm is not established homogeneously along the column anymore, but microbial cells need to attach first before they can convert amendment or coal. With this, the output of the model is also dependent on where amendment is trapped and resuspended, as not all resuspended amendment necessarily passes by a location with active biofilm. If the amendment deposition or resuspension is occurring too fast or too slow, the corresponding biofilm potentially has not established along the column yet, or decayed already.

Even though no clear pattern of parameters can be shown, the heatmap illustrates how the interactions between the parameters can have an influence on the Sobol index of each parameter. It is also interesting to see, that with changing physical processes for each case study (amendment retardation in Case 3, cell attachment in Case 4), the importance of the reaction parameters varies, while the corresponding physical parameters, e.g. for deposition or attachment, stay of minor importance in most cases. While this is also an effect of the limited simulation time, the effect of changing physical processes can be seen clearly in the variation of the other parameters. So even if they show lower total-order Sobol indices for a variation, they obviously influence the entire model response. Therefore, when talking about important or unimportant parameters, one has to keep in mind, that "unimportant" in the light of this SA only means that the variation of this parameter in its specified range does not have a large effect on the methane production i.e. the model output.

7.3 Discussion and conclusion of sensitivity analysis

With the data of the SA described, explained and briefly discussed in Sections 7.2.1, 7.2.2, and 7.2.3, this section has its focus on the main conclusion that can be drawn from this SA. It was performed to identify and potentially prioritize important modelling factors to validate the model and to provide a basis for potential future parameter fixing. While the last point is not investigated any further for this thesis, the other two aims were achieved. Important factors for each test case were identified, and with varying test cases, the parameters showed to behave differently when compared between another. The results are in line with the experimental and numerical results from Chapter 6, as different microbial pathways are supported with different physical settings.

An interesting observation for Case 1 is, that when only the microbial reactions were varied, most parameters were of almost equal importance. This is in contrast, to the other two test cases, where two parameters showed to be dominating the models output, while the remaining parameters only had minimal or almost no influence. Box and Meyer [1986] state that when performing a statistical analysis and determining important or unimportant parameters, the unimportance of certain parameters is necessary for optimization. As only with factor sparsity, meaning that most parameters are unimportant and that not all can be relatively important, further optimization is possible. While Box and Meyer [1986]'s statement holds true for Case 3 and Case 4, it does not for Case 1. Wider parameter ranges for Case 1 could be a way to clearly determine more important and less important parameters. However, this result also indicates that the pre-calculated values from the batch scenarios and the design of the model yield a result where all the microbial reaction pathways represent almost equal possibilities to produce methane and therefore, no clearly dominating parameter can be determined.
For Cases 3 and 4, the introduction of amendment deposition as well as microbial attachment and detachment leads to systems that clearly show the importance of certain parameters and the unimportance of others. For further studies, this knowledge could be used to employ e.g. factor fixing as a method to remove unimportant parameters from a future recalibration of the system. Additionally, a focus on the key inputs and parameters is now possible and code optimization, by simplification of e.g. partial reactions could be of interest in the future.

In summary, this SA demonstrated the importance of various parameters within the modelling setup. It was shown how the parameters interact and their influence on the methane production in total is illustrated for each test case individually and also in comparison with another by the heatmap. While each individual test case resolves temporal changes of each parameter, the heatmap averages over the entire modelling period. With changing the cases, and thereby changing the modelling basis, differences in parameter sensitivities can be observed, which are in line with findings from previous simulations. Therefore, a validation, meaning that the processes in the model behave as expected to input variations, is achieved. However, no clear most-important parameter for all different setups is identified. This is partially attributed to the three competing methanogenic pathways of producing methane, but also to the limited time-frame of the SA. However, when looking at the results of e.g. the substrate consumption in Chapter 6, the sensitivity analysis confirms these results and matches well to the applied assumptions.

8 Application of operator splitting to column scenarios

When modelling flow and transport with many components and complex, interacting reactions, a robust and efficient solution strategy is essential. The existing MECBM model was set up as a fully implicit (global implicit) model that solves flow, transport and reactions simultaneously, so far. Sequentially iterative or sequentially non-iterative schemes are reported to be more efficient in some modelling cases [Steefel et al., 2015, Carrayrou et al., 2004], while often only introducing small splitting errors. Therefore, sequential non-iterative approaches are investigated as a first step towards a potentially more efficient MECBM model solution strategy.

For this special test case, the fully (or global) implicit approach (GIA) is solved as a reference test case with a high spatial resolution (80 cells over the height of the column). We use the same spatial resolution for all OS methods, and consequently compare against the reference solution using the same time steps and time-step sizes. Historically, the GIA shows a potential limitation when modelling large systems with many components and many grid cells as e.g. for a field scale simulation. There, the Jacobian matrix needs to be computed, stored, and inverted, which results in massive memory usage and CPU time when the system is solved. However, with evolving computer technology, memory usage and CPU time are not as restricted anymore and the GIA is also applied to larger systems [Helmig et al., 1997, Class et al., 2009, Steefel et al., 2015].
Nevertheless, we investigate operator splitting approaches here to see if they can be a valuable and efficient tool to enhance the solution strategy of MECBM models. Especially for future studies and investigations on the field-scale, this preliminary work can be of interest. In general, OS methods have been investigated for many reactive transport problems and applications [Lichtner, 1996, Steefel et al., 2015, Hron,

2015]. Theoretically, the different parts of a reactive-transport system can be solved separately, and thereby a speed-up is achieved. The hyperbolic transport equations are solved first, and the reactions reduce to local ODEs at each node or grid cell, which theoretically is good for parallelization. However, no parallel computation is implemented and presented in this thesis. Therefore, a computational speed-up is only achieved by separating the non-linear reaction terms from the flow and transport term in the context of this thesis.

8.1 Adaption of column test case

To investigate the behaviour of the MECBM model with applied OS techniques, only Case 1 with the DuMu$^{\text{x}}$ Coal^{+-} setup from Chapter 6 is investigated for 115 days of simulation time. Case 1 can be adapted to match similar reactive-transport models listed in literature rather easy, while all other cases would impose further challenges to the OS schemes. A study by Wang [2019] already investigated decoupled solution schemes for a MECBM model. One of the findings is, that phase transitions from two-phase to single-phase flow or vice versa, increase computational demand and introduce further error for OS methods compared to the GIA. Therefore, the column investigated for this study, is constantly injected with an additional gas phase ($v_n = 1 \times 10^{-6}\,\mathrm{mol/m^3}$), keeping the two-phase flow regime more stable over the entire study. Since additional errors from phase transitions would decrease the significance of the results, we take these steps for now.

Wang [2019] also presents that an iterative OS scheme, which essentially refines the SNIA approach by iterating the solution until some convergence limit ϵ is matched, does not converge well and does not yield reasonable results due to microbial growth rates. SIA methods are used for reaction systems that either define an equilibrium state or implement a reversible kinetic. However, the Monod kinetics do not show this reversible behaviour for the microbial growth, therefore, the growth of microbes is accumulated during iterations. Consequently, no dynamic equilibrium can be found within a reasonable time and the iteration step fails. Therefore, only non-iterative approaches are investigated here further.

8.2 Operator splitting schemes in DuMu^x

A short summary of the different OS approaches, explained in Section 3.6.2, alongside details on the implementation in the numerical software framework DuMu^x is presented in this section. We investigate two general splitting techniques, see Section 3.6.2: First the so-called sequential non-iterative approach (SNIA), where a transport step is solved and the solution of the transport step is then inserted as initial condition into the reaction step. This simple scheme introduces a first-order splitting error of $\mathcal{O}(\Delta t)$.
The second scheme is the Strang sequential non-iterative approach (S-SNIA), where transport is solved for a half-timestep, then the reactions are solved for a full timestep and finally the second transport half-timestep is performed. The S-SNIA is reported to gain computational efficiency with linear reactions, at the cost of an error with $\mathcal{O}(\Delta t^2)$. Hundsdorfer and Verwer [1995] propose to switch the order of transport and reactions, as this might result in better convergence for some reactive-transport simulations. The approach from Hundsdorfer and Verwer [1995] is investigated, but shows to produce slightly larger errors while taking approx. the same CPU time for our investigations. Therefore, the results are not further explained and shown.

The accuracy of the OS approach is assessed by comparing all concentration profiles obtained with the OS method against the GIA results, which is assumed to give the correct reference solution. The errors can be quantified after Steefel and MacQuarrie [1996] either with the L^2 norm or with the relative L^2 norm. The L^2 norm is defined as:

$$||y||_2 = \sqrt{\sum_{i=1}^{N_y} y_i^2}, \tag{8.1}$$

with N_y as the number of data points and y_i as the vector of concentration differences between the reference solution and the corresponding OS method $C_{\text{ref}} - C_{\text{OSmethod}}$. Note, that the L^2 norm has the units of molar concentration (mol/m^3), which is not further indicated throughout this work. The relative L^2 norm scales the value of the L^2 norm by the L^2 norm of the reference with $||y||_2/||C_{\text{ref}}||_2$. We use the relative L^2 norm for all further comparisons.

A study by Wang [2019] showed, that solving only the reactions and updating the concentrations did not work as expected, due to the highly coupled and interacting MECBM reaction system. Some reaction products (e.g. CH_4, CO_2, and H_2) are prone

to form a gas-phase and influence the local pressure and saturation and thereby the local mole fractions of all components. During each reaction step, these components are formed and influence the phase composition. If the phase composition is not updated in a reaction step, the following transport step is prone to converge slowly, or as in most cases, not at all. Additionally, some reactions might be influenced by the changed phase composition. To solve this problem, each reaction step is now accompanied by a phase-composition step, where the new composition of each phase with its resulting new pressure and saturation is calculated. This can be done explicitly or implicitly using a set of mass-balance equations that solve the reactions alongside the phase composition in the same step. Due to convergence problems for larger timesteps, this might result in a short series of reduced timestep sizes. The convergence issues occur with timestep sizes larger than approx. 1000 s. Results of SNIA and S-SNIA for these larger timesteps are shown nevertheless. However, the measured computational time might increase due to the temporal reduction of timestep sizes. Error calculations for these cases are also affected and are reduced, as reduced timestep sizes are assumed to better approximate the reactions.

8.3 Results of operator splitting approach

The results for the OS approaches are always compared against a reference solution that was obtained using the GIA approach with the same timesteps. Accuracy is measured using the relative L^2-norm defined in Section 8.2 after Eq. (8.1). Corresponding Damköhler numbers introduced in Eq. (3.31) are only assessed as a post-processing step at the end of the study. Total CPU times for the different approaches are compared in Table 8.1 and are explained in detail in Section 8.3.1. The total CPU time is defined as the entire time taken to set up the equations, solve them and write all output for the 115 simulated days. In addition to the total CPU time, the CPU time per timestep or OS-subprocess can be analysed. When not otherwise mentioned, the times always include set-up of the equations, solving the system and writing output.
First time measurements show, that for the SNIA the transport and reaction step take approx. the same CPU time. However, the explicit solve of the reaction ODE system e.g. with a $\Delta t = 100\,\mathrm{s}$ takes only 0.0054 s, while the equation assembly, total calculation of the new phase composition with all new variables takes 0.491 s. Solving the transport

step, with the phase composition automatically included, implicitly takes 0.69 s. While the exact times vary with different timestep-sizes as well as during the simulation, the relation stays approx. the same. The relatively simple ODE solve of the reactions is by up to two orders of magnitude faster, but calculating the phase-composition and all secondary variables takes up almost as much time as the transport step. A similar behaviour is observed for the S-SNIA, where the solve of the transport step is approx. two times faster than for the SNIA, but has to be done twice with a timestep size of $\Delta t/2$.

Overall, these first measurements show that while a computational speed-up can be observed for the individual sub-problems, the assembly of all equations, calculation of secondary variables, and the phase state and composition takes up significant amounts of computational time. This is due to the fact, that still all components are solved for each phase. This could be reduced theoretically, if the reaction system would be reduced and potentially only tracer components are used. Tracer components would only be transported with the phase-velocity and do not couple back to the phase composition. Additionally, these tracers could be solved explicitly again, which would increase speed-up as shown in a study by Peter [2019].

8.3.1 Comparison of runtime and accuracy

The runtime and accuracy of the SNIA and S-SNIA approach are compared against the GIA in this section. Table 8.1 compares the total runtime in seconds for the GIA, SNIA, and S-SNIA for varied timestep sizes, while Table 8.2 relates the runtime of the OS approaches to the corresponding runtime of the GIA approach, resulting in a "ratio of speed-up". Table 8.2 also calculates the relative L^2 error of the OS approach to the reference solution (GIA).
As shown in Table 8.1, different timestep sizes were investigated for all models. Only the results corresponding to the same timestep size are compared to ensure the exact same behaviour of all different approaches and allow for a fair comparison. However, not all OS approaches were able to run through with the defined timesteps. Especially for timestep sizes larger than 1000 s the OS approaches failed to converge. To solve this problem, the OS models are allowed to dynamically reduce the timestep size over a short period to ensure convergence. Therefore, the interpretation of runtimes, as well as

the error calculations are not as straightforward anymore for results with $\Delta t > 1000\,\mathrm{s}$. Runtimes are potentially overestimated, while errors might be underestimated for these results.

A general and obvious finding from Table 8.1 is that setting a smaller timestep size results in a larger total runtime. The SNIA is significantly faster than the GIA for all timestep sizes smaller 1000 s, while the S-SNIA shows to be faster for all variations performed in this study. The total runtimes of the GIA increase by a factor of almost 17 when comparing $\Delta t = 1000\,\mathrm{s}$ with $\Delta t = 50\,\mathrm{s}$, while the SNIA and S-SNIA only show an increase in runtime of approx. 10 or 12.

Table 8.1: Runtime comparison for three different operator splitting approaches in comparison to the GIA (as reference) for Δt ranging from 50 s to 6000 s.

Runtime [s]			
Δt [s]	GIA (ref)	SNIA	S-SNIA
50	2.23×10^5	1.31×10^5	1.31×10^5
100	1.15×10^5	6.68×10^4	6.58×10^4
200	5.89×10^4	3.44×10^4	3.28×10^4
500	2.58×10^4	1.44×10^4	1.45×10^4
1000	1.32×10^4	7.77×10^3	1.10×10^4
2000	6.97×10^3	7.03×10^3	5.70×10^3
4000	3.98×10^3	6.72×10^3	3.07×10^3
6000	3.04×10^3	5.15×10^3	2.45×10^3

We are now interested at the goodness of our reference solution by taking a look at the GIA solution with the largest Δt (12 000 s) to the GIA solution of the smallest Δt (50 s). They produce the same result with a relative L^2 error smaller 1×10^{-7}. It is therefore accepted as a reference for all other approaches.
All OS approaches with their relative L^2 errors and the ratio of speed-up in comparison to the GIA for the OS approaches are shown in Table 8.2.

For the SNIA, the runtime ratio is larger than 1 for all $\Delta t > 1000\,\mathrm{s}$, while it reduces significantly to approx. 0.6 or below for all other Δt. Not only runtime is important, but especially the relative L^2 error is of interest for this study. Relative L^2 errors reduce from 2.24×10^{-3} for $\Delta t = 6000\,\mathrm{s}$ to 3.02×10^{-5} for $\Delta t = 50\,\mathrm{s}$, which is as expected and reported from other studies [Steefel et al., 2015, Hron, 2015, Carrayrou et al., 2004].
The S-SNIA has a runtime ratio of 0.81 for $\Delta t = 6000\,\mathrm{s}$ that decreases to below 0.6 for all $\Delta t < 500\,\mathrm{s}$. Regarding L^2 errors, S-SNIA shows smaller or almost identical errors

for all Δt-variations as the SNIA approach. S-SNIA reduces the error from 2.09×10^{-4} $\Delta t = 6000\,\mathrm{s}$ to as low as 2.86×10^{-5} for $\Delta t = 200\,\mathrm{s}$. Further reduction of the timestep size does not show a decrease of L^2 error anymore for this study. An additional run of the S-SNIA with $\Delta t = 5\,\mathrm{s}$ showed an estimated error of 1.34×10^{-6}. However, the simulation was only run for the first 50 days of simulated time, while all other simulations were run for 115 days of simulated time. Therefore, the relative L^2 error is not given in the table and is potentially underestimated.

Nevertheless, both OS approaches show an increase in runtime and an increase in accuracy with reducing Δt. The speed-up in comparison to the GIA approach is obvious for all studies with $\Delta t < 1000\,\mathrm{s}$, while the S-SNIA performs better in terms of accuracy and speed-up for all but one case.

However, the real speed-up of interest is not when comparing against the runtimes of the corresponding GIA runs (with reduced Δt), but when comparing to the runtimes of a GIA solution with e.g. $\Delta t = 6000\,\mathrm{s}$. The major advantage of the GIA is the stability of the approach and its low errors. It even converges well with a maximum (adaptive) timestep size of $\Delta t = 12\,000\,\mathrm{s}$ and takes only $2.04 \times 10^3\,\mathrm{s}$ of total CPU time, making it faster and more accurate than all OS approaches, independent of the timestep size "refinement".

Table 8.2: Runtime comparison relative to GIA runtime and L^2 error comparison for Δt ranging from 50 s to 6000 s.

Δt [s]	t_{SNIA}/t_{ref}	$\|\|C_{ref} - C_{SNIA}\|\|_2/\|\|C_{ref}\|\|_2$	t_{S-SNIA}/t_{ref}	$\|\|C_{ref} - C_{S-NIA}\|\|_2/\|\|C_{ref}\|\|_2$
50	0.59	3.02×10^{-5}	0.59	2.89×10^{-5}
100	0.58	3.15×10^{-5}	0.57	2.88×10^{-5}
200	0.58	3.47×10^{-5}	0.56	2.86×10^{-5}
500	0.56	4.72×10^{-5}	0.56	3.76×10^{-5}
1000	0.59	7.23×10^{-5}	0.83	7.13×10^{-5}
2000	1.01	2.19×10^{-4}	0.82	1.42×10^{-4}
4000	1.69	1.39×10^{-3}	0.77	1.72×10^{-4}
6000	1.70	2.24×10^{-3}	0.81	2.09×10^{-4}

Visualization of runtime and accuracy results A combination of the runtimes from Table 8.1 and the relative L^2 error from Table 8.2 is visualized in the log-log plots of Figure 8.1. The top plot shows variations of the timestep sizes over the mass error calculated using the relative L^2 error defined after Eq. (8.1). The green dots represent the results of the SNIA, while the orange triangles represent the results for the S-SNIA. The same trends as previously described for Table 8.2 are observed. The S-SNIA generally produces smaller errors than the SNIA for this study. With reduced Δt both approaches show smaller errors, but error reduction slows down with $\Delta t < 100\,\mathrm{s}$. The error of the SNIA seems to reduce with $\mathcal{O}(\Delta t)$ for $\Delta t > 100\,\mathrm{s}$, which is as expected from literature [Steefel et al., 2015, Hron, 2015, Carrayrou et al., 2004]. Only the error of S-SNIA does not reduce as expected ($\mathcal{O}(\Delta t^2)$). Regarding Δt from 2000 s to 6000 s, the error stays approximately in the same order of magnitude for S-SNIA. This can be attributed to the convergence problems of the S-SNIA and the resulting reduction of timestep sizes. Since the timestep sizes were reduced to ensure convergence, the errors are reduced, too. From timestep sizes of 200 s to 2000 s, the expected reduction of error can be observed, but for all timesteps smaller than 200 s, no further reduction is visible in the case of S-SNIA. If this already is the splitting error, or due to the interacting reactions that build on each other, is not clear at this point. However, with sub-steps for the reactions, the problem of interacting and depending reactions could potentially be overcome and the error could be reduced even further.

When taking a look at the bottom plot of Figure 8.1, the timestep sizes are plotted against the total CPU time needed to solve the problem. The reference times for the GIA are plotted with blue squares, in addition to the SNIA and S-SNIA results explained above. This plot visualizes the results of Table 8.1 and demonstrates that the S-SNIA is generally the fastest approach for most investigated timestep sizes, closely followed by the SNIA. Only for larger timestep sizes the previously mentioned reduction of timestep sizes due to convergence problems leads to the shift in results. Interestingly, the S-SNIA stays faster for $\Delta t \geq 1000\,\mathrm{s}$. However, a small jump can be seen for $\Delta t = 1000\,\mathrm{s}$, indicating that the first convergence problems occur, which lead to an increase of total CPU time. Even though the reduction of timestep sizes was necessary for $\Delta t > 1000\,\mathrm{s}$, the approach stays the fastest overall.

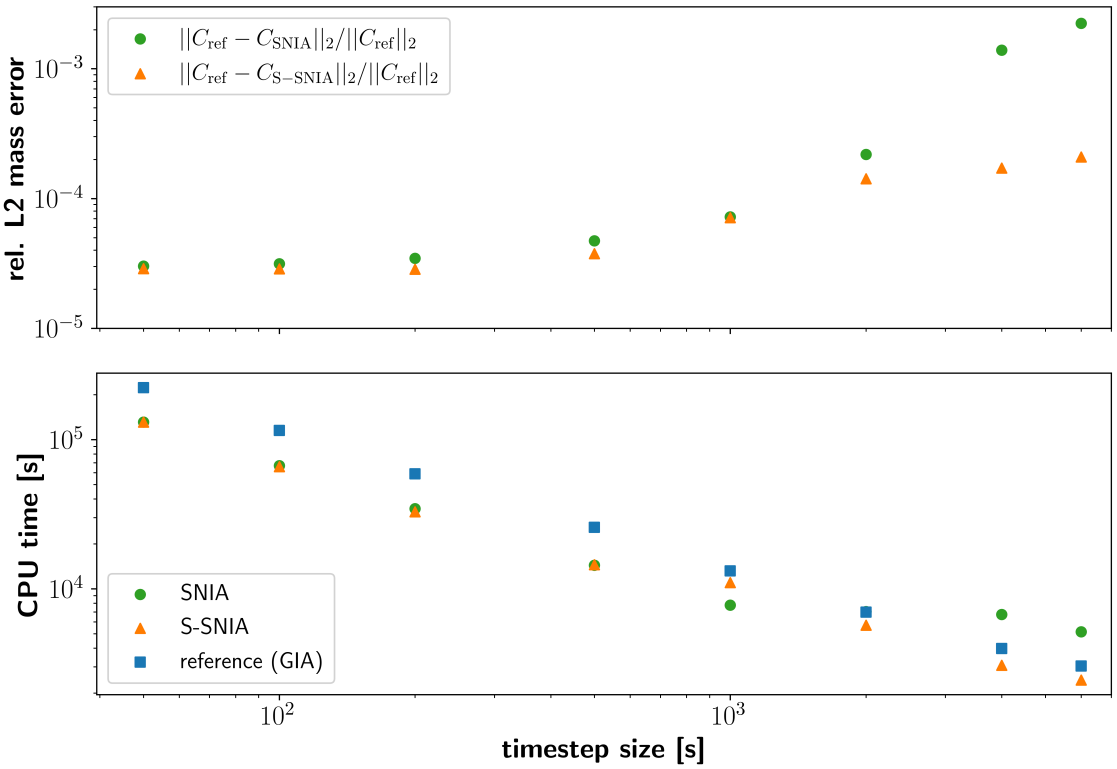

Figure 8.1: Comparison plots of operator splitting techniques for relative L^2 error and CPU time over varying timestep sizes. The splitting techniques of SNIA (green dots) and S-SNIA (orange triangles) are compared against the GIA (blue squares), which serves as reference. A reduction of the timestep size generally leads to a reduction of the relative L^2 error and an increase in CPU time.

Evolution of errors over time and "food-web"

Only total errors averaged over all mass balance equations were evaluated so far. However, each reaction and each component can have its own error and contributes to the total errors analysed previously. With Figure 8.2, the aim is to show the evolution of errors over time and over the different components of a reaction system as it was explained in Chapter 2. Figure 8.2 shows the values of the reference solution (GIA) plotted against the values of the SNIA solution for different Δt evaluated at the middle of the column. The aim of this plot is to show where the different components or reactants deviate from the reference solution. Since the errors are quite small, zoomed regions are added to each plot. The introduced zoom is always for a time of 0.5 d and is a 100x zoom of the original image. According to the reaction system explained in

Figure 2.1, one microbial species of bacteria (coal consuming bacteria), archaea (acetoclastic archaea), one intermediate product (acetate), and one end product (methane) is plotted. With this selection, one of the three main pathways through the reaction system is evaluated and potential accumulation of errors can be estimated. The reference solution is depicted with a blue line, SNIA with $\Delta t = 1000\,\mathrm{s}$ with a purple dotted line, SNIA with $\Delta t = 500\,\mathrm{s}$ with a green dash-dotted line, and SNIA with $\Delta t = 50\,\mathrm{s}$ with an orange dashed line.

In the top left plot of Figure 8.2 the volume fraction of coal consuming bacteria (CoalBac) is plotted over time. No visible deviations (without zoom) from the reference can be observed, as this is only dependent on the available volume fraction of coal, that is assumed to be immobile.
The top right plot of Figure 8.2 evaluates the mole fraction of acetate in the wetting phase over time. The SNIA solution with $\Delta t = 1000\,\mathrm{s}$ is slightly overestimating acetate mole fraction, especially towards Day 38, while $\Delta t = 500\,\mathrm{s}$ is slightly underestimating the acetate mole fraction for the first 20 days and the peak on Day 38 is slightly underestimated. SNIA with $\Delta t = 50\,\mathrm{s}$ coincides with the reference for most parts of the plotted line.
The volume fraction of acetoclastic archaea (AcetoArch) are shown in the bottom left plot. As acetoclastic archaea use acetate as their substrate, therefore, this result is coupled to the previously discussed mole fraction of acetate. The difference between the SNIA results is rarely visible and also the difference to the reference is small, but increasing with time. The SNIA results are closer to the reference at the first zoomed image, whereas they are further away at the second zoomed image.

The bottom right plot shows the mole fraction of methane evaluated over time. Especially during the first 60 days, a deviation from the reference is observed for all SNIA approaches. For regions with large changes or gradients, the SNIA results deviate from the reference, but the deviation is reduced with smaller Δt in most cases. Only the local minimum in methane mole fraction on Day 46 is underestimated by $\Delta t = 50\,\mathrm{s}$, while the other Δt variations slightly overestimate the mole fraction.

Figure 8.2 shows that the different components in the system contribute with different amounts to the total error previously discussed. A general trend is that the deviations increase with longer runtime and in regions with strong gradients or large changes in concentrations. Especially for the "solid" species in the reaction system, as e.g.

acetoclastic archaea, the error is accumulating over time as they can not move, but only grow or decay depending on the substrate that is available to them. Therefore, the error increases the further back they are with respect to the MECBM food-web (Figure 2.1). For components that are transported through the system, as e.g. methane or acetate, the error increases and decreases depending on the reaction rates at that point in space and time. While reactants arrive, the error increases, but if all reactants passed through this point, the error is reduced again.

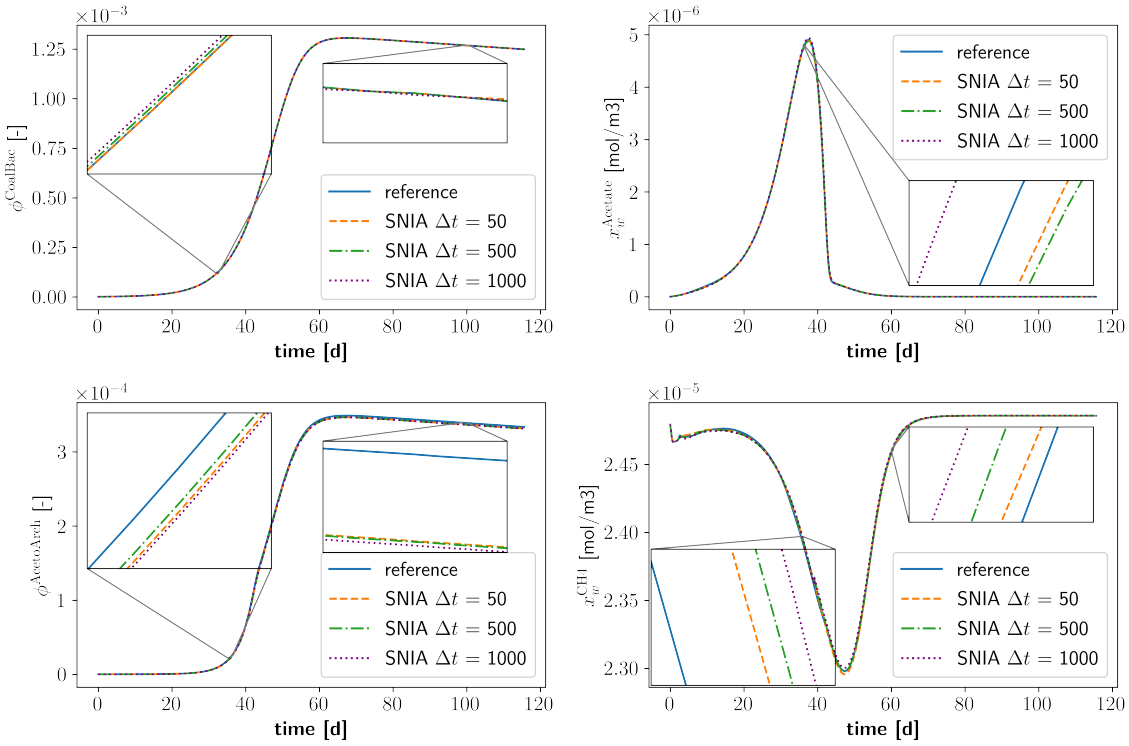

Figure 8.2: Mole fraction and volume fraction comparison of SNIA Δt variations against reference solution (blue). SNIA with $\Delta t = 50\,\mathrm{s}$ is shown with dashed orange line and matches the reference best, while SNIA $\Delta t = 500\,\mathrm{s}$ (green dash-dotted line) and SNIA $\Delta t = 1000\,\mathrm{s}$ (purple dotted line) deviate more from the reference for all four depicted mole or volume fractions. Each plot has zoomed regions (100xzoom), representing a timespan of 0.5 d to better visualize the differences.
Top left shows the volume fraction of the coal consuming bacteria and generally the curves almost coincide. The mole fraction of acetate in water is shown on the top right and the larger deviations are observed with larger Δt. The bottom left shows the volume fraction of acetoclastic archaea, which depends on the mole fraction of acetate in water and the deviation increases over time for all SNIA Δt variations. The mole fraction of methane in water shows a distinct difference especially for the first 60 days with all SNIA Δt variations.

8.3.2 Damköhler numbers for SNIA

A common indicator in estimating the timestep size for OS approaches with decoupled reaction terms are Damköhler numbers. As already explained in Section 3.6.3, we investigated the advective Damköhler number which relates the characteristic advective timescales to the reaction timescales in the column.
Since the Damköhler numbers for the previously calculated variations vary over orders of magnitude, only those with $Da < 1$ are shown here. Systems with $\Delta t \geq 2000\,\mathrm{s}$ showed to have Damköhler numbers in the range of $Da = 10$ or greater. Additionally, those systems also showed convergence issues, which is likely caused by the decoupled solution of the reaction problem. For the other timestep sizes, Damköhler numbers of each reactant are shown in Figure 8.3. Only methane is excluded, as those Damköhler numbers were always one order of magnitude below the others. Figure 8.3 shows the different components on the x-axis with two bar-plots for each Δt. The first bar-plot with a light colour gives the Damköhler number for the first 20 days. At the same location, a second bar-plot for the same Δt indicates the maximum Damköhler number from Day 20 to Day 115 with a more intense colour. This shows e.g. in the case of Acetate with $\Delta t = 1000\,\mathrm{s}$ that the maximum Damköhler number in the initial period (Day 0 to 20) is 0.087, while the Damköhler number for the remaining days is only 0.015. This behaviour is observed for all illustrated cases and the Damköhler numbers in the initial 20 days are generally almost one order of magnitude larger than for the remaining days of the study.

8.4 Discussion

The presented results show, as already indicated in the study of Wang [2019], that OS methods for the highly interacting MECBM food-web yield mostly accurate results within reasonable time-constraints for this simple study. Other studies e.g. by Lichtner [1996], Xu et al. [1999], Saaltink et al. [2001], Cirpka and Helmig [1997] already compare SNIA, SIA and GIA approaches and conclude, that for complex reaction systems the GIA performs better than any OS method. Even though the GIA is more demanding regarding computer requirements, it can perform better without introducing OS errors. SIA are commonly used and accepted for relatively simple reaction problems, but even

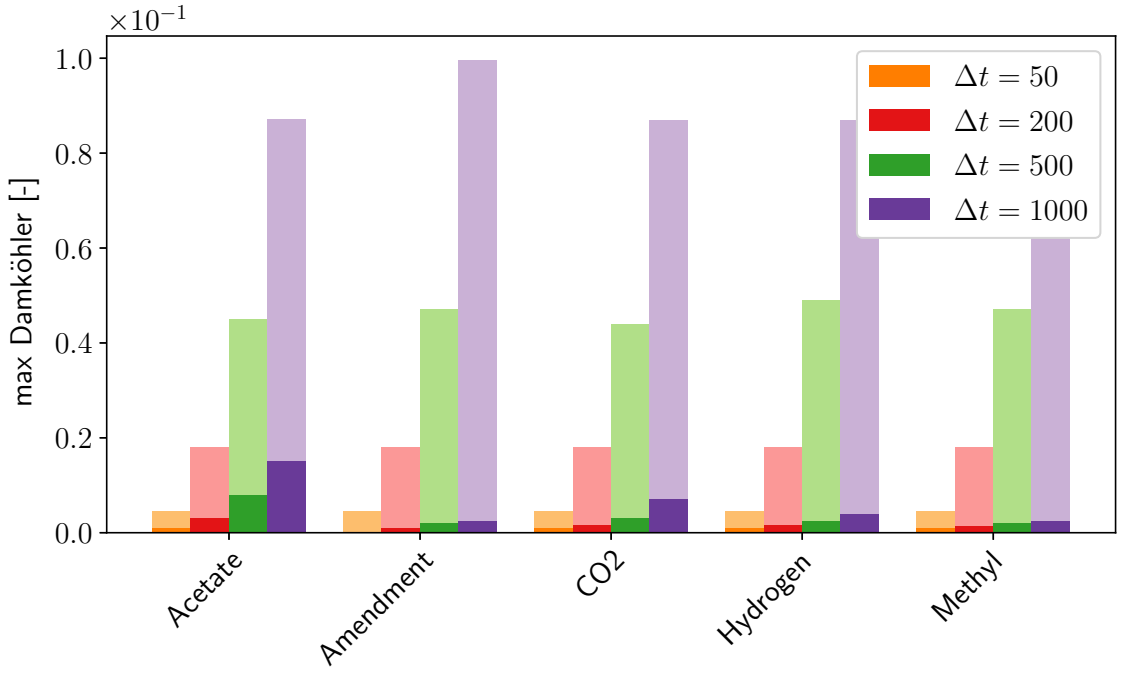

Figure 8.3: Damköhler numbers for different components as a result of the SNIA for four different Δt. One bar-plot with a light colour shows the maximum Damköhler number during the first 20 days. At the same location, a second bar-plot for the same Δt indicates the maximum Damköhler number from Day 20 to Day 115 with a more intense colour. Damköhler numbers generally decrease with reducing Δt.

there Cirpka and Helmig [1997] as well as Hron [2015] show that the computational times for an OS system, which combines slow and fast reaction kinetics is less efficient than the GIA, due to the required small size of timesteps.

Especially for equilibrium reactions or for fast reactions as e.g. filtration or retardation (which was not investigated for now), the OS approach struggles to match the exact solution [Hron, 2015]. With respect to these findings from literature, the MECBM model produces reasonable results, while running into the same problems as reported in literature. However, the discussed speed-ups are considered to be of minor relevance, as the presented results are a rather simple setup. For field-scale applications, OS approaches could be necessary and faster than the GIA.
While decreasing Δt generally leads to an increase in accuracy for the presented case study, the computational time increases. This can be partially attributed to the way the splitting is performed. The same amount of equations was used to model this

study for both the transport and the reaction part, as the presented MECBM system is highly interacting. However, no time or memory reduction regarding the equation assembly is achieved with this method. As assembly of equations does take a large amount of time, further computational speed-up could be achieved with a reduction of modelled equations e.g. for the transport part of the equations. A reduction of equations for the reaction does not seem reasonable, as all fluid components are part of the reaction system. The transport of the remaining components in a two-phase context could be achieved with implementation of so-called "tracer" components for the wetting phase, as presented in a study by Peter [2019] which is available in the framework of DuMu^{x}. A reduced set of equations for the transport part has a large potential for faster computation.

Regarding the Damköhler numbers presented here, they appear to be in ranges well below one for $\Delta t \leq 1000\,\mathrm{s}$. Only for $\Delta t \geq 2000\,\mathrm{s}$, Damköhler numbers above one were observed. As the reaction part is dominating for Damköhler numbers greater than one, it is likely that the convergence problems for these timestep sizes are also caused by the large influence of the reactions. Therefore, the reduction of timestep sizes, as reported for $\Delta t \geq 2000\,\mathrm{s}$, also helps in lowering the Damköhler numbers. Only for comparison reasons the timestep size was fixed for this study, but the correlation between poor convergence and Damköhler numbers greater one, indicates that also for this model, the advective Damköhler numbers presented here could be used to determine an adaptive timestep size for future applications.

8.5 Conclusion

For lab-scale simulations, as performed so far, the GIA produces the most accurate and also the fastest results. However, when envisioning field-scale applications for the model in the future, OS approaches could be of importance, as the resulting Jacobian Matrix for GIA could become too large to be solved efficiently. For field-scale applications, more work on the grid dependence needs to be done. All of this is to be investigated thoroughly for the MECBM model in a separate study.

We showed here, that splitting transport and reactions for the MECBM model is generally possible while some constraints and challenges remain. Future challenges will

include handling of the phase-change, exact determination of the Damköhler numbers, as well as determining a reasonable balance between accuracy and CPU time. All of these can be investigated in a future study combined with multi-step reactions, more complex column scenarios and further decoupling of transport with tracer-like components.
Especially when working with multiple small steps for the reactions, the performance in terms of accuracy could be improved as multiple small steps are likely to estimate the reaction network better. However, Damköhler numbers need to be defined carefully then, to ensure good convergence of the solution at all times. More complex and realistic scenarios, as presented in Case 4 of Chapter 6, are to be included in a future OS study. Before this is performed, a separate investigation with tracer components is potentially of interest. Such an investigation could show how to reduce computational demand in the assembly of equations when modelling attaching and detaching microbial cells. However, each of these processes is best investigated separately at first to measure and determine the error contribution of each subprocess.

Last but not least, the correct splitting of sub-processes should be investigated further. The presented MECBM model is highly interacting and connected, which does not allow for an easy splitting along physical independent processes. Therefore, when investigating OS approaches introduction of an OS error is assumed to be always present. It should be good practice to check if commutativity of advection, diffusion, and reaction, as presented by Lanser and Verwer [1999] is actually given.

9 Summary and outlook

9.1 Summary

This thesis focuses on the development, calibration and validation of a numerical model capable of describing the biogeochemical reactions with flow and transport features in the subsurface in the context of microbially enhanced coal-bed methane production. As biogeochemical processes occur on many temporal and spatial scales, numerical modelling is an efficient and instrumental tool to enhance understanding of complex processes and interactions. However, not all processes with their complex interactions and interdependencies can be approximated with the same level of detail, which is the motivation for this work to develop a substantial conceptual model that parametrizes the complex reality in subsurface reaction systems. This is performed in a step-wise development of the numerical model, using extensive experimental investigations from Davis et al. [2018a], Davis and Gerlach [2018], Davis et al. [2019]. All modelling schemes have been implemented into the open-source simulator DuMu^{x} [Flemisch et al., 2011, Koch et al., 2020], allowing for a comparison of the different methods within the same software framework, which is continuously validated with benchmark studies [Class et al., 2009, Flemisch et al., 2011, 2018].

Chapter 2 provides an overview of the fundamental biogeochemical processes and how they can be described in a conceptual model. Each reaction is derived using Gibbs free energy calculations and according to those the products and microbial growth are calculated.

Chapter 3 outlines the fundamental quantities and processes of flow and transport in porous media. Two-phase flow with multiple components and multiple biofilm species is considered. This chapter also includes a short summary on filtration laws, attachment, and detachment processes in porous media for microbial cells or particulate matter as e.g. amendments. Additionally, the differences between the fully-implicit

and fully-coupled approach (GIA) to solve the model and so-called operator splitting (OS) methods are explained and introduced.
Chapter 4 recapitulates and summarizes the main findings of the external experimental investigations this study is based on. Limitations and restrictions regarding the model, as a result of the experimental results are explained therein.

The first numerical study using the conceptual and mathematical model which was explained in the previous chapters, is presented in Chapter 5. The numerical model is calibrated using only two out of nine datasets, with a substrate specific setup in mind. By calibrating two sub-processes (coal and amendment consumption) independently, and combining them afterwards, a cross-validation is achieved on top of the already good calibration and validation using the nine datasets. The batch model is able to effectively predict the results of the experimental studies within less than 10 % error, and thereby mostly within the confidence intervals of the experimental study. With this, the mathematical and conceptual model shows the importance of specific substrate utilization by microbes in the subsurface and provides a tool for further investigations in the field of MECBM production.

The logical next step is presented in Chapter 6, where the validated batch model is extended to model flow and transport for upflow column reactors. The numerical model is now used to test various hypotheses, which were derived from the experimental study. These hypotheses are then compared between each other and to the experimental results and show to give valuable insight into the processes involved in MECBM production. It can be shown that microbial cell attachment and detachment are of importance, when modelling MECBM production on the column scale with flow and transport features. Filtration or retardation of the amendment seem to have a large influence on the results of the numerical model. Additionally, first indications that the distribution of microbial cells along the column could have an influence on the methane production are presented. If a subsequent microorganism is not located downstream of its precursor that should produce a substrate for him, they can decay and the conversion chain from coal or amendment over intermediate products to methane is stopped.

Chapter 7 discusses three of the four case studies introduced in Chapter 6 in the light of sensitivity of the input parameters with respect to methane output. The MECBM model is a highly parametrized model, where a sensitivity analysis relates the different parameters and their uncertainty in modelling to one another using Sobol indices. The

three cases and their different parameters are analysed individually over time. Additionally, a heatmap comparing the total sensitivities of the parameters between the different cases is created. From the heatmap, it can be observed which parameters are or are not of importance in all cases and which gain or lose importance with changing physical processes in the columns. It is interesting to observe, that with changing physical behaviour of the columns or introduction of new processes, the Sobol indices change and the model output is dominated by other parameters. The findings of the sensitivity analysis help in identifying relevant parameters for two of the three investigated cases and show to support and further validate the findings of Chapter 6.

In the last part of this thesis, a numerical decoupling strategy is investigated by the means of operator splitting. Two different operator-splitting approaches are investigated for a MECBM column case, but all show to be not efficient enough and only partially precise enough, when compared to the fully-implicit model for this simple study. However, when moving to more complex scenarios or larger modelling systems, the presented results can be used as a guideline to study OS approaches for MECBM production. The main challenges for the OS approaches are related to the highly interdependent processes involved in MECBM production, which do not allow for a feasible decoupling of all flow, transport and reactions. However, a simple decoupling is obtained and when comparing against the GIA with the same low timestep size, the OS approaches show to be up to 40 % more efficient than the GIA. Further studies could focus on keeping the main components and phases solved fully coupled, while only the solution for tracer-like components, particles and reactions are decoupled. For the reaction part, a multi-reaction-step approach, including multiple sub-reaction-steps per global timestep, is advised.

Concluding, we have successfully developed, calibrated, and validated a numerical model for microbially enhanced coal-bed methane production. The implemented food-web was validated by the experimental and the modelling data; however, further confirmation by new experimental evidence would be good (see Section 9.2). The model is extended to simulate column studies and investigate the role of retardation and filtration of particulate matter as well as attachment and detachment processes of microbial cells. Amendment injections are prone to being retarded and the attachment and detachment of microbial cells are essential to match the experimental results. A sensitivity analysis is performed, which provides further insight into the results of the column study and the importance of the respective modelling parameters. The numerical decoupling

of the MECBM model shows to present reasonable results, yet the investigated system is too small to allow for a significant computational gain in performance. Possible extensions and recommendations for future studies are presented.

9.2 Outlook

This thesis focuses on the description and implementation of a numerical model that can be applied to lab-study experiments. The capabilities of the model, embedded in the advanced simulation framework DuMu^x, can be extended further to larger laboratory studies or potentially even field-scale studies. However, there is much room for model improvement along this path to a field-scale numerical model.

Conceptual and numerical model improvements As this model focuses mainly on the conceptual model with calibration and validation of the basic processes, more work on a better description of each of these processes can be done. Also, some simplifications and assumptions in the model have to be tested over and over again. Obviously, the food-web and all metabolic pathways can be investigated further with more dedicated experimental investigations on certain sub-processes.
More joint experimental and numerical investigations are also essential for future modelling of cell attachment, biofilm detachment, and amendment retardation. These processes deserve further investigation as we have shown their large effect on the modelling results on the column scale. Adsorption should be studied for each type of coal, and relevant adsorption isotherms are to be included in future models.
The field-scale has not been investigated by us so far and only crushed and therefore homogenized coal was used in the presented numerical and experimental studies. However, with the field-scale application in mind, further modelling challenges are posed by the structure of the coal. A real coal bed is known to be structured and usually anisotropic with a much more challenging flow field. A study by Zhi et al. [2018] uses a discrete fracture model to model CBM production at the field scale with natural and hydraulic fractures. Such a model is already available in the software framework DuMu^x [Gläser et al., 2019] and could be coupled to the MECBM model in the future.

Numerical investigations Regarding the numerical framework, future studies should focus on a process-dependent decoupling study, as the general decoupling strategy seems to reach its limitations already for small problems. More work investigating each sub-process and decoupling each sub-process is advised if OS approaches are studied further for the MECBM model. With the individual splitting of each sub-process, a contribution of speed-up and error can be estimated. With these estimates, a better distinction of the different splitting steps can be discussed. Afterwards, the most feasible splitting process, in terms of accuracy and speed-up, can be implemented and applied to the MECBM model.

Other experimental MECBM studies This study has focused on a number of experimental studies from the Powder River Basin (PRB) [Barnhart et al., 2017, Davis et al., 2018a, Davis and Gerlach, 2018, Davis et al., 2018b, 2019]. This focus allowed for an easy transfer of assumptions as the bioavailable fraction of coal, the type of amendment, and the microbial community stay similar throughout the experiments. However, other experimental investigations might need some adjustments in the numerical model, as the reactions and kinetics are calibrated to data from the PRB. These further experimental studies as presented by Beckmann et al. [2019] or Lupton et al. [2020] could be used to adapt the model and test it on this new data. Obviously, new challenges would occur when trying to transfer the different coal types, potentially different microorganisms, and different amendments of these studies.
As most of the presented work focused on MECBM production in the USA so far, it is important to mention, that MECBM production is a process investigated around the world and could also be applied in Germany, as presented by Thielemann et al. [2004] for abandoned coal-mines in the Ruhr area. Similar experimental studies and potential further joint experimental and numerical studies could be performed in the future. With such studies, the knowledge about MECBM-related biological and chemical processes could be enhanced and the rising global energy demand could partially be satisfied with microbially generated gas from otherwise unmineable coal-beds.

A Energetics and bacterial growth

Table A.1: Energetics and reactions system for bacteria using glucose. Reprinted with permission from Emmert et al. [2020a], © 2020 Elsevier Inc.

ΔG in kJ/mol	Equation		
-41.924	$\frac{1}{24}C_6H_{12}O_6 + \frac{1}{4}H_2O = \frac{1}{4}CO_2 + 1H^+ + 1e^-$	(A.1)	Eq. 29 in McCarty [1972]
100.00	$\frac{1}{4}CO_2 + \frac{1}{20}NH_3 + 1H^+ + 1e^- = \frac{1}{20}C_5H_7O_2N + \frac{2}{5}H_2O$	(A.2)	Eq. 32 in McCarty [1972]
27.652	$\frac{1}{8}CO_2 + \frac{1}{8}HCO_3^- + 1H^+ + 1e^- = \frac{1}{8}CH_3COO^- + \frac{3}{8}H_2O$	(A.3)	Eq. 14 in McCarty [1972]
40.459	$1H^+ + 1e^- = \frac{1}{2}H_2$	(A.4)	Eq. 28 in McCarty [1972]
37.510	$\frac{1}{6}CO_2 + 1H^+ + 1e^- = \frac{1}{6}CH_3COH + \frac{1}{6}H_2O$	(A.5)	Eq. 26 in McCarty [1972]

Table A.2: Energetics and reactions system for archaea using intermediates. Reprinted with permission from Emmert et al. [2020a], © 2020 Elsevier Inc.

ΔG **in** kJ/mol	**Equation**		
24.112	$\frac{1}{8}\mathrm{CO_2} + 1\mathrm{H^+} + 1\mathrm{e^-} = \frac{1}{8}\mathrm{CH_4} + \frac{1}{4}\mathrm{H_2O}$	(A.6)	Eq. 12 in McCarty [1972]
100.00	$\frac{1}{4}\mathrm{CO_2} + \frac{1}{20}\mathrm{NH_3} + 1\mathrm{H^+} + 1\mathrm{e^-} = \frac{1}{20}\mathrm{C_5H_7O_2N} + \frac{2}{5}\mathrm{H_2O}$	(A.7)	Eq. 32 in McCarty [1972]
-27.652	$\frac{1}{8}\mathrm{CH_3COO^-} + \frac{3}{8}\mathrm{H_2O} = \frac{1}{8}\mathrm{CO_2} + \frac{1}{8}\mathrm{HCO_3^-} + 1\mathrm{H^+} + 1\mathrm{e^-}$	(A.8)	Eq. 14 in McCarty [1972]
-40.459	$\frac{1}{2}\mathrm{H_2} = 1\mathrm{H^+} + 1\mathrm{e^-}$	(A.9)	Eq. 28 in McCarty [1972]
-37.510	$\frac{1}{6}\mathrm{CH_3COH} + \frac{1}{6}\mathrm{H_2O} = \frac{1}{6}\mathrm{CO_2} + 1\mathrm{H^+} + 1\mathrm{e^-}$	(A.10)	Eq. 26 in McCarty [1972]

B Parameter ranges, initial conditions and sources

Table B.1: Initial biomass conditions and densities. Reprinted with permission from Emmert et al. [2020a], © 2020 Elsevier Inc.

Parameter	Value	Source	Brief Description
$\phi_{\mathrm{cb},0}$	$1 * 10^{-5}$ [−]	Estimated	Initial volume fraction of coal consuming bacteria
$\phi_{\mathrm{ab},0}$	$1 * 10^{-5}$ [−]	Estimated	Initial volume fraction of amendment and coal consuming bacteria
$\phi_{\mathrm{ha},0}$	$1 * 10^{-6}$ [−]	Estimated, approx. one order of magnitude lower than bacteria	Initial volume fraction of hydrogenotrophic archaea
$\phi_{\mathrm{aa},0}$	$1 * 10^{-6}$ [−]	Estimated, approx. one order of magnitude lower than bacteria	Initial volume fraction of acetoclastic archaea
$\phi_{\mathrm{ma},0}$	$1 * 10^{-6}$ [−]	Estimated, approx. one order of magnitude lower than bacteria	Initial volume fraction of methylotrophic archaea
$\phi_{\mathrm{Cc},0}$	$2.53{\cdot}10^{-2}$ [−]	Derived from experimental concentration	Initial volume fraction of coal, corresponding to 100 g/L
ρ_{Cc}	1250 $\frac{kg}{m^3}$	Average measurement value [Davis et al., 2019]	Density of coal
ρ_i	10 $\frac{kg}{m^3}$	Estimated, see Hommel et al. [2015]	Dry density of all microbes

Table B.2: Initial component concentrations. Reprinted with permission from Emmert et al. [2020a], © 2020 Elsevier Inc.

Parameter	Value	Source	Brief Description
$C_{\mathrm{Am},0}$	0.1 g/L	Experimental value [Davis et al., 2018a]	Initial concentration of amendment
$C_{\mathrm{H_2},0}$	0.0 g/L	Experimental value [Davis et al., 2018a]	Initial concentration of hydrogen
$C_{\mathrm{Ac},0}$	0.0 g/L	Experimental value [Davis et al., 2018a]	Initial concentration of acetate
$C_{\mathrm{CH_3},0}$	0.0 g/L	Experimental value [Davis et al., 2018a]	Initial concentration of methyl-groups

Table B.3: Microbial growth rates: The rates are named $\mu^{\mathrm{P}}_{X,S}$ after the microbe X they are growing, their substrate (S) and where applicable the product P that is forming corresponding to the respective growth. Reprinted with permission from Emmert et al. [2020a], © 2020 Elsevier Inc.

Parameter	Value	Source	Brief Description
$\mu^{\mathrm{Ac}}_{\mathrm{cb,Cc}}$	0.308 d^{-1}	Estimated range: 0.05 - 0.5 d^{-1}	Maximum specific growth rate constant of coal consuming bacteria on coal producing acetate
$\mu^{\mathrm{H_2}}_{\mathrm{cb,Cc}}$	0.308 d^{-1}	Estimated range: 0.05 - 0.5 d^{-1}	Maximum specific growth rate constant of coal consuming bacteria on coal producing hydrogen
$\mu^{\mathrm{Ac}}_{\mathrm{ab,Cc}}$	0.054 d^{-1}	Estimated range: 0.05 - 0.5 d^{-1}	Maximum specific growth rate constant of amendment and coal consuming bacteria on coal producing acetate
$\mu^{\mathrm{H_2}}_{\mathrm{ab,Cc}}$	0.054 d^{-1}	Estimated range: 0.05 - 0.5 d^{-1}	Maximum specific growth rate constant of amendment and coal consuming bacteria on coal producing hydrogen
$\mu^{\mathrm{Ac}}_{\mathrm{ab,Am}}$	0.771 d^{-1}	Estimated range: 0.1 - 1.5 d^{-1}	Maximum specific growth rate constant of amendment and coal consuming bacteria on amendment producing acetate

Continued on next page

Table B.3 – continued from previous page

Parameter	Value	Source	Brief Description
$\mu_{ab,Am}^{H_2}$	0.771 d^{-1}	Estimated range: 0.1 - 1.5 d^{-1}	Maximum specific growth rate constant of amendment and coal consuming bacteria on amendment producing hydrogen
$\mu_{ab,Am}^{CH_3}$	1.06 d^{-1}	Estimated range: 0.1 - 1.5 d^{-1}	Maximum specific growth rate constant of amendment and coal consuming bacteria on amendment producing methylgroups
μ_{ha}	0.253 d^{-1}	Range [Archer and Powell, 1985]: 0.05 - 4.07 d^{-1}	Maximum specific growth rate constant of hydrogenotrophic archaea
μ_{aa}	0.279 d^{-1}	Range [Pan et al., 2016, Archer and Powell, 1985]: 0.08 - 2.49 d^{-1}	Maximum specific growth rate constant of acetoclastic archaea
μ_{ma}	1.06 d^{-1}	Range [Welander, 2007]: 0.2 - 6 d^{-1}	Maximum specific growth rate constant of methylotrophic archaea

Table B.4: Monod half saturations: The monod half saturations for every component that is involved in a reaction. Reprinted with permission from Emmert et al. [2020a], © 2020 Elsevier Inc.

Parameter	Value	Source	Brief Description
K_{Cc}	0.52 g/L	Estimated range: 0.1 - 2 g/L	Monod half saturation constant for coal
K_{Am}	1.17 g/L	Estimated range: 0.1 - 5 g/L	Monod half saturation constant for amendment
$K_{\mathrm{H_2}}$	$7.65{\cdot}10^{-5}$ g/L	Fitted, [Robinson and Tiedje, 1984] estimates: 10^{-5} g/L	Monod half saturation constant for hydrogen
K_{Ac}	$1.37{\cdot}10^{-3}$ g/L	Fitted, estimated range: $1 \cdot 10^{-3}$ - 0.24 g/L [Sørensen and Ahring, 1993]	Monod half saturation constant for acetate
$K_{\mathrm{CH_3}}$	$2.0 \cdot 10^{-3}$ g/L	Fixed, according to Zhang et al. [2008]	Monod half saturation constant for methyl-groups
k_{X}	$1 \cdot 10^{-4}\mathrm{d}^{-1}$	Fixed, estimated to approx. min growth rate / 100	Decay coefficient of all microorganisms

The respective yields for all the reactions for biomass or components are listed in Table B.5 and B.6.

Table B.5: Biomass yields: The yields $Y^P_{X,S}$ are named after the microbe that is growing X, the substrate S and, where applicable, the product they are producing P. Reprinted with permission from Emmert et al. [2020a], © 2020 Elsevier Inc.

Parameter	Value	Source	Brief Description
$Y^{\mathrm{Ac}}_{\mathrm{cb,Cc}}$	$1.14 \cdot 10^{-1}$ $\frac{g\ X_{cb}}{g\ Cc}$	Calculated range using Eqs. A.1, A.3, A.2: $7.43 \cdot 10^{-2} - 2.23 \cdot 10^{-1}$	Coal consuming bacteria biomass yield on coal producing acetate
$Y^{\mathrm{H2}}_{\mathrm{cb,Cc}}$	$3.52 \cdot 10^{-2}$ $\frac{g\ X_{cb}}{g\ Cc}$	Calculated range using Eqs. A.1, A.4, A.2: $1.48 \cdot 10^{-2} - 3.52 \cdot 10^{-2}$	Coal consuming bacteria biomass yield on coal producing hydrogen
$Y^{\mathrm{Ac}}_{\mathrm{ab,Cc}}$	$1.14 \cdot 10^{-1}$ $\frac{g\ X_{ab}}{g\ Cc}$	Calculated range using Eqs. A.1, A.3, A.2: $7.43 \cdot 10^{-2} - 2.23 \cdot 10^{-1}$	Amendment and coal consuming bacteria biomass yield on coal producing acetate
$Y^{\mathrm{H2}}_{\mathrm{ab,Cc}}$	$3.52 \cdot 10^{-2}$ $\frac{g\ X_{ab}}{g\ Cc}$	Calculated range using Eqs. A.1, A.4, A.2: $1.48 \cdot 10^{-2} - 3.52 \cdot 10^{-2}$	Amendment and coal consuming bacteria biomass yield on coal producing hydrogen
$Y^{\mathrm{Ac}}_{\mathrm{ab,Am}}$	$1.13 \cdot 10^{-1}$ $\frac{g\ X_{ab}}{g\ Am}$	Calculated range using Eqs. A.1, A.3, A.2: $7.43 \cdot 10^{-2} - 2.23 \cdot 10^{-1}$	Amendment and coal consuming bacteria biomass yield on amendment producing acetate
$Y^{\mathrm{H2}}_{\mathrm{ab,Am}}$	$9.41 \cdot 10^{-3}$ $\frac{g\ X_{ab}}{g\ Am}$	Calculated range using Eqs. A.1, A.4, A.2: $9.26 \cdot 10^{-3} - 2.78 \cdot 10^{-2}$	Amendment and coal consuming bacteria biomass yield on amendment producing hydrogen
$Y^{\mathrm{CH3}}_{\mathrm{ab,Am}}$	$5.04 \cdot 10^{-2}$ $\frac{g\ X_{ab}}{g\ Am}$	Calculated range using Eqs. A.1, A.5, A.2: $4.26 \cdot 10^{-2} - 7.89 \cdot 10^{-2}$	Amendment and coal consuming bacteria biomass yield on amendment producing methyl groups
$Y_{\mathrm{aa,Ac}}$	$3.10 \cdot 10^{-2}$ $\frac{g\ X_{aa}}{g\ Ac}$	Calculated range using Eqs. A.6, A.8, A.7: $2.86 \cdot 10^{-2} - 5.36 \cdot 10^{-2}$	Acetoclastic archaea biomass yield on acetate
$Y_{\mathrm{ha,H_2}}$	$1.22 \cdot 10^{-1}$ $\frac{g\ X_{ha}}{g\ H_2}$	Calculated range using Eqs. A.6, A.9, A.7: $1.22 \cdot 10^{-1} - 1.83$	Hydrogenotrophic archaea biomass yield on hydrogen

Continued on next page

Table B.5 – continued from previous page

Parameter	Value	Source	Brief Description
$Y_{\mathrm{ma,CH_3}}$	$1.74{\cdot}10^{-1}$ $\frac{g\ X_{ma}}{g\ CH_3}$	Calculated range using Eqs. A.6, A.10, A.7: $1.5 \cdot 10^{-1} - 2.81 \cdot 10^{-1}$	Methylotrophic archaea biomass yield on methyl-groups

Table B.6: Component yields: The yields are named $Y_{P,S}$ after their substrate S and products P, where S and P are substituted for the respective components. Reprinted with permission from Emmert et al. [2020a], © 2020 Elsevier Inc.

Parameter	**Value**	**Source**	**Brief Description**
$Y_{\mathrm{Ac,Cc}}$	$9.73 \cdot 10^{-1}$ $\frac{g\ Ac}{g\ Cc}$	Calculated range using Eqs. A.1, A.3, A.2: $6.31 \cdot 10^{-2} - 1.18$	Yield of acetate from coal
$Y_{\mathrm{H_2,Cc}}$	$1.3 \cdot 10^{-2}$ $\frac{g\ H_2}{g\ Cc}$	Calculated range using Eqs. A.1, A.4, A.2: $1.30 \cdot 10^{-2} - 1.95 \cdot 10^{-1}$	Yield of hydrogen from coal
$Y_{\mathrm{Ac,Am}}$	$9.79 \cdot 10^{-1}$ $\frac{g\ Ac}{g\ Am}$	Calculated range using Eqs. A.1, A.3, A.2: $6.31 \cdot 10^{-1} - 1.18$	Yield of acetate from amendment
$Y_{\mathrm{H_2,Am}}$	$1.94 \cdot 10^{-01}$ $\frac{g\ H_2}{g\ Am}$	Calculated range using Eqs. A.1, A.4, A.2: $1.04 \cdot 10^{-1} - 1.95 \cdot 10^{-1}$	Yield of hydrogen from amendment
$Y_{\mathrm{CH_3,Am}}$	$6.96 \cdot 10^{-1}$ $\frac{g\ CH_3}{g\ Am}$	Calculated range using Eqs. A.1, A.5, A.2: $5.29 \cdot 10^{-1} - 9.91 \cdot 10^{-1}$	Yield of methyl-groups from amendment
$Y_{\mathrm{CH_4,Ac}}$	$2.93 \cdot 10^{-1}$ $\frac{g\ CH_4}{g\ Ac}$	Calculated range using Eqs. A.6, A.8, A.7: $2.07 \cdot 10^{-1} - 3.88 \cdot 10^{-1}$	Yield of CH_4 from acetate
$Y_{\mathrm{CH_4,H_2}}$	2.89 $\frac{g\ CH_4}{g\ H_2}$	Calculated range using Eqs. A.6, A.9, A.7: $1.26 \cdot 10^{-1} - 2.98$	Yield of CH_4 from hydrogen
$Y_{\mathrm{CH_4,CH_3}}$	$3.3 \cdot 10^{-1}$ $\frac{g\ CH_4}{g\ CH_3}$	Calculated range using Eqs. A.6, A.10, A.7: $2.47 \cdot 10^{-2} - 4.63 \cdot 10^{-1}$	Yield of CH_4 from methyl-groups
$Y_{\mathrm{CO_2,Ac}}$	$8.05 \cdot 10^{-1}$ $\frac{g\ CO_2}{g\ Ac}$	Calculated range using Eqs. A.6, A.8, A.7: $5.69 \cdot 10^{-1} - 1.07$	Yield of CO_2 from acetate

Continued on next page

Table B.6 – continued from previous page

Parameter	Value	Source	Brief Description
Y_{CO_2,H_2}	$4.46 \cdot 10^{-1}$ $\frac{g\ CO_2}{g\ H_2}$	Calculated range using Eqs. A.6, A.9, A.7: $1.88 \cdot 10^{-1} - 4.46 \cdot 10^{-1}$	Yield of CO_2 from hydrogen
Y_{CO_2,CH_3}	$1.73 \cdot 10^{-1}$ $\frac{g\ CO_2}{g\ CH_3}$	Calculated range using Eqs. A.6, A.10, A.7: $1.29 \cdot 10^{-1} - 2.43 \cdot 10^{-1}$	Yield of CO_2 from methyl-groups

C MECBM summary of equations

Table C.1: MECBM microbial growth and decay rate equations with the resulting net. specific growth rates. Reprinted with permission from Emmert et al. [2020a], © 2020 Elsevier Inc.

Microbe	**Net specific growth**	**Growth rate**	**Decay rate**
Coal consuming bacteria	$q^{\mathrm{cb}} = \frac{d(\rho_{\mathrm{cb}}\phi_{\mathrm{cb}})}{dt}$ $= r^{\mathrm{Ac}}_{\mathrm{cb,Cc}} + r^{\mathrm{H_2}}_{\mathrm{cb,Cc}} - r^{\mathrm{cb}}_{\mathrm{d}}$	$r^{\mathrm{X}}_{\mathrm{cb,CC}} = \mu^{\mathrm{X}}_{\mathrm{cb,Cc}} \left(\frac{\rho_{\mathrm{Cc}}\phi_{\mathrm{Cc}}}{K_{\mathrm{Cc}}+\rho_{\mathrm{Cc}}\phi_{\mathrm{Cc}}}\right) \cdot \rho_{\mathrm{cb}}\phi_{\mathrm{cb}}$ with $\mathrm{X} \in \{\mathrm{Ac}; \mathrm{H_2}; \mathrm{CH_3}\}$	$r^{\mathrm{cb}}_{\mathrm{d}} = k_0 \cdot \rho_{\mathrm{cb}}\phi_{\mathrm{cb}}$
Amendment and coal consuming bacteria	$q^{\mathrm{ab}} = \frac{d(\rho_{\mathrm{ab}}\phi_{\mathrm{ab}})}{dt}$ $= r^{\mathrm{Ac}}_{\mathrm{ab,Cc}} + r^{\mathrm{H_2}}_{\mathrm{ab,Cc}} + r^{\mathrm{Ac}}_{\mathrm{ab,Am}} + r^{\mathrm{H_2}}_{\mathrm{ab,Am}} + r^{\mathrm{CH_3}}_{\mathrm{ab,Am}} - r^{\mathrm{ab}}_{\mathrm{d}}$	$r^{\mathrm{X}}_{\mathrm{ab,Cc}} = \mu^{\mathrm{X}}_{\mathrm{ab,Cc}} \left(\frac{\rho_{\mathrm{Cc}}\phi_{\mathrm{Cc}}}{K_{\mathrm{Cc}}+\rho_{\mathrm{Cc}}\phi_{\mathrm{Cc}}}\right) \cdot \rho_{\mathrm{ab}}\phi_{\mathrm{ab}}$, $r^{\mathrm{X}}_{\mathrm{ab,Am}} = \mu^{\mathrm{X}}_{\mathrm{ab,Am}} \left(\frac{\rho_{\mathrm{Am}}\phi_{\mathrm{Am}}}{K_{\mathrm{Am}}+\rho_{\mathrm{Am}}\phi_{\mathrm{Am}}}\right) \cdot \rho_{\mathrm{ab}}\phi_{\mathrm{ab}}$	$r^{\mathrm{ab}}_{\mathrm{d}} = k_0 \cdot \rho_{\mathrm{ab}}\phi_{\mathrm{ab}}$
Acetoclastic archaea	$q^{\mathrm{aa}} = \frac{d(\rho_{\mathrm{aa}}\phi_{\mathrm{aa}})}{dt} = r^{\mathrm{aa}}_{\mathrm{g}} - r^{\mathrm{aa}}_{\mathrm{d}}$	$r^{\mathrm{aa}}_{\mathrm{g}} = \mu_{\mathrm{aa}} \left(\frac{\rho_{\mathrm{Ac}}\phi_{\mathrm{Ac}}}{K_{\mathrm{Ac}}+\rho_{\mathrm{Ac}}\phi_{\mathrm{Ac}}}\right) \cdot \rho_{\mathrm{aa}}\phi_{\mathrm{aa}}$	$r^{\mathrm{aa}}_{\mathrm{d}} = k_0 \cdot \rho_{\mathrm{aa}}\phi_{\mathrm{aa}}$
Hydrogenotrophic archaea	$q^{\mathrm{ha}} = \frac{d(\rho_{\mathrm{ha}}\phi_{\mathrm{ha}})}{dt} = r^{\mathrm{ha}}_{\mathrm{g}} - r^{\mathrm{ha}}_{\mathrm{d}}$	$r^{\mathrm{ha}}_{\mathrm{g}} = \mu_{\mathrm{ha}} \left(\frac{\rho_{\mathrm{H_2}}\phi_{\mathrm{H_2}}}{K_{\mathrm{H_2}}+\rho_{\mathrm{H_2}}\phi_{\mathrm{H_2}}}\right) \cdot \rho_{\mathrm{ha}}\phi_{\mathrm{ha}}$	$r^{\mathrm{ha}}_{\mathrm{d}} = k_0 \cdot \rho_{\mathrm{ha}}\phi_{\mathrm{ha}}$
Methylotrophic archaea	$q^{\mathrm{ma}} = \frac{d(\rho_{\mathrm{ma}}\phi_{\mathrm{ma}})}{dt} = r^{\mathrm{ma}}_{\mathrm{g}} - r^{\mathrm{ma}}_{\mathrm{d}}$	$r^{\mathrm{ma}}_{\mathrm{g}} = \mu_{\mathrm{ma}} \left(\frac{\rho_{\mathrm{CH_3}}\phi_{\mathrm{CH_3}}}{K_{\mathrm{CH_3}}+\rho_{\mathrm{CH_3}}\phi_{\mathrm{CH_3}}}\right) \cdot \rho_{\mathrm{ma}}\phi_{\mathrm{ma}}$	$r^{\mathrm{ma}}_{\mathrm{d}} = k_0 \cdot \rho_{\mathrm{ma}}\phi_{\mathrm{ma}}$

Table C.2: Relevant MECBM component reaction equations. Reprinted with permission from Emmert et al. [2020a], © 2020 Elsevier Inc.

Component	**Source and sink term**
Acetate	$q^{\mathrm{Ac}} = r^{\mathrm{Ac}}_{\mathrm{cb,Cc}} \cdot \frac{Y_{\mathrm{Ac,Cc}}}{Y^{\mathrm{Ac}}_{\mathrm{cb,Cc}}} + r^{\mathrm{Ac}}_{\mathrm{ab,Cc}} \cdot \frac{Y_{\mathrm{Ac,Cc}}}{Y^{\mathrm{Ac}}_{\mathrm{ab,Cc}}} + r^{\mathrm{Ac}}_{\mathrm{ab,Am}} \cdot \frac{Y_{\mathrm{Ac,Am}}}{Y^{\mathrm{Ac}}_{\mathrm{ab,Am}}} - \frac{r_{\mathrm{aa}}}{Y_{\mathrm{aa,Ac}}}$
Amendment	$q^{\mathrm{Am}} = -\left(\frac{r^{\mathrm{Ac}}_{\mathrm{ab,Am}}}{Y^{\mathrm{Ac}}_{\mathrm{ab,Am}}} + \frac{r^{\mathrm{H_2}}_{\mathrm{ab,Am}}}{Y^{\mathrm{H_2}}_{\mathrm{ab,Am}}} + \frac{r^{\mathrm{CH_3}}_{\mathrm{ab,Am}}}{Y^{\mathrm{CH_3}}_{\mathrm{ab,Am}}}\right)$
CH_4	$q^{\mathrm{CH_4}} = r_{\mathrm{aa}} \cdot \frac{Y_{\mathrm{CH_4,Ac}}}{Y_{\mathrm{aa,Ac}}} + r_{\mathrm{ha}} \cdot \frac{Y_{\mathrm{CH_4,H_2}}}{Y_{\mathrm{ha,H_2}}} + r_{\mathrm{ma}} \cdot \frac{Y_{\mathrm{CH_4,CH_3}}}{Y_{\mathrm{ma,CH_3}}}$
CO_2	$q^{\mathrm{CO_2}} = r_{\mathrm{aa}} \cdot \frac{Y_{\mathrm{CO_2,Ac}}}{Y_{\mathrm{aa,Ac}}} + r_{\mathrm{ma}} \cdot \frac{Y_{\mathrm{CO_2,CH_3}}}{Y_{\mathrm{ma,CH_3}}} - \frac{r_{\mathrm{ha}}}{Y_{\mathrm{ha,CO_2}}}$
Coal	$q^{\mathrm{Cc}} = -\left(\frac{r^{\mathrm{Ac}}_{\mathrm{cb,Cc}}}{Y^{\mathrm{Ac}}_{\mathrm{cb,Cc}}} + \frac{r^{\mathrm{H_2}}_{\mathrm{cb,Cc}}}{Y^{\mathrm{H_2}}_{\mathrm{cb,Cc}}} + \frac{r^{\mathrm{Ac}}_{\mathrm{ab,Cc}}}{Y^{\mathrm{Ac}}_{\mathrm{ab,Cc}}} + \frac{r^{\mathrm{H_2}}_{\mathrm{ab,Cc}}}{Y^{\mathrm{H_2}}_{\mathrm{ab,Cc}}} + \frac{r^{\mathrm{CH_3}}_{\mathrm{ab,Cc}}}{Y^{\mathrm{CH_3}}_{\mathrm{ab,Cc}}}\right)$
Hydrogen	$q^{\mathrm{H_2}} = r^{\mathrm{H_2}}_{\mathrm{cb,Cc}} \cdot \frac{Y_{\mathrm{H_2,Cc}}}{Y^{\mathrm{H_2}}_{\mathrm{cb,Cc}}} + r^{\mathrm{H_2}}_{\mathrm{ab,Cc}} \cdot \frac{Y_{\mathrm{H_2,Cc}}}{Y^{\mathrm{H_2}}_{\mathrm{ab,Cc}}} + r^{\mathrm{H_2}}_{\mathrm{ab,Am}} \cdot \frac{Y_{\mathrm{H_2,Am}}}{Y^{\mathrm{H_2}}_{\mathrm{ab,Am}}} - \frac{r_{\mathrm{ha}}}{Y_{\mathrm{ha,H_2}}}$
Methyl-groups	$q^{\mathrm{CH_3}} = r^{\mathrm{CH_3}}_{\mathrm{ab,Am}} \cdot \frac{Y_{\mathrm{CH_3,Am}}}{Y^{\mathrm{CH_3}}_{\mathrm{ab,Am}}} - \frac{r_{\mathrm{ma}}}{Y_{\mathrm{ma,CH_3}}}$

D Column modelling parameters

Table D.1: List of used initial conditions, numerical, and physical parameters used in all simulations. Some parameters are given here again for completeness. Reaction parameters are presented and explained in Emmert et al. [2020a]. Reproduced with permission from Emmert et al. [2020b], CC BY 4.0 MDPI 2020.

Parameter	**Value**
Newton MaxRelativeShift	$1{\cdot}10^{-8}$
Newton ResidualReduction	$1{\cdot}10^{-8}$
Newton MinSteps	2
Newton MaxSteps	18
Newton TargetSteps	10
Newton RetryTimeStepReductionFactor	0.5
Newton MaxTimeStepDivisions	10
Linear Solver Reduction	$1{\cdot}10^{-7}$
MaxTimeStepSize	21600 [s]
Column height	0.13858 [m]
Column diameter	0.0525 [m]
Grid Cells	80
Amendment (and Biofilm) injection period	240 [s]
Water injection (flow rate)	$8.33{\cdot}10^{11}$ [m^3/s]
Decay rate coefficient Cases 1-3	$1 \cdot 10^{-3}$ [d^{-1}]
Decay rate coefficient Case 4	$1 \cdot 10^{-4}$ [d^{-1}]
Amendment attachment coefficient Case 3 $\lambda^{Am}_{attach,C3}$	$2.52 \cdot 10^{4}$ [m^{-1}]
Amendment detachment coefficient Case 3 $\lambda^{Am}_{detach,C3}$	$1.12 \cdot 10^{-4}$ [s^{-1}]
Amendment attachment coefficient Case 4 $\lambda^{Am}_{attach,C4}$	$5.14 \cdot 10^{4}$ [m^{-1}]

Continued on next page

Table D.1 – continued from previous page

Parameter	**Value**
Amendment detachment coefficient Case 4 $\lambda^{Am}_{detach,C4}$	$4.96 \cdot 10^{-6}$ $[s^{-1}]$
Cell attachment coefficient Case 4 $\lambda^{Bio}_{attach,C4}$	$7.51 \cdot 10^{5}$ $[m^{-1}]$
Cell detachment coefficient Case 4 $\lambda^{Bio}_{detach,C4}$	$1.11 \cdot 10^{-8}$ $[s^{-1}]$
Brooks Corey Lambda	2
Brooks Corey entry pressure	500 [Pa]
Irreducible Gas saturation	$1{\cdot}10^{-5}$ [-]
Irreducible Liquid saturation	$1{\cdot}10^{-3}$ [-]
Temperature	298.15 [K]
Initial porosity	0.48 [-]
Initial permeability	$2.23 \cdot 10^{-10}$ [cm^{-2}]
Initial pressure (top)	$1.113 \cdot 10^{5}$ [Pa]
Initial concentration of solutes	0.0 [mol/m^3]
Initial volume fraction archaea Case 1-3	$1{\cdot}10^{-7}$ [-]
Initial volume fraction bacteria Case 1-3	$1{\cdot}10^{-6}$ [-]
Initial volume fraction convertible coal	$4{\cdot}10^{-4}$ [-]

Bibliography

D. B. Archer and G. E. Powell. Dependence of the Specific Growth Rate of Methanogenic Mutualistic Cocultures on the Methanogen. *Archives of Microbiology*, 141(2):133–137, 1985.

R. T. Bachmann, A. C. Johnson, and R. G. Edyvean. Biotechnology in the petroleum industry: an overview. *International Biodeterioration & Biodegradation*, 86:225–237, 2014.

J. M. Bahr and J. Rubin. Direct comparison of kinetic and local equilibrium formulations for solute transport affected by surface reactions. *Water Resources Research*, 23(3):438–452, 1987.

E. P. Barnhart, E. P. Weeks, E. J. Jones, D. J. Ritter, J. C. McIntosh, A. C. Clark, L. F. Ruppert, A. B. Cunningham, D. S. Vinson, W. Orem, et al. Hydrogeochemistry and coal-associated bacterial populations from a methanogenic coal bed. *International Journal of Coal Geology*, 162:14–26, 2016.

E. P. Barnhart, K. J. Davis, M. Varonka, W. Orem, A. B. Cunningham, B. D. Ramsay, and M. W. Fields. Enhanced coal-dependent methanogenesis coupled with algal biofuels: Potential water recycle and carbon capture. *International Journal of Coal Geology*, 171:69–75, 2017.

P. Bastian, M. Blatt, A. Dedner, C. Engwer, R. Klöfkorn, R. Kornhuber, M. Ohlberger, and O. Sander. A generic grid interface for parallel and adaptive scientific computing. Part II: Implementation and tests in dune. *Computing*, 82(2-3):121–138, 2008a.

P. Bastian, M. Blatt, A. Dedner, C. Engwer, R. Klöfkorn, M. Ohlberger, and O. Sander. A generic grid interface for parallel and adaptive scientific computing. Part I: abstract framework. *Computing*, 82(2-3):103–119, 2008b.

P. Bastian, M. Blatt, A. Dedner, N.-A. Dreier, C. Engwer, R. Fritze, C. Gräser, C. Grüninger, D. Kempf, R. Klöfkorn, et al. The DUNE framework: basic concepts and recent developments. *Computers & Mathematics with Applications*, 2020.

J. Bear. *Dynamics of fluids in porous media*. Courier Corporation, 2013.

S. Beckmann, T. Lueders, M. Krüger, F. von Netzer, B. Engelen, and H. Cypionka. Acetogens and acetoclastic methanosarcinales govern methane formation in abandoned coal mines. *Applied and environmental microbiology*, 77(11):3749–3756, 2011.

S. Beckmann, A. W. Luk, M.-L. Gutierrez-Zamora, N. H. H. Chong, T. Thomas, M. Lee, and M. Manefield. Long-term succession in a coal seam microbiome during in situ biostimulation of coalbed-methane generation. *The ISME journal*, 13(3):632–650, 2019.

K. Besemer, G. Singer, R. Limberger, A.-K. Chlup, G. Hochedlinger, I. Hödl, C. Baranyi, and T. J. Battin. Biophysical controls on community succession in stream biofilms. *Applied and environmental microbiology*, 73(15):4966–4974, 2007.

F. Birol, C. Besson, et al. Golden rules for a golden age of gas—world energy outlook special report on unconventional gas. *International Energy Agency*, 12(12), 2012.

M. J. Blunt, B. Bijeljic, H. Dong, O. Gharbi, S. Iglauer, P. Mostaghimi, A. Paluszny, and C. Pentland. Pore-scale imaging and modelling. *Advances in Water resources*, 51:197–216, 2013.

G. E. Box and R. D. Meyer. An analysis for unreplicated fractional factorials. *Technometrics*, 28(1):11–18, 1986.

R. H. Brooks and A. T. Corey. Hydraulic properties of porous media. *Hydrology papers (Colorado State University); no. 3*, 1964.

T. Bruckner, I. A. Bashmakov, Y. Mulugetta, H. Chum, A. De la Vega Navarro, J. Edmonds, A. Faaij, B. Fungtammasan, A. Garg, E. Hertwich, et al. Energy systems climate change 2014: Mitigation of climate change. contribution of working group III to the fifth assessment report of the intergovernmental panel on climate change ed or edenhofer et al. *Cambridge and New York: Cambridge University Press. Available at: https://www. ipcc. ch/pdf/assessment-report/ar5/wg3/ipcc_wg3_ar5_chapter7. pdf*, 2014.

J. D. Bryers. *Biofilms II*. Wiley, 2000.

J. Carrayrou, R. Mosé, and P. Behra. Operator-splitting procedures for reactive transport and comparison of mass balance errors. *Journal of Contaminant Hydrology*, 68 (3-4):239–268, 2004.

T. Chai and R. R. Draxler. Root mean square error (RMSE) or mean absolute error (MAE)?–arguments against avoiding RMSE in the literature. *Geoscientific model development*, 7(3):1247–1250, 2014.

H. Chmiel, R. Takors, and D. Weuster-Botz. *Bioprozesstechnik*. Springer, 2018.

O. Cirpka and R. Helmig. Comparison of approaches for the coupling of chemistry to transport in groundwater systems. In *Modeling and Computation in Environmental Sciences*, pages 102–120. Springer, 1997.

H. Class. *Models for non-isothermal compositional gas-liquid flow and transport in porous media*. Habilitationsschrift, Universität Stuttgart, Institut für Wasserbau, 6 2007. URL `https://elib.uni-stuttgart.de/opus/volltexte/2009/3847/pdf/class_habil_version1.1.pdf`.

H. Class, R. Helmig, and P. Bastian. Numerical simulation of non-isothermal multiphase multicomponent processes in porous media.: 1. an efficient solution technique. *Advances in Water Resources*, 25(5):533–550, 2002.

H. Class, A. Ebigbo, R. Helmig, H. K. Dahle, J. M. Nordbotten, M. A. Celia, P. Audigane, M. Darcis, J. Ennis-King, Y. Fan, et al. A benchmark study on problems related to CO2 storage in geologic formations. *Computational Geosciences*, 13(4): 409, 2009.

D. R. Cullimore. *Microbiology of well biofouling*, volume 3. CRC press, 1999.

A. B. Cunningham, R. R. Sharp, R. Hiebert, and G. James. Subsurface biofilm barriers for the containment and remediation of contaminated groundwater. *Bioremediation Journal*, 7(3-4):151–164, 2003.

A. B. Cunningham, H. Class, A. Ebigbo, R. Gerlach, A. J. Phillips, and J. Hommel. Field-scale modeling of microbially induced calcite precipitation. *Computational Geosciences*, 23(2):399–414, 2019.

H. P. G. Darcy. *Les Fontaines publiques de la ville de Dijon. Exposition et application des principes à suivre et des formules à employer dans les questions de distribution d'eau, etc.* V. Dalamont, 1856.

K. Davis, G. Platt, E. Barnhart, R. Hiebert, R. Hyatt, M. Fields, and R. Gerlach. Biogenic coal-to-methane conversion can be enhanced with small additions of algal amendment in field-relevant upflow column reactors. *Fuel*, 256, 08 2019. doi: 10.1016/j.fuel.2019.115905.

K. J. Davis and R. Gerlach. Transition of biogenic coal-to-methane conversion from the laboratory to the field: A review of important parameters and studies. *International Journal of Coal Geology*, 185:33–43, 2018.

K. J. Davis, E. P. Barnhart, M. W. Fields, and R. Gerlach. Biogenic coal-to-methane conversion efficiency decreases after repeated organic amendment. *Energy & Fuels*, 32(3):2916–2925, 2018a.

K. J. Davis, S. Lu, E. P. Barnhart, A. E. Parker, M. W. Fields, and R. Gerlach. Type and amount of organic amendments affect enhanced biogenic methane production from coal and microbial community structure. *Fuel*, 211:600–608, 2018b.

D. De Beer and P. Stoodley. Microbial biofilms. *Prokaryotes*, 1:904–937, 2006.

J. Doherty. *Calibration and uncertainty analysis for complex environmental models.* Watermark Numerical Computing, 2015.

M. A. Dojka, P. Hugenholtz, S. K. Haack, and N. R. Pace. Microbial diversity in a hydrocarbon-and chlorinated-solvent-contaminated aquifer undergoing intrinsic bioremediation. *Applied and Environmental Microbiology*, 64(10):3869–3877, 1998.

B. Dudley et al. BP statistical review of world energy. *BP Statistical Review, London, UK, accessed Aug*, 6:2018, 2018.

A. Ebigbo, R. Helmig, A. B. Cunningham, H. Class, and R. Gerlach. Modelling biofilm growth in the presence of carbon dioxide and water flow in the subsurface. *Advances in Water Resources*, 33(7):762–781, 2010.

S. Emmert, H. Class, K. J. Davis, and R. Gerlach. Importance of specific substrate utilization by microbes in microbially enhanced coal-bed methane production: A

modelling study. *International Journal of Coal Geology*, 229:103567, 2020a. ISSN 0166-5162. doi: 10.1016/j.coal.2020.103567.

S. Emmert, K. Davis, R. Gerlach, and H. Class. The role of retardation, attachment and detachment processes during microbial coal-bed methane production after organic amendment. *Water*, 12(11):3008, 2020b. doi: 10.3390/w12113008.

M. Fahs, J. Carrayrou, A. Younes, and P. Ackerer. On the efficiency of the direct substitution approach for reactive transport problems in porous media. *Water, air, and soil pollution*, 193(1-4):299–308, 2008.

H. Fang, Y. Chen, L. Huang, and G. He. Analysis of biofilm bacterial communities under different shear stresses using size-fractionated sediment. *Scientific Reports*, 7 (1):1–14, 2017.

B. Flemisch, M. Darcis, K. Erbertseder, B. Faigle, A. Lauser, K. Mosthaf, S. Müthing, P. Nuske, A. Tatomir, M. Wolff, and R. Helmig. DuMux: DUNE for multi-phase,component,scale,physics,... flow and transport in porous media. *Advances in Water Resources*, 34(9):1102 – 1112, 2011. doi: 10.1016/j.advwatres.2011.03.007. New Computational Methods and Software Tools.

B. Flemisch, I. Berre, W. Boon, A. Fumagalli, N. Schwenck, A. Scotti, I. Stefansson, and A. Tatomir. Benchmarks for single-phase flow in fractured porous media. *Advances in Water Resources*, 111:239–258, 2018.

R. M. Flores, C. A. Rice, G. D. Stricker, A. Warden, and M. S. Ellis. Methanogenic pathways of coal-bed gas in the Powder River Basin, United States: the geologic factor. *International Journal of Coal Geology*, 76(1-2):52–75, 2008.

H. Freundlich et al. Over the adsorption in solution. *Journal of Physical Chemistry*, 57(385471):1100–1107, 1906.

J.-L. Garcia, B. Ollivier, and W. B. Whitman. The order methanomicrobiales. *The prokaryotes: Volume 3: Archaea. Bacteria: Firmicutes, actinomycetes*, pages 208–230, 2006.

S. Geetha, I. M. Banat, and S. J. Joshi. Biosurfactants: Production and potential applications in microbial enhanced oil recovery (MEOR). *Biocatalysis and Agricultural Biotechnology*, 14:23–32, 2018.

D. Gläser, B. Flemisch, R. Helmig, and H. Class. A hybrid-dimensional discrete fracture model for non-isothermal two-phase flow in fractured porous media. *GEM-International Journal on Geomathematics*, 10(1):5, 2019.

M. S. Green, K. C. Flanegan, and P. C. Gilcrease. Characterization of a methanogenic consortium enriched from a coalbed methane well in the Powder River Basin, USA. *International Journal of Coal Geology*, 76(1-2):34–45, 2008.

M. Grösbacher, D. Eckert, O. A. Cirpka, and C. Griebler. Contaminant concentration versus flow velocity: drivers of biodegradation and microbial growth in groundwater model systems. *Biodegradation*, 29(3):211–232, 2018.

P. Gupta and A. Gupta. Biogas production from coal via anaerobic fermentation. *Fuel*, 118:238 – 242, 2014. ISSN 0016-2361. doi: 10.1016/j.fuel.2013.10.075.

S. Harpalani and X. Zhao. Microstructure of coal and its influence on flow of gas. *Energy Sources*, 13(2):229–242, 1991.

S. H. Harris, R. L. Smith, and C. E. Barker. Microbial and chemical factors influencing methane production in laboratory incubations of low-rank subsurface coals. *International Journal of Coal Geology*, 76(1-2):46–51, 2008.

R. Helmig et al. *Multiphase flow and transport processes in the subsurface: a contribution to the modeling of hydrosystems.* Springer-Verlag, 1997.

J. Herman and W. Usher. SALib: An open-source python library for sensitivity analysis. *The Journal of Open Source Software*, 2(9), jan 2017. doi: 10.21105/joss.00097.

J. Hommel, E. Lauchnor, A. Phillips, R. Gerlach, A. B. Cunningham, R. Helmig, A. Ebigbo, and H. Class. A Revised Model for Microbially Induced Calcite Precipitation: Improvements and new Insights Based on Recent Experiments. *Water Resources Research*, 51(5):3695–3715, 2015.

J. Hommel, E. Coltman, and H. Class. Porosity-permeability relations for evolving pore space: a review with a focus on (bio-)geochemically altered porous media. *Transport in Porous Media*, 124:589–629, 2018.

T. Hower, J. Jones, D. Goldstein, W. Harbridge, et al. Development of the wyodak coalbed methane resource in the powder river basin. In *SPE Annual Technical Conference and Exhibition*. Society of Petroleum Engineers, 2003.

P. Hron. *Numerical Simulation of Multi-Phase Multi-Component Reactive Flow in Porous Media*. PhD thesis, 2015.

W. Hundsdorfer and J. G. Verwer. A note on splitting errors for advection-reaction equations. *Applied Numerical Mathematics*, 18(1-3):191–199, 1995.

T. Iwasaki, J. Slade, and W. E. Stanley. Some notes on sand filtration [with discussion]. *Journal (American Water Works Association)*, 29(10):1591–1602, 1937.

C. J. Willmott and K. Matsuura. Advantages of the Mean Absolute Error (MAE) over the Root Mean Square Error (RMSE) in Assessing Average Model Performance. *Climate Research*, 30:79, 12 2005. doi: 10.3354/cr030079.

V. Jegatheesan and S. Vigneswaran. Deep bed filtration: mathematical models and observations. *Critical Reviews in Environmental Science and Technology*, 35(6):515–569, 2005.

A. Jones, G. Bell, R. Morales, and R. Schraufnagel. The influence of coal fines/chips on the behavior of hydraulic fracture stimulation treatments. In *The 1987 Coalbed Methane Symposium Proceedings, The University of Alabama, Tuscaloosa, Alabama,(November) pp*, pages 93–102, 1987.

E. J. Jones, M. A. Voytek, M. D. Corum, and W. H. Orem. Stimulation of methane generation from nonproductive coal by addition of nutrients or a microbial consortium. *Applied and environmental microbiology*, 76(21):7013–7022, 2010.

J.-W. Kim, H. Choi, and Y. A. Pachepsky. Biofilm morphology as related to the porous media clogging. *Water Research*, 44(4):1193–1201, 2010.

D. J. Kirkner and H. Reeves. Multicomponent mass transport with homogeneous and heterogeneous chemical reactions: effect of the chemistry on the choice of numerical algorithm: 1. theory. *Water Resources Research*, 24(10):1719–1729, 1988.

T. Koch, D. Gläser, K. Weishaupt, S. Ackermann, M. Beck, B. Becker, S. Burbulla, H. Class, E. Coltman, S. Emmert, et al. Dumux 3–an open-source simulator for solving flow and transport problems in porous media with a focus on model coupling. *Computers & Mathematics with Applications*, 2020.

I. Langmuir. The constitution and fundamental properties of solids and liquids. II. Liquids. *Journal of the American chemical society*, 39(9):1848–1906, 1917.

D. Lanser and J. G. Verwer. Analysis of operator splitting for advection–diffusion–reaction problems from air pollution modelling. *Journal of computational and applied mathematics*, 111(1-2):201–216, 1999.

P. C. Lichtner. Reactive transport in porous media. *Mineralogical Society of America, Reviews in Mineralogy*, 34:438, 1996.

X. Liu, F. Civan, et al. Formation damage and filter cake buildup in laboratory core tests: modeling and model-assisted analysis. *SPE Formation Evaluation*, 11(01): 26–30, 1996.

N. Lupton, L. D. Connell, D. Heryanto, R. Sander, M. Camilleri, D. I. Down, and Z. Pan. Enhancing biogenic methane generation in coalbed methane reservoirs–core flooding experiments on coals at in-situ conditions. *International Journal of Coal Geology*, 219:103377, 2020.

E. Lyautey, C. R. Jackson, J. Cayrou, J.-L. Rols, and F. Garabétian. Bacterial community succession in natural river biofilm assemblages. *Microbial Ecology*, 50(4): 589–601, 2005.

M. Magot, B. Ollivier, and B. K. Patel. Microbiology of petroleum reservoirs. *Antonie van Leeuwenhoek*, 77(2):103–116, 2000.

P. McCarty. Energetics of organic matter degradation. *Water pollution microbiology*, pages 91–108, 1972.

M. Meslé, G. Dromart, and P. Oger. Microbial methanogenesis in subsurface oil and coal. *Research in microbiology*, 164(9):959–972, 2013.

I. L. Molnar, W. P. Johnson, J. I. Gerhard, C. S. Willson, and D. M. O'Carroll. Predicting colloid transport through saturated porous media: A critical review. *Water Resources Research*, 51(9):6804–6845, 2015.

J. Monod. Recherches sur la croissance des cultures bacteriennes. 1942.

X. Pan, I. Angelidaki, M. Alvarado-Morales, H. Liu, Y. Liu, X. Huang, and G. Zhu. Methane production from formate, acetate and H2/CO2; focusing on kinetics and microbial characterization. *Bioresource Technology*, 218:796 – 806, 2016. ISSN 0960-8524. doi: 10.1016/j.biortech.2016.07.032.

S. Y. Park and Y. Liang. Biogenic methane production from coal: A review on recent research and development on microbially enhanced coalbed methane (mecbm). *Fuel*, 166:258–267, 2016.

M. Peter. Implementierung eines numerischen Modells für den Transport von Tracerkomponenten in Zweiphasenströmungen. Projektarbeit, Universität Stuttgart, Institut für Wasser-und Umweltsystemmodellierung, Januar 2019.

A. J. Phillips, R. Gerlach, E. Lauchnor, A. C. Mitchell, A. B. Cunningham, and L. Spangler. Engineered applications of ureolytic biomineralization: a review. *Biofouling*, 29 (6):715–733, 2013.

A. J. Phillips, E. Troyer, R. Hiebert, C. Kirkland, R. Gerlach, A. B. Cunningham, L. Spangler, J. Kirksey, W. Rowe, and R. Esposito. Enhancing wellbore cement integrity with microbially induced calcite precipitation (MICP): a field scale demonstration. *Journal of petroleum science and engineering*, 171:1141–1148, 2018.

D. Ritter, D. Vinson, E. Barnhart, D. M. Akob, M. W. Fields, A. B. Cunningham, W. Orem, and J. C. McIntosh. Enhanced microbial coalbed methane generation: A review of research, commercial activity, and remaining challenges. *International Journal of Coal Geology*, 146:28 – 41, 2015. ISSN 0166-5162. doi: 10.1016/j.coal.2015.04.013.

B. E. Rittman. The effect of shear stress on biofilm loss rate. *Biotechnology and bioengineering*, 24(2):501–506, 1982.

B. E. Rittmann. The significance of biofilms in porous media. *Water Resources Research*, 29(7):2195–2202, 1993.

J. A. Robinson and J. M. Tiedje. Competition Between Sulfate-Reducing and Methanogenic Bacteria for H 2 under Resting and Growing Conditions. *Archives of Microbiology*, 137(1):26–32, 1984.

A. Rochex, J.-J. Godon, N. Bernet, and R. Escudié. Role of shear stress on composition, diversity and dynamics of biofilm bacterial communities. *Water Research*, 42(20): 4915–4922, 2008.

M. L. Rockhold, R. Yarwood, and J. S. Selker. Coupled microbial and transport processes in soils. *Vadose Zone Journal*, 3(2):368–383, 2004.

M. W. Saaltink, J. Carrera, and C. Ayora. On the behavior of approaches to simulate reactive transport. *Journal of Contaminant Hydrology*, 48(3-4):213–235, 2001.

A. Saltelli, S. Tarantola, F. Campolongo, and M. Ratto. *Sensitivity analysis in practice: a guide to assessing scientific models*, volume 1. Wiley Online Library, 2004.

O. Sander, T. Koch, N. Schröder, and B. Flemisch. The Dune FoamGrid implementation for surface and network grids. *Archive of Numerical Software*, 5(1):217–244, 2017.

A. Saravanan, P. S. Kumar, K. H. Vardhan, S. Jeevanantham, S. B. Karishma, P. R. Yaashikaa, and P. Vellaichamy. A review on systematic approach for microbial enhanced oil recovery technologies: opportunities and challenges. *Journal of Cleaner Production*, page 120777, 2020.

S. Saurabh and S. Harpalani. Modeling of microbial methane generation from coal and assessment of its impact on flow behavior. *Fuel*, 216:274–283, 2018.

D. Scheer, H. Class, and B. Flemisch. *Subsurface Environmental Modelling Between Science and Policy*. Springer International Publishing, 2021. ISBN 978-3-030-51177-7. doi: 10.1007/978-3-030-51178-4.

T. Scheibe and S. Yabusaki. Scaling of flow and transport behavior in heterogeneous groundwater systems. *Advances in Water Resources*, 22(3):223 – 238, 1998. ISSN 0309-1708. doi: 10.1016/S0309-1708(98)00014-1.

B. Schink. Energetics of Syntrophic Cooperation in Methanogenic Degradation. *Microbiology and Molecular Biology Reviews*, 61(2):262–280, 1997.

S. Scholz. Modeling microbially enhanced coal-bed methane production. Masterarbeit, Universität Stuttgart, Institut für Wasser-und Umweltsystemmodellierung, February 2017.

G. Senthamaraikkannan, K. Budwill, I. Gates, S. Mitra, and V. Prasad. Kinetic modeling of the biogenic production of coalbed methane. *Energy & Fuels*, 30(2):871–883, 2016a.

G. Senthamaraikkannan, I. Gates, and V. Prasad. Development of a Multiscale Microbial Kinetics Coupled Gas Transport Model for the Simulation of Biogenic Coalbed Methane Production. *Fuel*, 167:188–198, 2016b.

V. Smil. *Energy transitions: global and national perspectives*. ABC-CLIO, 2016.

I. M. Sobol. Global sensitivity indices for nonlinear mathematical models and their monte carlo estimates. *Mathematics and computers in simulation*, 55(1-3):271–280, 2001.

A. H. Sørensen and B. K. Ahring. Measurements of the Specific Methanogenic Activity of Anaerobic Digestor Biomass. *Applied Microbiology and Biotechnology*, 40(2):427–431, 1993.

R. Span and W. Wagner. A new equation of state for carbon dioxide covering the fluid region from the triple-point temperature to 1100 k at pressures up to 800 mpa. *Journal of physical and chemical reference data*, 25(6):1509–1596, 1996.

G. E. Speitel Jr and F. A. DiGiano. Biofilm shearing under dynamic conditions. *Journal of Environmental Engineering*, 113(3):464–475, 1987.

C. Steefel, C. Appelo, B. Arora, D. Jacques, T. Kalbacher, O. Kolditz, V. Lagneau, P. Lichtner, K. U. Mayer, J. Meeussen, et al. Reactive transport codes for subsurface environmental simulation. *Computational Geosciences*, 19(3):445–478, 2015.

C. I. Steefel and K. T. MacQuarrie. Approaches to modeling of reactive transport in porous media. *Reviews in Mineralogy and Geochemistry*, 34(1):85–129, 1996.

G. Strang. On the construction and comparison of difference schemes. *SIAM journal on numerical analysis*, 5(3):506–517, 1968.

D. Strapoc, F. W. Picardal, C. Turich, I. Schaperdoth, J. L. Macalady, J. S. Lipp, Y.-S. Lin, T. F. Ertefai, F. Schubotz, K.-U. Hinrichs, et al. Methane-producing microbial community in a coal bed of the Illinois Basin. *Applied and environmental microbiology*, 74(8):2424–2432, 2008.

D. Strapoc, M. Mastalerz, K. Dawson, J. Macalady, A. V. Callaghan, B. Wawrik, C. Turich, and M. Ashby. Biogeochemistry of microbial coal-bed methane. *Annual Review of Earth and Planetary Sciences*, 39, 2011.

E. L. Taylor, T. N. Taylor, and M. Krings. *Paleobotany: the biology and evolution of fossil plants*. Academic Press, 2009.

T. Thielemann, B. Cramer, and A. Schippers. Coalbed methane in the ruhr basin, germany: a renewable energy resource? *Organic Geochemistry*, 35(11-12):1537–1549, 2004.

C. Tien, R. M. Turian, and H. Pendse. Simulation of the dynamic behavior of deep bed filters. *AIChE Journal*, 25(3):385–395, 1979.

H. A. Van der Vorst. Bi-CGSTAB: A fast and smoothly converging variant of Bi-CG for the solution of nonsymmetric linear systems. *SIAM Journal on scientific and Statistical Computing*, 13(2):631–644, 1992.

W. Wagner, J. R. Cooper, A. Dittmann, J. Kijima, H.-J. Kretzschmar, A. Kruse, R. Mareš, K. Oguchi, H. Sato, I. Stöcker, O. Šifner, Y. Takaishi, I. Tanishita, J. Trübenbach, and T. Willkommen. The IAPWS Industrial Formulation 1997 for the Thermodynamic Properties of Water and Steam . *Journal of Engineering for Gas Turbines and Power*, 122(1):150–184, 01 2000. ISSN 0742-4795. doi: 10.1115/1.483186.

Y. Wang. Decoupled solution of flow, transport and reactions for microbially enhanced coal bed methane scenarios. Masterarbeit, Universität Stuttgart, Institut für Wasser- und Umweltsystemmodellierung, October 2019.

P. V. Welander. *Analysis of Methylotrophic Methanogenesis in Methanosarcina Barkeri Fusaro*. ProQuest, 2007.

V. S. Whiffin, L. A. Van Paassen, and M. P. Harkes. Microbial carbonate precipitation as a soil improvement technique. *Geomicrobiology Journal*, 24(5):417–423, 2007.

D. White et al. *Physiology and biochemistry of prokaryotes*. Oxford University Press, 2000.

T. Xu, J. Samper, C. Ayora, M. Manzano, and E. Custodio. Modeling of non-isothermal multi-component reactive transport in field scale porous media flow systems. *Journal of Hydrology*, 214(1-4):144–164, 1999.

G. Zhang, N. Jiang, X. Liu, and X. Dong. Methanogenesis from Methanol at Low Temperatures by a Novel Psychrophilic Methanogen,"Methanolobus psychrophilus" sp. nov., prevalent in Zoige Wetland of the Tibetan Plateau. *Applied and Environmental Microbiology*, 74(19):6114–6120, 2008.

J. Zhao, T. D. Scheibe, and R. Mahadevan. Model-based analysis of the role of biological, hydrological and geochemical factors affecting uranium bioremediation. *Biotechnology and Bioengineering*, 108(7):1537–1548, 2011. doi: 10.1002/bit.23096.

S. Zhi, D. Elsworth, J. Wang, Q. Gan, and S. Lio. Hydraulic fracturing for improved nutrient delivery in microbially-enhanced coalbed-methane (MECBM) production. *Journal of Natural Gas Science and Engineering*, 60:294–311, 2018. doi: 10.1016/j.jngse.2018.10.012.

S. Zinder. Microbiology of anaerobic conversion of organic wastes to methane: recent developments. *American Society for Microbiology News;(United States)*, 50(7), 1984.

S. H. Zinder. Physiological ecology of methanogens. In *Methanogenesis*, pages 128–206. Springer, 1993.

Institut für Wasser- und Umweltsystemmodellierung
Universität Stuttgart

Pfaffenwaldring 61
70569 Stuttgart (Vaihingen)
Telefon (0711) 685 - 60156
Telefax (0711) 685 - 51073
E-Mail: iws@iws.uni-stuttgart.de
http://www.iws.uni-stuttgart.de

Verzeichnis der Mitteilungshefte

1 Röhnisch, Arthur: *Die Bemühungen um eine Wasserbauliche Versuchsanstalt an der Technischen Hochschule Stuttgart*, und
Fattah Abouleid, Abdel: *Beitrag zur Berechnung einer in lockeren Sand gerammten, zweifach verankerten Spundwand*, 1963

2 Marotz, Günter: *Beitrag zur Frage der Standfestigkeit von dichten Asphaltbelägen im Großwasserbau*, 1964

3 Gurr, Siegfried: *Beitrag zur Berechnung zusammengesetzter ebener Flächentrag-werke unter besonderer Berücksichtigung ebener Stauwände, mit Hilfe von Rand-wert- und Lastwertmatrizen*, 1965

4 Plica, Peter: *Ein Beitrag zur Anwendung von Schalenkonstruktionen im Stahlwasserbau*, und
Petrikat, Kurt: *Möglichkeiten und Grenzen des wasserbaulichen Versuchswesens*, 1966

5 Plate, Erich: *Beitrag zur Bestimmung der Windgeschwindigkeitsverteilung in der durch eine Wand gestörten bodennahen Luftschicht*, und
Röhnisch, Arthur; Marotz, Günter: *Neue Baustoffe und Bauausführungen für den Schutz der Böschungen und der Sohle von Kanälen, Flüssen und Häfen; Gestehungskosten und jeweilige Vorteile*, sowie
Unny, T.E.: *Schwingungsuntersuchungen am Kegelstrahlschieber*, 1967

6 Seiler, Erich: *Die Ermittlung des Anlagenwertes der bundeseigenen Binnenschiffahrtsstraßen und Talsperren und des Anteils der Binnenschiffahrt an diesem Wert*, 1967

7 *Sonderheft anläßlich des 65. Geburtstages von Prof. Arthur Röhnisch mit Beiträgen von* Benk, Dieter; Breitling, J.; Gurr, Siegfried; Haberhauer, Robert; Honekamp, Hermann; Kuz, Klaus Dieter; Marotz, Günter; Mayer-Vorfelder, Hans-Jörg; Miller, Rudolf; Plate, Erich J.; Radomski, Helge; Schwarz, Helmut; Vollmer, Ernst; Wildenhahn, Eberhard; 1967

8 Jumikis, Alfred: *Beitrag zur experimentellen Untersuchung des Wassernachschubs in einem gefrierenden Boden und die Beurteilung der Ergebnisse*, 1968

9 Marotz, Günter: *Technische Grundlagen einer Wasserspeicherung im natürlichen Untergrund*, 1968

10 Radomski, Helge: *Untersuchungen über den Einfluß der Querschnittsform wellenförmiger Spundwände auf die statischen und rammtechnischen Eigenschaften*, 1968

11 Schwarz, Helmut: *Die Grenztragfähigkeit des Baugrundes bei Einwirkung vertikal gezogener Ankerplatten als zweidimensionales Bruchproblem*, 1969

12 Erbel, Klaus: *Ein Beitrag zur Untersuchung der Metamorphose von Mittelgebirgsschneedecken unter besonderer Berücksichtigung eines Verfahrens zur Bestimmung der thermischen Schneequalität*, 1969

13 Westhaus, Karl-Heinz: *Der Strukturwandel in der Binnenschiffahrt und sein Einfluß auf den Ausbau der Binnenschiffskanäle*, 1969

14 Mayer-Vorfelder, Hans-Jörg: *Ein Beitrag zur Berechnung des Erdwiderstandes unter Ansatz der logarithmischen Spirale als Gleitflächenfunktion*, 1970

15 Schulz, Manfred: *Berechnung des räumlichen Erddruckes auf die Wandung kreiszylindrischer Körper*, 1970

16 Mobasseri, Manoutschehr: *Die Rippenstützmauer. Konstruktion und Grenzen ihrer Standsicherheit*, 1970

17 Benk, Dieter: *Ein Beitrag zum Betrieb und zur Bemessung von Hochwasserrückhaltebecken*, 1970

18 Gàl, Attila: *Bestimmung der mitschwingenden Wassermasse bei überströmten Fischbauchklappen mit kreiszylindrischem Staublech*, 1971, vergriffen

19 Kuz, Klaus Dieter: *Ein Beitrag zur Frage des Einsetzens von Kavitationserscheinungen in einer Düsenströmung bei Berücksichtigung der im Wasser gelösten Gase*, 1971, vergriffen

20 Schaak, Hartmut: *Verteilleitungen von Wasserkraftanlagen*, 1971

21 *Sonderheft zur Eröffnung der neuen Versuchsanstalt des Instituts für Wasserbau der Universität Stuttgart mit Beiträgen von* Brombach, Hansjörg; Dirksen, Wolfram; Gàl, Attila; Gerlach, Reinhard; Giesecke, Jürgen; Holthoff, Franz-Josef; Kuz, Klaus Dieter; Marotz, Günter; Minor, Hans-Erwin; Petrikat, Kurt; Röhnisch, Arthur; Rueff, Helge; Schwarz, Helmut; Vollmer, Ernst; Wildenhahn, Eberhard; 1972

22 Wang, Chung-su: *Ein Beitrag zur Berechnung der Schwingungen an Kegelstrahlschiebern*, 1972

23 Mayer-Vorfelder, Hans-Jörg: *Erdwiderstandsbeiwerte nach dem Ohde-Variationsverfahren*, 1972

24 Minor, Hans-Erwin: *Beitrag zur Bestimmung der Schwingungsanfachungsfunktionen überströmter Stauklappen*, 1972, vergriffen

25 Brombach, Hansjörg: *Untersuchung strömungsmechanischer Elemente (Fluidik) und die Möglichkeit der Anwendung von Wirbelkammerelementen im Wasserbau*, 1972, vergriffen

26 Wildenhahn, Eberhard: *Beitrag zur Berechnung von Horizontalfilterbrunnen*, 1972

27 Steinlein, Helmut: *Die Eliminierung der Schwebstoffe aus Flußwasser zum Zweck der unterirdischen Wasserspeicherung, gezeigt am Beispiel der Iller*, 1972

28 Holthoff, Franz Josef: *Die Überwindung großer Hubhöhen in der Binnenschiffahrt durch Schwimmerhebewerke*, 1973

29 Röder, Karl: *Einwirkungen aus Baugrundbewegungen auf trog- und kastenförmige Konstruktionen des Wasser- und Tunnelbaues*, 1973

30 Kretschmer, Heinz: *Die Bemessung von Bogenstaumauern in Abhängigkeit von der Talform*, 1973

31 Honekamp, Hermann: *Beitrag zur Berechnung der Montage von Unterwasserpipelines*, 1973

32 Giesecke, Jürgen: *Die Wirbelkammertriode als neuartiges Steuerorgan im Wasserbau*, und Brombach, Hansjörg: *Entwicklung, Bauformen, Wirkungsweise und Steuereigenschaften von Wirbelkammerverstärkern*, 1974

33 Rueff, Helge: *Untersuchung der schwingungserregenden Kräfte an zwei hintereinander angeordneten Tiefschützen unter besonderer Berücksichtigung von Kavitation*, 1974

34 Röhnisch, Arthur: *Einpreßversuche mit Zementmörtel für Spannbeton - Vergleich der Ergebnisse von Modellversuchen mit Ausführungen in Hüllwellrohren*, 1975

35 *Sonderheft anläßlich des 65. Geburtstages von Prof. Dr.-Ing. Kurt Petrikat mit Beiträgen von*: Brombach, Hansjörg; Erbel, Klaus; Flinspach, Dieter; Fischer jr., Richard; Gàl, Attila; Gerlach, Reinhard; Giesecke, Jürgen; Haberhauer, Robert; Hafner Edzard; Hausenblas, Bernhard; Horlacher, Hans-Burkhard; Hutarew, Andreas; Knoll, Manfred; Krummet, Ralph; Marotz, Günter; Merkle, Theodor; Miller, Christoph; Minor, Hans-Erwin; Neumayer, Hans; Rao, Syamala; Rath, Paul; Rueff, Helge; Ruppert, Jürgen; Schwarz, Wolfgang; Topal-Gökceli, Mehmet; Vollmer, Ernst; Wang, Chung-su; Weber, Hans-Georg; 1975

36 Berger, Jochum: *Beitrag zur Berechnung des Spannungszustandes in rotationssymmetrisch belasteten Kugelschalen veränderlicher Wandstärke unter Gas- und Flüssigkeitsdruck durch Integration schwach singulärer Differentialgleichungen*, 1975

37 Dirksen, Wolfram: *Berechnung instationärer Abflußvorgänge in gestauten Gerinnen mittels Differenzenverfahren und die Anwendung auf Hochwasserrückhaltebecken*, 1976

38 Horlacher, Hans-Burkhard: *Berechnung instationärer Temperatur- und Wärmespannungsfelder in langen mehrschichtigen Hohlzylindern*, 1976

39 Hafner, Edzard: *Untersuchung der hydrodynamischen Kräfte auf Baukörper im Tiefwasserbereich des Meeres*, 1977, ISBN 3-921694-39-6

40 Ruppert, Jürgen: *Über den Axialwirbelkammerverstärker für den Einsatz im Wasserbau*, 1977, ISBN 3-921694-40-X

41 Hutarew, Andreas: *Beitrag zur Beeinflußbarkeit des Sauerstoffgehalts in Fließgewässern an Abstürzen und Wehren*, 1977, ISBN 3-921694-41-8, *vergriffen*

42 Miller, Christoph: *Ein Beitrag zur Bestimmung der schwingungserregenden Kräfte an unterströmten Wehren*, 1977, ISBN 3-921694-42-6

43 Schwarz, Wolfgang: *Druckstoßberechnung unter Berücksichtigung der Radial- und Längsverschiebungen der Rohrwandung*, 1978, ISBN 3-921694-43-4

44 Kinzelbach, Wolfgang: *Numerische Untersuchungen über den optimalen Einsatz variabler Kühlsysteme einer Kraftwerkskette am Beispiel Oberrhein*, 1978, ISBN 3-921694-44-2

45 Barczewski, Baldur: *Neue Meßmethoden für Wasser-Luftgemische und deren Anwendung auf zweiphasige Auftriebsstrahlen*, 1979, ISBN 3-921694-45-0

46 Neumayer, Hans: *Untersuchung der Strömungsvorgänge in radialen Wirbelkammerverstärkern*, 1979, ISBN 3-921694-46-9

47 Elalfy, Youssef-Elhassan: *Untersuchung der Strömungsvorgänge in Wirbelkammerdioden und -drosseln*, 1979, ISBN 3-921694-47-7

48 Brombach, Hansjörg: *Automatisierung der Bewirtschaftung von Wasserspeichern*, 1981, ISBN 3-921694-48-5

49 Geldner, Peter: *Deterministische und stochastische Methoden zur Bestimmung der Selbstdichtung von Gewässern*, 1981, ISBN 3-921694-49-3, *vergriffen*

50 Mehlhorn, Hans: *Temperaturveränderungen im Grundwasser durch Brauchwassereinleitungen*, 1982, ISBN 3-921694-50-7, *vergriffen*

51 Hafner, Edzard: *Rohrleitungen und Behälter im Meer*, 1983, ISBN 3-921694-51-5

52 Rinnert, Bernd: *Hydrodynamische Dispersion in porösen Medien: Einfluß von Dichteunterschieden auf die Vertikalvermischung in horizontaler Strömung*, 1983, ISBN 3-921694-52-3, *vergriffen*

53 Lindner, Wulf: *Steuerung von Grundwasserentnahmen unter Einhaltung ökologischer Kriterien*, 1983, ISBN 3-921694-53-1, *vergriffen*

54 Herr, Michael; Herzer, Jörg; Kinzelbach, Wolfgang; Kobus, Helmut; Rinnert, Bernd: *Methoden zur rechnerischen Erfassung und hydraulischen Sanierung von Grundwasserkontaminationen*, 1983, ISBN 3-921694-54-X

55 Schmitt, Paul: *Wege zur Automatisierung der Niederschlagsermittlung*, 1984, ISBN 3-921694-55-8, *vergriffen*

56 Müller, Peter: *Transport und selektive Sedimentation von Schwebstoffen bei gestautem Abfluß*, 1985, ISBN 3-921694-56-6

57 El-Qawasmeh, Fuad: *Möglichkeiten und Grenzen der Tropfbewässerung unter besonderer Berücksichtigung der Verstopfungsanfälligkeit der Tropfelemente*, 1985, ISBN 3-921694-57-4, *vergriffen*

58 Kirchenbaur, Klaus: *Mikroprozessorgesteuerte Erfassung instationärer Druckfelder am Beispiel seegangsbelasteter Baukörper*, 1985, ISBN 3-921694-58-2

59 Kobus, Helmut (Hrsg.): *Modellierung des großräumigen Wärme- und Schadstofftransports im Grundwasser*, Tätigkeitsbericht 1984/85 (DFG-Forschergruppe an den Universitäten Hohenheim, Karlsruhe und Stuttgart), 1985, ISBN 3-921694-59-0, *vergriffen*

60 Spitz, Karlheinz: *Dispersion in porösen Medien: Einfluß von Inhomogenitäten und Dichteunterschieden*, 1985, ISBN 3-921694-60-4, *vergriffen*

61 Kobus, Helmut: *An Introduction to Air-Water Flows in Hydraulics*, 1985, ISBN 3-921694-61-2

62 Kaleris, Vassilios: *Erfassung des Austausches von Oberflächen- und Grundwasser in horizontalebenen Grundwassermodellen*, 1986, ISBN 3-921694-62-0

63 Herr, Michael: *Grundlagen der hydraulischen Sanierung verunreinigter Porengrundwasserleiter*, 1987, ISBN 3-921694-63-9

64 Marx, Walter: *Berechnung von Temperatur und Spannung in Massenbeton infolge Hydratation*, 1987, ISBN 3-921694-64-7

65 Koschitzky, Hans-Peter: *Dimensionierungskonzept für Sohlbelüfter in Schußrinnen zur Vermeidung von Kavitationsschäden*, 1987, ISBN 3-921694-65-5

66 Kobus, Helmut (Hrsg.): *Modellierung des großräumigen Wärme- und Schadstofftransports im Grundwasser*, Tätigkeitsbericht 1986/87 (DFG-Forschergruppe an den Universitäten Hohenheim, Karlsruhe und Stuttgart) 1987, ISBN 3-921694-66-3

67 Söll, Thomas: *Berechnungsverfahren zur Abschätzung anthropogener Temperaturanomalien im Grundwasser*, 1988, ISBN 3-921694-67-1

68 Dittrich, Andreas; Westrich, Bernd: *Bodenseeufererosion, Bestandsaufnahme und Bewertung*, 1988, ISBN 3-921694-68-X, *vergriffen*

69 Huwe, Bernd; van der Ploeg, Rienk R.: *Modelle zur Simulation des Stickstoffhaushaltes von Standorten mit unterschiedlicher landwirtschaftlicher Nutzung*, 1988, ISBN 3-921694-69-8, *vergriffen*

70 Stephan, Karl: *Integration elliptischer Funktionen*, 1988, ISBN 3-921694-70-1

71 Kobus, Helmut; Zilliox, Lothaire (Hrsg.): *Nitratbelastung des Grundwassers, Auswirkungen der Landwirtschaft auf die Grundwasser- und Rohwasserbeschaffenheit und Maßnahmen zum Schutz des Grundwassers*. Vorträge des deutsch-französischen Kolloquiums am 6. Oktober 1988, Universitäten Stuttgart und Louis Pasteur Strasbourg (Vorträge in deutsch oder französisch, Kurzfassungen zweisprachig), 1988, ISBN 3-921694-71-X

72 Soyeaux, Renald: *Unterströmung von Stauanlagen auf klüftigem Untergrund unter Berücksichtigung laminarer und turbulenter Fließzustände*,1991, ISBN 3-921694-72-8

73 Kohane, Roberto: *Berechnungsmethoden für Hochwasserabfluß in Fließgewässern mit überströmten Vorländern*, 1991, ISBN 3-921694-73-6

74 Hassinger, Reinhard: *Beitrag zur Hydraulik und Bemessung von Blocksteinrampen in flexibler Bauweise*, 1991, ISBN 3-921694-74-4, vergriffen

75 Schäfer, Gerhard: *Einfluß von Schichtenstrukturen und lokalen Einlagerungen auf die Längsdispersion in Porengrundwasserleitern*, 1991, ISBN 3-921694-75-2

76 Giesecke, Jürgen: *Vorträge, Wasserwirtschaft in stark besiedelten Regionen; Umweltforschung mit Schwerpunkt Wasserwirtschaft*, 1991, ISBN 3-921694-76-0

77 Huwe, Bernd: *Deterministische und stochastische Ansätze zur Modellierung des Stickstoffhaushalts landwirtschaftlich genutzter Flächen auf unterschiedlichem Skalenniveau*, 1992, ISBN 3-921694-77-9, vergriffen

78 Rommel, Michael: *Verwendung von Kluftdaten zur realitätsnahen Generierung von Kluftnetzen mit anschließender laminar-turbulenter Strömungsberechnung*, 1993, ISBN 3-92 1694-78-7

79 Marschall, Paul: *Die Ermittlung lokaler Stofffrachten im Grundwasser mit Hilfe von Einbohrloch-Meßverfahren*, 1993, ISBN 3-921694-79-5, vergriffen

80 Ptak, Thomas: *Stofftransport in heterogenen Porenaquiferen: Felduntersuchungen und stochastische Modellierung*, 1993, ISBN 3-921694-80-9, vergriffen

81 Haakh, Frieder: *Transientes Strömungsverhalten in Wirbelkammern,* 1993, ISBN 3-921694-81-7

82 Kobus, Helmut; Cirpka, Olaf; Barczewski, Baldur; Koschitzky, Hans-Peter: *Versuchseinrichtung zur Grundwasser- und Altlastensanierung VEGAS, Konzeption und Programmrahmen*, 1993, ISBN 3-921694-82-5

83 Zang, Weidong: *Optimaler Echtzeit-Betrieb eines Speichers mit aktueller Abflußregenerierung*, 1994, ISBN 3-921694-83-3, vergriffen

84 Franke, Hans-Jörg: *Stochastische Modellierung eines flächenhaften Stoffeintrages und Transports in Grundwasser am Beispiel der Pflanzenschutzmittelproblematik*, 1995, ISBN 3-921694-84-1

85 Lang, Ulrich: *Simulation regionaler Strömungs- und Transportvorgänge in Karstaquiferen mit Hilfe des Doppelkontinuum-Ansatzes: Methodenentwicklung und Parameteridentifikation*, 1995, ISBN 3-921694-85-X, vergriffen

86 Helmig, Rainer: *Einführung in die Numerischen Methoden der Hydromechanik*, 1996, ISBN 3-921694-86-8, vergriffen

87 Cirpka, Olaf: *CONTRACT: A Numerical Tool for Contaminant Transport and Chemical Transformations - Theory and Program Documentation -*, 1996, ISBN 3-921694-87-6

88 Haberlandt, Uwe: *Stochastische Synthese und Regionalisierung des Niederschlages für Schmutzfrachtberechnungen*, 1996, ISBN 3-921694-88-4

89 Croisé, Jean: *Extraktion von flüchtigen Chemikalien aus natürlichen Lockergesteinen mittels erzwungener Luftströmung*, 1996, ISBN 3-921694-89-2, vergriffen

90 Jorde, Klaus: *Ökologisch begründete, dynamische Mindestwasserregelungen bei Ausleitungskraftwerken*, 1997, ISBN 3-921694-90-6, vergriffen

91 Helmig, Rainer: *Gekoppelte Strömungs- und Transportprozesse im Untergrund - Ein Beitrag zur Hydrosystemmodellierung-*, 1998, ISBN 3-921694-91-4, vergriffen

92 Emmert, Martin: *Numerische Modellierung nichtisothermer Gas-Wasser Systeme in porösen Medien,* 1997, ISBN 3-921694-92-2

93 Kern, Ulrich: *Transport von Schweb- und Schadstoffen in staugeregelten Fließgewässern am Beispiel des Neckars*, 1997, ISBN 3-921694-93-0, vergriffen

94 Förster, Georg: *Druckstoßdämpfung durch große Luftblasen in Hochpunkten von Rohrleitungen 1997*, ISBN 3-921694-94-9

95 Cirpka, Olaf: *Numerische Methoden zur Simulation des reaktiven Mehrkomponententransports im Grundwasser*, 1997, ISBN 3-921694-95-7, *vergriffen*

96 Färber, Arne: *Wärmetransport in der ungesättigten Bodenzone: Entwicklung einer thermischen In-situ-Sanierungstechnologie*, 1997, ISBN 3-921694-96-5

97 Betz, Christoph: *Wasserdampfdestillation von Schadstoffen im porösen Medium: Entwicklung einer thermischen In-situ-Sanierungstechnologie*, 1998, SBN 3-921694-97-3

98 Xu, Yichun: *Numerical Modeling of Suspended Sediment Transport in Rivers*, 1998, ISBN 3-921694-98-1, *vergriffen*

99 Wüst, Wolfgang: *Geochemische Untersuchungen zur Sanierung CKW-kontaminierter Aquifere mit Fe(0)-Reaktionswänden,* 2000, ISBN 3-933761-02-2

100 Sheta, Hussam: *Simulation von Mehrphasenvorgängen in porösen Medien unter Einbeziehung von Hysterese-Effekten*, 2000, ISBN 3-933761-03-4

101 Ayros, Edwin: *Regionalisierung extremer Abflüsse auf der Grundlage statistischer Verfahren*, 2000, ISBN 3-933761-04-2, *vergriffen*

102 Huber, Ralf: *Compositional Multiphase Flow and Transport in Heterogeneous Porous Media*, 2000, ISBN 3-933761-05-0

103 Braun, Christopherus: *Ein Upscaling-Verfahren für Mehrphasenströmungen in porösen Medien*, 2000, ISBN 3-933761-06-9

104 Hofmann, Bernd: *Entwicklung eines rechnergestützten Managementsystems zur Beurteilung von Grundwasserschadensfällen*, 2000, ISBN 3-933761-07-7

105 Class, Holger: *Theorie und numerische Modellierung nichtisothermer Mehrphasenprozesse in NAPL-kontaminierten porösen Medien,* 2001, ISBN 3-933761-08-5

106 Schmidt, Reinhard: *Wasserdampf- und Heißluftinjektion zur thermischen Sanierung kontaminierter Standorte*, 2001, ISBN 3-933761-09-3

107 Josef, Reinhold: *Schadstoffextraktion mit hydraulischen Sanierungsverfahren unter Anwendung von grenzflächenaktiven Stoffen*, 2001, ISBN 3-933761-10-7

108 Schneider, Matthias: *Habitat- und Abflussmodellierung für Fließgewässer mit unscharfen Berechnungsansätzen*, 2001, ISBN 3-933761-11-5

109 Rathgeb, Andreas: *Hydrodynamische Bemessungsgrundlagen für Lockerdeckwerke an überströmbaren Erddämmen*, 2001, ISBN 3-933761-12-3

110 Lang, Stefan: *Parallele numerische Simulation instätionärer Probleme mit adaptiven Methoden auf unstrukturierten Gittern*, 2001, ISBN 3-933761-13-1

111 Appt, Jochen; Stumpp Simone: *Die Bodensee-Messkampagne 2001, IWS/CWR Lake Constance Measurement Program 2001*, 2002, ISBN 3-933761-14-X

112 Heimerl, Stephan: *Systematische Beurteilung von Wasserkraftprojekten,* 2002, ISBN 3-933761-15-8, *vergriffen*

113 Iqbal, Amin: *On the Management and Salinity Control of Drip Irrigation,* 2002, ISBN 3-933761-16-6

114 Silberhorn-Hemminger, Annette: *Modellierung von Kluftaquifersystemen: Geostatistische Analyse und deterministisch-stochastische Kluftgenerierung,* 2002, ISBN 3-933761-17-4

115 Winkler, Angela: *Prozesse des Wärme- und Stofftransports bei der In-situ-Sanierung mit festen Wärmequellen,* 2003, ISBN 3-933761-18-2

116 Marx, Walter: *Wasserkraft, Bewässerung, Umwelt - Planungs- und Bewertungsschwerpunkte der Wasserbewirtschaftung,* 2003, ISBN 3-933761-19-0

117 Hinkelmann, Reinhard: *Efficient Numerical Methods and Information-Processing Techniques in Environment Water,* 2003, ISBN 3-933761-20-4

118 Samaniego-Eguiguren, Luis Eduardo: *Hydrological Consequences of Land Use / Land Cover and Climatic Changes in Mesoscale Catchments*, 2003, ISBN 3-933761-21-2

119 Neunhäuserer, Lina: *Diskretisierungsansätze zur Modellierung von Strömungs- und Transportprozessen in geklüftet-porösen Medien*, 2003, ISBN 3-933761-22-0

120 Paul, Maren: *Simulation of Two-Phase Flow in Heterogeneous Poros Media with Adaptive Methods*, 2003, ISBN 3-933761-23-9

121 Ehret, Uwe: *Rainfall and Flood Nowcasting in Small Catchments using Weather Radar*, 2003, ISBN 3-933761-24-7

122 Haag, Ingo: *Der Sauerstoffhaushalt staugeregelter Flüsse am Beispiel des Neckars - Analysen, Experimente, Simulationen -,* 2003, ISBN 3-933761-25-5

123 Appt, Jochen: *Analysis of Basin-Scale Internal Waves in Upper Lake Constance,* 2003, ISBN 3-933761-26-3

124 Hrsg.: Schrenk, Volker; Batereau, Katrin; Barczewski, Baldur; Weber, Karolin und Koschitzky, Hans-Peter: *Symposium Ressource Fläche und VEGAS - Statuskolloquium 2003, 30. September und 1. Oktober 2003,* 2003, ISBN 3-933761-27-1

125 Omar Khalil Ouda: *Optimisation of Agricultural Water Use: A Decision Support System for the Gaza Strip,* 2003, ISBN 3-933761-28-0

126 Batereau, Katrin: *Sensorbasierte Bodenluftmessung zur Vor-Ort-Erkundung von Schadensherden im Untergrund*, 2004, ISBN 3-933761-29-8

127 Witt, Oliver: *Erosionsstabilität von Gewässersedimenten mit Auswirkung auf den Stofftransport bei Hochwasser am Beispiel ausgewählter Stauhaltungen des Oberrheins*, 2004, ISBN 3-933761-30-1

128 Jakobs, Hartmut: *Simulation nicht-isothermer Gas-Wasser-Prozesse in komplexen Kluft-Matrix-Systemen*, 2004, ISBN 3-933761-31-X

129 Li, Chen-Chien: *Deterministisch-stochastisches Berechnungskonzept zur Beurteilung der Auswirkungen erosiver Hochwasserereignisse in Flussstauhaltungen,* 2004, ISBN 3-933761-32-8

130 Reichenberger, Volker; Helmig, Rainer; Jakobs, Hartmut; Bastian, Peter; Niessner, Jennifer: *Complex Gas-Water Processes in Discrete Fracture-Matrix Systems: Up-scaling, Mass-Conservative Discretization and Efficient Multilevel Solution,* 2004, ISBN 3-933761-33-6

131 Hrsg.: Barczewski, Baldur; Koschitzky, Hans-Peter; Weber, Karolin; Wege, Ralf: *VEGAS - Statuskolloquium 2004,* Tagungsband zur Veranstaltung am 05. Oktober 2004 an der Universität Stuttgart, Campus Stuttgart-Vaihingen, 2004, ISBN 3-933761-34-4

132 Asie, Kemal Jabir: *Finite Volume Models for Multiphase Multicomponent Flow through Porous Media*. 2005, ISBN 3-933761-35-2

133 Jacoub, George: *Development of a 2-D Numerical Module for Particulate Contaminant Transport in Flood Retention Reservoirs and Impounded Rivers,* 2004, ISBN 3-933761-36-0

134 Nowak, Wolfgang: *Geostatistical Methods for the Identification of Flow and Transport Parameters in the Subsurface,* 2005, ISBN 3-933761-37-9

135 Süß, Mia: *Analysis of the influence of structures and boundaries on flow and transport processes in fractured porous media*, 2005, ISBN 3-933761-38-7

136 Jose, Surabhin Chackiath: *Experimental Investigations on Longitudinal Dispersive Mixing in Heterogeneous Aquifers,* 2005, ISBN: 3-933761-39-5

137 Filiz, Fulya: *Linking Large-Scale Meteorological Conditions to Floods in Mesoscale Catchments,* 2005, ISBN 3-933761-40-9

138 Qin, Minghao: *Wirklichkeitsnahe und recheneffiziente Ermittlung von Temperatur und Spannungen bei großen RCC-Staumauern*, 2005, ISBN 3-933761-41-7

139 Kobayashi, Kenichiro: *Optimization Methods for Multiphase Systems in the Subsurface - Application to Methane Migration in Coal Mining Areas*, 2005, ISBN 3-933761-42-5

140 Rahman, Md. Arifur: *Experimental Investigations on Transverse Dispersive Mixing in Heterogeneous Porous Media,* 2005, ISBN 3-933761-43-3

141 Schrenk, Volker: *Ökobilanzen zur Bewertung von Altlastensanierungsmaßnahmen,* 2005, ISBN 3-933761-44-1

142 Hundecha, Hirpa Yeshewatesfa: *Regionalization of Parameters of a Conceptual Rainfall-Runoff Model*, 2005, ISBN: 3-933761-45-X

143 Wege, Ralf: *Untersuchungs- und Überwachungsmethoden für die Beurteilung natürlicher Selbstreinigungsprozesse im Grundwasser,* 2005, ISBN 3-933761-46-8

144 Breiting, Thomas: *Techniken und Methoden der Hydroinformatik - Modellierung von komplexen Hydrosystemen im Untergrund*, 2006, ISBN 3-933761-47-6

145 Hrsg.: Braun, Jürgen; Koschitzky, Hans-Peter; Müller, Martin: *Ressource Untergrund: 10 Jahre VEGAS: Forschung und Technologieentwicklung zum Schutz von Grundwasser und Boden,* Tagungsband zur Veranstaltung am 28. und 29. September 2005 an der Universität Stuttgart, Campus Stuttgart-Vaihingen, 2005, ISBN 3-933761-48-4

146 Rojanschi, Vlad: *Abflusskonzentration in mesoskaligen Einzugsgebieten unter Berücksichtigung des Sickerraumes,* 2006, ISBN 3-933761-49-2

147 Winkler, Nina Simone: *Optimierung der Steuerung von Hochwasserrückhaltebeckensystemen,* 2006, ISBN 3-933761-50-6

148 Wolf, Jens: *Räumlich differenzierte Modellierung der Grundwasserströmung alluvialer Aquifere für mesoskalige Einzugsgebiete*, 2006, ISBN: 3-933761-51-4

149 Kohler, Beate: *Externe Effekte der Laufwasserkraftnutzung*, 2006, ISBN 3-933761-52-2

150 Hrsg.: Braun, Jürgen; Koschitzky, Hans-Peter; Stuhrmann, Matthias: *VEGAS-Statuskolloquium 2006,* Tagungsband zur Veranstaltung am 28. September 2006 an der Universität Stuttgart, Campus Stuttgart-Vaihingen, 2006, ISBN 3-933761-53-0

151 Niessner, Jennifer: *Multi-Scale Modeling of Multi-Phase - Multi-Component Processes in Heterogeneous Porous Media*, 2006, ISBN 3-933761-54-9

152 Fischer, Markus: *Beanspruchung eingeerdeter Rohrleitungen infolge Austrocknung bindiger Böden,* 2006, ISBN 3-933761-55-7

153 Schneck, Alexander: *Optimierung der Grundwasserbewirtschaftung unter Berücksichtigung der Belange der Wasserversorgung, der Landwirtschaft und des Naturschutzes*, 2006, ISBN 3-933761-56-5

154 Das, Tapash: *The Impact of Spatial Variability of Precipitation on the Predictive Uncertainty of Hydrological Models,* 2006, ISBN 3-33761-57-3

155 Bielinski, Andreas: *Numerical Simulation of CO_2 sequestration in geological formations*, 2007, ISBN 3-933761-58-1

156 Mödinger, Jens: *Entwicklung eines Bewertungs- und Entscheidungsunterstützungssystems für eine nachhaltige regionale Grundwasserbewirtschaftung*, 2006, ISBN 3-933761-60-3

157 Manthey, Sabine: *Two-phase flow processes with dynamic effects in porous media - parameter estimation and simulation,* 2007, ISBN 3-933761-61-1

158 Pozos Estrada, Oscar: *Investigation on the Effects of Entrained Air in Pipelines,* 2007, ISBN 3-933761-62-X

159 Ochs, Steffen Oliver: *Steam injection into saturated porous media – process analysis including experimental and numerical investigations*, 2007, ISBN 3-933761-63-8

160 Marx, Andreas: *Einsatz gekoppelter Modelle und Wetterradar zur Abschätzung von Niederschlagsintensitäten und zur Abflussvorhersage, 2007,* ISBN 3-933761-64-6

161 Hartmann, Gabriele Maria: *Investigation of Evapotranspiration Concepts in Hydrological Modelling for Climate Change Impact Assessment*, 2007, ISBN 3-933761-65-4

162 Kebede Gurmessa, Tesfaye: *Numerical Investigation on Flow and Transport Characteristics to Improve Long-Term Simulation of Reservoir Sedimentation*, 2007, ISBN 3-933761-66-2

163 Trifković, Aleksandar: *Multi-objective and Risk-based Modelling Methodology for Planning, Design and Operation of Water Supply Systems*, 2007, ISBN 3-933761-67-0

164 Götzinger, Jens: *Distributed Conceptual Hydrological Modelling - Simulation of Climate, Land Use Change Impact and Uncertainty Analysis*, 2007, ISBN 3-933761-68-9

165 Hrsg.: Braun, Jürgen; Koschitzky, Hans-Peter; Stuhrmann, Matthias: *VEGAS – Kolloquium 2007,* Tagungsband zur Veranstaltung am 26. September 2007 an der Universität Stuttgart, Campus Stuttgart-Vaihingen, 2007, ISBN 3-933761-69-7

166 Freeman, Beau: *Modernization Criteria Assessment for Water Resources Planning; Klamath Irrigation Project, U.S.*, 2008, ISBN 3-933761-70-0

167 Dreher, Thomas: *Selektive Sedimentation von Feinstschwebstoffen in Wechselwirkung mit wandnahen turbulenten Strömungsbedingungen*, 2008, ISBN 3-933761-71-9

168 Yang, Wei: *Discrete-Continuous Downscaling Model for Generating Daily Precipitation Time Series*, 2008, ISBN 3-933761-72-7

169 Kopecki, Ianina: *Calculational Approach to FST-Hemispheres for Multiparametrical Benthos Habitat Modelling,* 2008*,* ISBN 3-933761-73-5

170 Brommundt, Jürgen: *Stochastische Generierung räumlich zusammenhängender Niederschlagszeitreihen*, 2008, ISBN 3-933761-74-3

171 Papafotiou, *Alexandros: Numerical Investigations of the Role of Hysteresis in Heterogeneous Two-Phase Flow Systems*, 2008, ISBN 3-933761-75-1

172 He, Yi: *Application of a Non-Parametric Classification Scheme to Catchment Hydrology*, 2008, ISBN 978-3-933761-76-7

173 Wagner, Sven: *Water Balance in a Poorly Gauged Basin in West Africa Using Atmospheric Modelling and Remote Sensing Information*, 2008, ISBN 978-3-933761-77-4

174 Hrsg.: Braun, Jürgen; Koschitzky, Hans-Peter; Stuhrmann, Matthias; Schrenk, Volker: *VEGAS-Kolloquium 2008 Ressource Fläche III*, Tagungsband zur Veranstaltung am 01. Oktober 2008 an der Universität Stuttgart, Campus Stuttgart-Vaihingen, 2008, ISBN 978-3-933761-78-1

175 Patil, Sachin: *Regionalization of an Event Based Nash Cascade Model for Flood Predictions in Ungauged Basins*, 2008, ISBN 978-3-933761-79-8

176 Assteerawatt, Anongnart: *Flow and Transport Modelling of Fractured Aquifers based on a Geostatistical Approach,* 2008, ISBN 978-3-933761-80-4

177 Karnahl, Joachim Alexander: *2D numerische Modellierung von multifraktionalem Schwebstoff- und Schadstofftransport in Flüssen*, 2008, ISBN 978-3-933761-81-1

178 Hiester, Uwe: *Technologieentwicklung zur In-situ-Sanierung der ungesättigten Bodenzone mit festen Wärmequellen,* 2009, ISBN 978-3-933761-82-8

179 Laux, Patrick: *Statistical Modeling of Precipitation for Agricultural Planning in the Volta Basin of West Africa,* 2009, ISBN 978-3-933761-83-5

180 Ehsan, Saqib: *Evaluation of Life Safety Risks Related to Severe Flooding,* 2009, ISBN 978-3-933761-84-2

181 Prohaska, Sandra: *Development and Application of a 1D Multi-Strip Fine Sediment Transport Model for Regulated Rivers,* 2009, ISBN 978-3-933761-85-9

182 Kopp, Andreas: *Evaluation of CO_2 Injection Processes in Geological Formations for Site Screening,* 2009, ISBN 978-3-933761-86-6

183 Ebigbo, Anozie: *Modelling of biofilm growth and its influence on CO_2 and water (two-phase) flow in porous media,* 2009, ISBN 978-3-933761-87-3

184 Freiboth, Sandra: *A phenomenological model for the numerical simulation of multiphase multicomponent processes considering structural alterations of porous media*, 2009, ISBN 978-3-933761-88-0

185 Zöllner, Frank: *Implementierung und Anwendung netzfreier Methoden im Konstruktiven Wasserbau und in der Hydromechanik*, 2009, ISBN 978-3-933761-89-7

186 Vasin, Milos: *Influence of the soil structure and property contrast on flow and transport in the unsaturated zone*, 2010, ISBN 978-3-933761-90-3

187 Li, Jing: *Application of Copulas as a New Geostatistical Tool*, 2010, ISBN 978-3-933761-91-0

188 AghaKouchak, Amir: *Simulation of Remotely Sensed Rainfall Fields Using Copulas*, 2010, ISBN 978-3-933761-92-7

189 Thapa, Pawan Kumar: *Physically-based spatially distributed rainfall runoff modelling for soil erosion estimation*, 2010, ISBN 978-3-933761-93-4

190 Wurms, Sven: *Numerische Modellierung der Sedimentationsprozesse in Retentionsanlagen zur Steuerung von Stoffströmen bei extremen Hochwasserabflussereignissen*, 2011, ISBN 978-3-933761-94-1

191 Merkel, Uwe: *Unsicherheitsanalyse hydraulischer Einwirkungen auf Hochwasserschutzdeiche und Steigerung der Leistungsfähigkeit durch adaptive Strömungsmodellierung*, 2011, ISBN 978-3-933761-95-8

192 Fritz, Jochen: *A Decoupled Model for Compositional Non-Isothermal Multiphase Flow in Porous Media and Multiphysics Approaches for Two-Phase Flow*, 2010, ISBN 978-3-933761-96-5

193 Weber, Karolin (Hrsg.): *12. Treffen junger WissenschaftlerInnen an Wasserbauinstituten*, 2010, ISBN 978-3-933761-97-2

194 Bliefernicht, Jan-Geert: *Probability Forecasts of Daily Areal Precipitation for Small River Basins,* 2011, ISBN 978-3-933761-98-9

195 Hrsg.: Koschitzky, Hans-Peter; Braun, Jürgen: *VEGAS-Kolloquium 2010 In-situ-Sanierung - Stand und Entwicklung Nano und ISCO -,* Tagungsband zur Veranstaltung am 07. Oktober 2010 an der Universität Stuttgart, Campus Stuttgart-Vaihingen*,* 2010*,* ISBN 978-3-933761-99-6

196 Gafurov, Abror: *Water Balance Modeling Using Remote Sensing Information - Focus on Central Asia,* 2010, ISBN 978-3-942036-00-9

197 Mackenberg, Sylvia: *Die Quellstärke in der Sickerwasserprognose: Möglichkeiten und Grenzen von Labor- und Freilanduntersuchungen,* 2010, ISBN 978-3-942036-01-6

198 Singh, Shailesh Kumar: *Robust Parameter Estimation in Gauged and Ungauged Basins,* 2010, ISBN 978-3-942036-02-3

199 Doğan, Mehmet Onur: *Coupling of porous media flow with pipe flow,* 2011, ISBN 978-3-942036-03-0

200 Liu, Min: *Study of Topographic Effects on Hydrological Patterns and the Implication on Hydrological Modeling and Data Interpolation,* 2011, ISBN 978-3-942036-04-7

201 Geleta, Habtamu Itefa: *Watershed Sediment Yield Modeling for Data Scarce Areas,* 2011, ISBN 978-3-942036-05-4

202 Franke, Jörg: *Einfluss der Überwachung auf die Versagenswahrscheinlichkeit von Staustufen,* 2011, ISBN 978-3-942036-06-1

203 Bakimchandra, Oinam: *Integrated Fuzzy-GIS approach for assessing regional soil erosion risks,* 2011, ISBN 978-3-942036-07-8

204 Alam, Muhammad Mahboob: *Statistical Downscaling of Extremes of Precipitation in Mesoscale Catchments from Different RCMs and Their Effects on Local Hydrology,* 2011, ISBN 978-3-942036-08-5

205 Hrsg.: Koschitzky, Hans-Peter; Braun, Jürgen: *VEGAS-Kolloquium 2011 Flache Geothermie - Perspektiven und Risiken,* Tagungsband zur Veranstaltung am 06. Oktober 2011 an der Universität Stuttgart, Campus Stuttgart-Vaihingen*,* 2011*,* ISBN 978-3-933761-09-2

206 Haslauer, Claus: *Analysis of Real-World Spatial Dependence of Subsurface Hydraulic Properties Using Copulas with a Focus on Solute Transport Behaviour,* 2011, ISBN 978-3-942036-10-8

207 Dung, Nguyen Viet: *Multi-objective automatic calibration of hydrodynamic models – development of the concept and an application in the Mekong Delta,* 2011, ISBN 978-3-942036-11-5

208 Hung, Nguyen Nghia: *Sediment dynamics in the floodplain of the Mekong Delta, Vietnam,* 2011, ISBN 978-3-942036-12-2

209 Kuhlmann, Anna: *Influence of soil structure and root water uptake on flow in the unsaturated zone,* 2012, ISBN 978-3-942036-13-9

210 Tuhtan, Jeffrey Andrew: *Including the Second Law Inequality in Aquatic Ecodynamics: A Modeling Approach for Alpine Rivers Impacted by Hydropeaking,* 2012, ISBN 978-3-942036-14-6

211 Tolossa, Habtamu: *Sediment Transport Computation Using a Data-Driven Adaptive Neuro-Fuzzy Modelling Approach,* 2012, ISBN 978-3-942036-15-3

212 Tatomir, Alexandru-Bodgan: *From Discrete to Continuum Concepts of Flow in Fractured Porous Media,* 2012, ISBN 978-3-942036-16-0

213 Erbertseder, Karin: *A Multi-Scale Model for Describing Cancer-Therapeutic Transport in the Human Lung,* 2012, ISBN 978-3-942036-17-7

214 Noack, Markus: *Modelling Approach for Interstitial Sediment Dynamics and Reproduction of Gravel Spawning Fish,* 2012, ISBN 978-3-942036-18-4

215 De Boer, Cjestmir Volkert: *Transport of Nano Sized Zero Valent Iron Colloids during Injection into the Subsurface*, 2012, ISBN 978-3-942036-19-1

216 Pfaff, Thomas: *Processing and Analysis of Weather Radar Data for Use in Hydrology*, 2013, ISBN 978-3-942036-20-7

217 Lebrenz, Hans-Henning: *Addressing the Input Uncertainty for Hydrological Modeling by a New Geostatistical Method*, 2013, ISBN 978-3-942036-21-4

218 Darcis, Melanie Yvonne: *Coupling Models of Different Complexity for the Simulation of CO_2 Storage in Deep Saline Aquifers*, 2013, ISBN 978-3-942036-22-1

219 Beck, Ferdinand: *Generation of Spatially Correlated Synthetic Rainfall Time Series in High Temporal Resolution - A Data Driven Approach*, 2013, ISBN 978-3-942036-23-8

220 Guthke, Philipp: *Non-multi-Gaussian spatial structures: Process-driven natural genesis, manifestation, modeling approaches, and influences on dependent processes*, 2013, ISBN 978-3-942036-24-5

221 Walter, Lena: *Uncertainty studies and risk assessment for CO_2 storage in geological formations*, 2013, ISBN 978-3-942036-25-2

222 Wolff, Markus: *Multi-scale modeling of two-phase flow in porous media including capillary pressure effects,* 2013, ISBN 978-3-942036-26-9

223 Mosthaf, Klaus Roland: *Modeling and analysis of coupled porous-medium and free flow with application to evaporation processes,* 2014, ISBN 978-3-942036-27-6

224 Leube, Philipp Christoph: *Methods for Physically-Based Model Reduction in Time: Analysis, Comparison of Methods and Application*, 2013, ISBN 978-3-942036-28-3

225 Rodríguez Fernández, Jhan Ignacio: *High Order Interactions among environmental variables: Diagnostics and initial steps towards modeling*, 2013, ISBN 978-3-942036-29-0

226 Eder, Maria Magdalena: *Climate Sensitivity of a Large Lake*, 2013, ISBN 978-3-942036-30-6

227 Greiner, Philipp: *Alkoholinjektion zur In-situ-Sanierung von CKW Schadensherden in Grundwasserleitern: Charakterisierung der relevanten Prozesse auf unterschiedlichen Skalen*, 2014, ISBN 978-3-942036-31-3

228 Lauser, Andreas: *Theory and Numerical Applications of Compositional Multi-Phase Flow in Porous Media*, 2014, ISBN 978-3-942036-32-0

229 Enzenhöfer, Rainer: *Risk Quantification and Management in Water Production and Supply Systems*, 2014, ISBN 978-3-942036-33-7

230 Faigle, Benjamin: *Adaptive modelling of compositional multi-phase flow with capillary pressure*, 2014, ISBN 978-3-942036-34-4

231 Oladyshkin, Sergey: *Efficient modeling of environmental systems in the face of complexity and uncertainty*, 2014, ISBN 978-3-942036-35-1

232 Sugimoto, Takayuki: *Copula based Stochastic Analysis of Discharge Time Series*, 2014, ISBN 978-3-942036-36-8

233 Koch, Jonas: *Simulation, Identification and Characterization of Contaminant Source Architectures in the Subsurface*, 2014, ISBN 978-3-942036-37-5

234 Zhang, Jin: *Investigations on Urban River Regulation and Ecological Rehabilitation Measures, Case of Shenzhen in China*, 2014, ISBN 978-3-942036-38-2

235 Siebel, Rüdiger: *Experimentelle Untersuchungen zur hydrodynamischen Belastung und Standsicherheit von Deckwerken an überströmbaren Erddämmen,* 2014, ISBN 978-3-942036-39-9

236 Baber, Katherina: *Coupling free flow and flow in porous media in biological and technical applications: From a simple to a complex interface description,* 2014, ISBN 978-3-942036-40-5

237 Nuske, Klaus Philipp: *Beyond Local Equilibrium — Relaxing local equilibrium assumptions in multiphase flow in porous media,* 2014, ISBN 978-3-942036-41-2

238 Geiges, Andreas: *Efficient concepts for optimal experimental design in nonlinear environmental systems*, 2014, ISBN 978-3-942036-42-9

239 Schwenck, Nicolas: *An XFEM-Based Model for Fluid Flow in Fractured Porous Media*, 2014, ISBN 978-3-942036-43-6

240 Chamorro Chávez, Alejandro: *Stochastic and hydrological modelling for climate change prediction in the Lima region, Peru*, 2015, ISBN 978-3-942036-44-3

241 Yulizar: *Investigation of Changes in Hydro-Meteorological Time Series Using a Depth-Based Approach*, 2015, ISBN 978-3-942036-45-0

242 Kretschmer, Nicole: *Impacts of the existing water allocation scheme on the Limarí watershed – Chile, an integrative approach*, 2015, ISBN 978-3-942036-46-7

243 Kramer, Matthias: *Luftbedarf von Freistrahlturbinen im Gegendruckbetrieb*, 2015, ISBN 978-3-942036-47-4

244 Hommel, Johannes: *Modeling biogeochemical and mass transport processes in the subsurface: Investigation of microbially induced calcite precipitation*, 2016, ISBN 978-3-942036-48-1

245 Germer, Kai: *Wasserinfiltration in die ungesättigte Zone eines makroporösen Hanges und deren Einfluss auf die Hangstabilität*, 2016, ISBN 978-3-942036-49-8

246 Hörning, Sebastian: *Process-oriented modeling of spatial random fields using copulas*, 2016, ISBN 978-3-942036-50-4

247 Jambhekar, Vishal: *Numerical modeling and analysis of evaporative salinization in a coupled free-flow porous-media system,* 2016, ISBN 978-3-942036-51-1

248 Huang, Yingchun: *Study on the spatial and temporal transferability of conceptual hydrological models*, 2016, ISBN 978-3-942036-52-8

249 Kleinknecht, Simon Matthias: *Migration and retention of a heavy NAPL vapor and remediation of the unsaturated zone*, 2016, ISBN 978-3-942036-53-5

250 Kwakye, Stephen Oppong: *Study on the effects of climate change on the hydrology of the West African sub-region*, 2016, ISBN 978-3-942036-54-2

251 Kissinger, Alexander: *Basin-Scale Site Screening and Investigation of Possible Impacts of CO_2 Storage on Subsurface Hydrosystems*, 2016, ISBN 978-3-942036-55-9

252 Müller, Thomas: *Generation of a Realistic Temporal Structure of Synthetic Precipitation Time Series for Sewer Applications*, 2017, ISBN 978-3-942036-56-6

253 Grüninger, Christoph: *Numerical Coupling of Navier-Stokes and Darcy Flow for Soil-Water Evaporation*, 2017, ISBN 978-3-942036-57-3

254 Suroso: *Asymmetric Dependence Based Spatial Copula Models: Empirical Investigations and Consequences on Precipitation Fields*, 2017, ISBN 978-3-942036-58-0

255 Müller, Thomas; Mosthaf, Tobias; Gunzenhauser, Sarah; Seidel, Jochen; Bárdossy, András: *Grundlagenbericht Niederschlags-Simulator (NiedSim3)*, 2017, ISBN 978-3-942036-59-7

256 Mosthaf, Tobias: *New Concepts for Regionalizing Temporal Distributions of Precipitation and for its Application in Spatial Rainfall Simulation,* 2017, ISBN 978-3-942036-60-3

257 Fenrich, Eva Katrin: *Entwicklung eines ökologisch-ökonomischen Vernetzungsmodells für Wasserkraftanlagen und Mehrzweckspeicher,* 2018, ISBN 978-3-942036-61-0

258 Schmidt, Holger: *Microbial stabilization of lotic fine sediments*, 2018, ISBN 978-3-942036-62-7

259 Fetzer, Thomas: *Coupled Free and Porous-Medium Flow Processes Affected by Turbulence and Roughness – Models, Concepts and Analysis*, 2018, ISBN 978-3-942036-63-4

260 Schröder, Hans Christoph: *Large-scale High Head Pico Hydropower Potential Assessment*, 2018, ISBN 978-3-942036-64-1

261 Bode, Felix: *Early-Warning Monitoring Systems for Improved Drinking Water Resource Protection*, 2018, ISBN 978-3-942036-65-8

262 Gebler, Tobias: *Statistische Auswertung von simulierten Talsperrenüberwachungsdaten zur Identifikation von Schadensprozessen an Gewichtsstaumauern*, 2018, ISBN 978-3-942036-66-5

263 Harten, Matthias von: *Analyse des Zuppinger-Wasserrades – Hydraulische Optimierungen unter Berücksichtigung ökologischer Aspekte*, 2018, ISBN 978-3-942036-67-2

264 Yan, Jieru: *Nonlinear estimation of short time precipitation using weather radar and surface observations*, 2018, ISBN 978-3-942036-68-9

265 Beck, Martin: *Conceptual approaches for the analysis of coupled hydraulic and geomechanical processes*, 2019, ISBN 978-3-942036-69-6

266 Haas, Jannik: *Optimal planning of hydropower and energy storage technologies for fully renewable power systems*, 2019, ISBN 978-3-942036-70-2

267 Schneider, Martin: *Nonlinear Finite Volume Schemes for Complex Flow Processes and Challenging Grids*, 2019, ISBN 978-3-942036-71-9

268 Most, Sebastian Christopher: *Analysis and Simulation of Anomalous Transport in Porous Media*, 2019, ISBN 978-3-942036-72-6

269 Buchta, Rocco: *Entwicklung eines Ziel- und Bewertungssystems zur Schaffung nachhaltiger naturnaher Strukturen in großen sandgeprägten Flüssen des norddeutschen Tieflandes*, 2019, ISBN 978-3-942036-73-3

270 Thom, Moritz: *Towards a Better Understanding of the Biostabilization Mechanisms of Sediment Beds*, 2019, ISBN 978-3-942036-74-0

271 Stolz, Daniel: *Die Nullspannungstemperatur in Gewichtsstaumauern unter Berücksichtigung der Festigkeitsentwicklung des Betons*, 2019, ISBN 978-3-942036-75-7

272 Rodriguez Pretelin, Abelardo: *Integrating transient flow conditions into groundwater well protection*, 2020, ISBN: 978-3-942036-76-4

273 Weishaupt, Kilian: *Model Concepts for Coupling Free Flow with Porous Medium Flow at the Pore-Network Scale: From Single-Phase Flow to Compositional Non-Isothermal Two-Phase Flow*, 2020, ISBN: 978-3-942036-77-1

274 Koch, Timo: *Mixed-dimension models for flow and transport processes in porous media with embedded tubular network systems*, 2020, ISBN: 978-3-942036-78-8

275 Gläser, Dennis: *Discrete fracture modeling of multi-phase flow and deformation in fractured poroelastic media*, 2020, ISBN: 978-3-942036-79-5

276 Seitz, Lydia: *Development of new methods to apply a multi-parameter approach – A first step towards the determination of colmation*, 2020, ISBN: 978-3-942036-80-1

277 Ebrahim Bakhshipour, Amin: *Optimizing hybrid decentralized systems for sustainable urban drainage infrastructures planning*, 2021, ISBN: 978-3-942036-81-8

278 Seitz, Gabriele: *Modeling Fixed-Bed Reactors for Thermochemical Heat Storage with the Reaction System CaO/Ca(OH)$_2$*, 2021, ISBN: 978-3-942036-82-5

279 Emmert, Simon: *Developing and Calibrating a Numerical Model for Microbially Enhanced Coal-Bed Methane Production*, 2021, ISBN: 978-3-942036-83-2

Die Mitteilungshefte ab der Nr. 134 (Jg. 2005) stehen als pdf-Datei über die Homepage des Instituts: www.iws.uni-stuttgart.de zur Verfügung.